Nematic ordering of wormlike polymers

by

Xiangqun Yuan

A thesis
presented to the University of Waterloo
in fulfillment of the
thesis requirement for the degree of
Master of Science
in
Physics

Waterloo, Ontario, Canada, 2005

AUTHOR'S DECLARATION FOR ELECTRONIC SUBMISSION OF A THESIS

I hereby declare that I am the sole author of this thesis. This is a true copy of the thesis, including any required final revisions, as accepted by my examiners.

I understand that my thesis may be made electronically available to the public.

Abstract

In this thesis, based on the Onsager excluded volume interaction model, two nematic ordering problems of wormlike (semiflexible) polymer are studied: one is to investigate the isotropic-nematic interface of polymers for three typical cases — the flexible one, the rigid-rod one and the intermediate one; the other is to investigate a very long polymer confined between two infinite flat hard walls.

Many previous studies of the isotropic-nematic phase coexistence are mainly focused on either rigid rod-like polymers with small flexibility, or flexible polymers with large flexibility. The phase coexistence of polymers with intermediate flexibility is desired to be investigated. For these three typical cases (flexible, rigid-rod and intermediate), the profiles for density, order parameter and tension contribution were shown for different tilt angles. The interface tension was studied. The simulation results are consistent with those reported by other people.

We investigated the confinement of a long polymer between two flat hard walls, which are separated by a distance comparable to the effective Kuhn length of polymer chain by the wormlike chain model with or without the Onsager excluded volume interaction. Without the interaction, the results are compared with those of the Gaussian chain model. Including the interaction, the phase diagram is analyzed.

Acknowledgements

I would like to gratefully acknowledge Dr. Jeff Z.Y. Chen for his enthusiastic supervision during this study. Without his common-sense, knowledge, perceptiveness and cracking-of-the-whip I would never have finished. I also deeply appreciate all other members of my committee for their care and help.

I am grateful to all my friends from Department of Physics, University of Waterloo, for being the surrogate family during the time here. From the staff, Judy McDonnell and Margaret O'Neill are especially thanked for their attention and help.

Finally, I am forever indebted to my parents and my wife for their understanding, endless patience and encouragement whenever mostly required.

Contents

List of Figures

Chapter 1

Introduction

1.1 Motivation

Liquid crystals (LC) are the states in which substances possess the flow properties of a liquid and, to a degree, the molecular order of a crystalline solid, i.e., the symmetric and mechanical properties of LC are intermediate between those of a crystalline solid and an isotopic liquid. The basic difference between crystals and liquids is that the molecules in a crystal are ordered whereas in a liquid they are not. The ordering of the molecules in a crystal is usually both positional and orientational, i.e., the molecules are constrained both to occupy specific sites in a lattice and to point their molecular axes in specific directions. Depending on different positional and orientational orders, liquid crystals can be classified into many types, such as (isotropic,) nematic, biaxial nematic, smectic A, smectic C, cholesteric phases, and so on. Figure 1.1 is the schematic plot for some popular liquid crystalline states. The phase without any positional and orientational orders is an isotropic phase. In the nematic phase the molecules maintain a preferred orientational direction called the nematic director, and they diffuse throughout the sample, i.e., the nematic phase has no positional order throughout the matter. The smectic phases are those where in addition to orientation order, the molecules are grouped into layers, enforcing long-range positional order in one or two directions. Liquid crystalline materials in general may have various types of molecular struc-

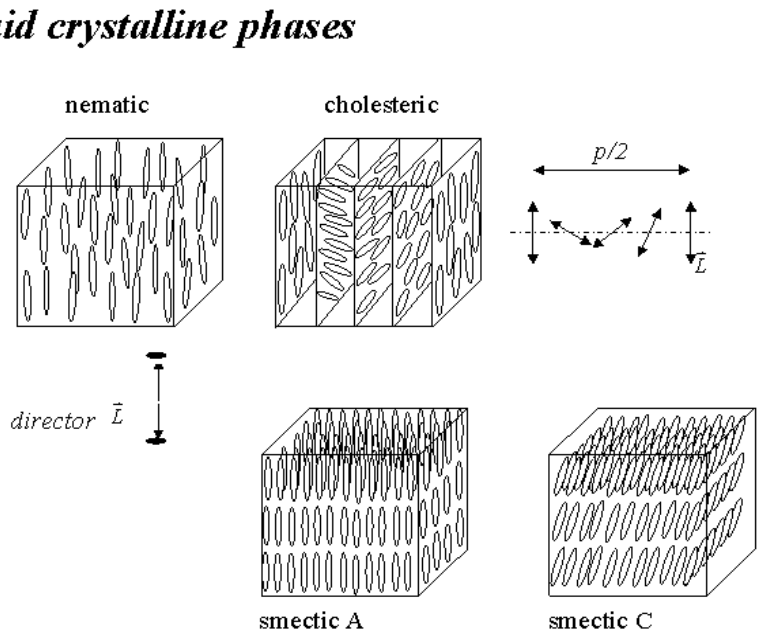

Figure 1.1: Illustration for some most popular liquid crystalline phases [1].

ture. What in common is that they are all anisotropic. Either their shape is such that one axis is very different from the other two or, in some cases, different parts of the molecules have very different solubility properties, or other unsymmetrical properties.

The study of polymeric liquid crystals is of high importance to improve our understanding of biological systems and because of various industrial applications [2, 3]. Most of the chemical compounds present in living organisms contain skeletons of covalently bonded carbon atoms (C-C-C). These compounds are known as organic compounds, because most of these are either present in, or produced by living things. Organic compounds are the major components of cells and tissues. They provide energy for life processes, participate in and regulate metabolic reactions, and transmit information. These macromolecules are polymers and made of smaller subunits (monomers). The subunits of macromolecules are held together with covalent bonds, and have different structures and properties. For example, the double helical DNA is a very long polymers with a large number of different subunits, formed by four bases: adenine (A), thymine (T), guanine (G) and cytosine

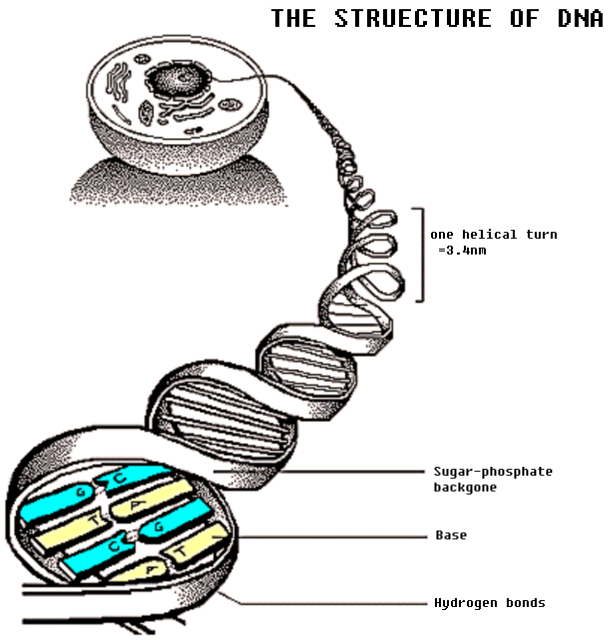

Figure 1.2: Illustration of the double helical structure of the DNA molecule [4].

(C). The schematic plot of the structure of DNA is shown in Fig. 1.2.

Their roles and the properties richness require much more work. We concentrate on one aspect, the dynamics of polymers in the liquid state, or in more detail, the phases formed by main-chain liquid crystalline polymers with or without external field, the phase transition and the phase coexistence.

One of the most successful models was introduced by Onsager [5]. In 1949, by considering the purely repulsive anisotropic interactions between molecules, Onsager showed that a phase transition exhibits in a system of long rigid rods from an isotropic phase to a denser anisotropic phase. The calculation was based on a cluster expansion to the second virial for the free energy, which is given as a functional of the distribution in orientation of the rigid molecules. The ratio of the length to the cross section diameter of rigid molecules must be high to make the second virial expansion valid (see A). The difference between the low density isotropic phase and the high density nematic phase is that the orientational sym-

metry of isotropic phase is broken in the nematic phase. This rigid-rod model was applied later to a certain idealized model by Zwanzig [6], in which the orientational direction is restricted to be parallel to the three coordinate axes and a first order phase transition was observed. Khokhlov and Semenov (KS) [7] extended this theory to very long semiflexible chains in order to describe the isotropic-nematic transition for long polymers. The liquid crystalline materials exhibit the richest varieties of polymorphism. The transition between different phases corresponds to the breaking of some symmetry. Phase transition of liquid crystalline polymers, such as isotropic-nematic transition, nematic-smectic transition, uniaxial nematic-biaxial nematic transition, etc., were studied by many different approaches, and is still a very active area with many problems unsolved.

Several simple models have been proposed ever since the beginning of microscopic modeling of polymers, two of the most important ones being the freely jointed chain model and the freely rotating chain model. In both models bond lengths are constrained to a fixed value. In the freely jointed chain model, the angle formed by the successive bonds is random, while in the freely rotating chain model, the polar angle is fixed and the bond can rotate freely about the adjacent bond. We will discuss these models in detail in the second chapter.

Stemming from these two models, the Gaussian chain model, and especially the wormlike one are also discussed and used as the basis of this thesis. The bond length of the Gaussian model is not fixed but it has the same macro-properties of the freely jointed chain model. The wormlike chain model involves the bending energy and regards the whole polymer as one continuous chain, characterized by the total contour length and the persistence length, in which length scale the correlation of the segments along the chain decays.

1.2 Contribution

The major contribution of this thesis is that two nematic ordering problems are solved. One is to investigate the phase coexistence of the isotropic phase and nematic phase, for three typical polymers, flexible, rigid-rod and the intermediate.

The other is to investigate a long polymer chain confined between two hard walls by considering the interaction with walls only by the geometric constraint. The numerical simulation is based on the wormlike chain model while the interaction between polymer segments is the Onsager type.

Current work on the interface between isotropic phase and nematic phase has focused either on the rigid rod-like polymers or on the flexible polymers. Even though some work claimed they have studied the semiflexible polymers by using the wormlike polymer chain model, they were focused on the two limits, one is that the persistence length of the polymers is much longer than the contour length, or vice versa. It is of importance to investigate the phases coexistence of the polymers with the persistence length comparable to the contour length. This study is presented in the third chapter.

In the fourth chapter, the confinement of a long polymer between two infinite hard walls is studied. The separation of two walls is comparable to the persistence length of polymers, which is much smaller than the contour length of the polymer chain, i.e., the chain is in the flexible limit. The walls are structureless and sterically contain the polymer. The study is conducted for wormlike chain with or without the Onsager excluded volume interaction. Without the interaction, the results are compared with those of the Gaussian chain. For inclusion of the interaction, the phase diagram is discussed.

Chapter 2

Theoretical Methods

A polymer is made up by linking many smaller molecules called monomers. Because of an enormous number of internal degrees of freedom for monomers which form the backbone of polymer chains, a polymer may take up virtually an infinite number of configurations, therefore it is very necessary to use the statistical mechanics to deal with the problem. Many ideal chain models [8] of varying levels of complexity and reality for ideal chains have been introduced to study the statistical properties of polymers in the equilibrium state.

2.1 Freely jointed chain model and Gaussian chain model

Freely jointed chain model is one of the most important models. Consider a single flexible polymer chain composed of n links, which can be described by the set of $(n+1)$ position vectors $\{\mathbf{r}_k\} = (\mathbf{r}_0, ..., \mathbf{r}_n)$ from one end of the chain to the other, or alternately, by (n) bond vectors $\{\mathbf{R}_k\} = (\mathbf{R}_1, ..., \mathbf{R}_n)$, where

$$\mathbf{R}_k = \mathbf{r}_k - \mathbf{r}_{k-1}, \qquad k = 1, 2, ..., n. \tag{2.1}$$

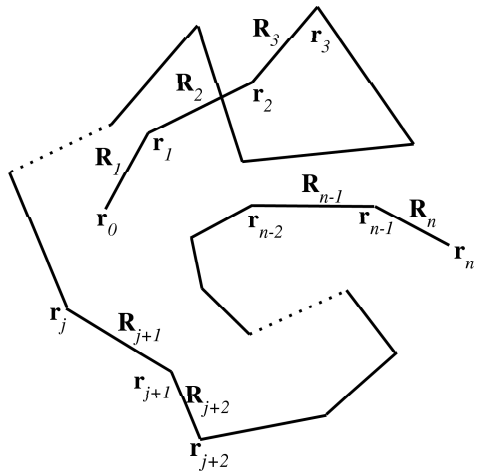

Figure 2.1: Freely jointed chain.

The potential energy of the chain is written in terms of bond vectors $\{\mathbf{R}_k\}$ as

$$U(\{\mathbf{R}_k\}) = \sum_{j=1}^{n} u_j(\mathbf{R}_j) + V(\{\mathbf{R}_k\}), \tag{2.2}$$

where, u_j accounts for the connectivity of the chain, V contains all other interactions. All of the statistical properties of a single chain are contained in the distribution

$$G(\{\mathbf{R}_k\}) = \prod_{j=1}^{n} \tau_j(\mathbf{R}_j) \exp[-\beta V(\{\mathbf{R}_k\})], \tag{2.3}$$

where

$$\tau_j(\mathbf{R}_j) = C \exp[-\beta u_j(\mathbf{R}_j)], \tag{2.4}$$

with the normalization condition

$$\int \mathrm{d}\mathbf{R}_j \tau_j(\mathbf{R}_j) = 1, \tag{2.5}$$

is the "probability" that the jth bond has length R_j, C the normalization constant, $\beta = 1/k_{\mathrm{B}}T$, k_{B} the Boltzmann constant and T the temperature. From Eq. (2.3),

in principle, we are able to calculate the partition function by

$$z = \int \mathrm{d}\{\mathbf{R}_k\} G(\{\mathbf{R}_k\}), \tag{2.6}$$

where

$$\mathrm{d}\{\mathbf{R}_k\} = \mathrm{d}\mathbf{R}_1 \mathrm{d}\mathbf{R}_2 ... \mathrm{d}\mathbf{R}_n = \prod_{j=1}^{n} \mathrm{d}\mathbf{R}_j, \tag{2.7}$$

and the distribution function for the entire chain is

$$P(\{\mathbf{R}_k\}) = z^{-1} G(\{\mathbf{R}_k\}). \tag{2.8}$$

If we only consider the interaction of connectivity of the chain, i.e., $V = 0$, the simplest model of a real polymer chain is the so-called freely jointed chain model in which all the bonds have the same length b, and is able to point in any direction independently of each other,

$$\tau(\mathbf{R}_j) = \frac{1}{4\pi b^2} \delta(|\mathbf{R}_j| - b), \tag{2.9}$$

where δ is the Dirac delta function. In this model, every bond has a fixed length b. The interesting thing is to calculate the end-to-end distribution of the chain, which is expressed in terms of the bond vectors

$$P(\mathbf{R}; n) = \int \left[\prod_{j=1}^{n} \tau(\mathbf{R}_j) \right] \delta \left(\sum_{j=1}^{n} \mathbf{R}_j - \mathbf{R} \right) \mathrm{d}\{\mathbf{R}_k\}, \tag{2.10}$$

where $\mathbf{R}$ is the end-to-end vector, and the delta function selects out all the configurations that $\mathbf{R} = \sum_{j=1}^{n} \mathbf{R}_j$. Note that Eq. (2.10) is, as usual, subjected to a normalization constant. By using the Fourier representation of the delta function

$$\delta \left(\sum_{j=1}^{n} \mathbf{R}_j - \mathbf{R} \right) = \int \frac{\mathrm{d}\mathbf{k}}{(2\pi)^3} \exp \left[i \left(\sum_{j=1}^{n} \mathbf{R}_j - \mathbf{R} \right) \cdot \mathbf{k} \right], \tag{2.11}$$

equation (2.10) gives a product of n identical factors

$$P(\mathbf{R}; n) = \int \frac{\mathrm{d}\mathbf{k}}{(2\pi)^3} \exp(-i\mathbf{k} \cdot \mathbf{R}) \left[\int \mathrm{d}\mathbf{R}_j \tau(\mathbf{R}_j) \exp(i\mathbf{R}_j \cdot \mathbf{k}) \right]^n. \tag{2.12}$$

Substitute Eq. (2.9) into Eq. (2.12), and the integral over $\mathbf{R}$ is evaluated by introducing polar coordinates ((r, θ, ψ), the reference axis of θ being taken along the vector $\mathbf{k}$), Eq. (2.12) would be

$$P(\mathbf{R}; n) = \int \frac{\mathrm{d}\mathbf{k}}{(2\pi)^3} \exp(-i\mathbf{k}\cdot\mathbf{R}) \left[\frac{\sin(kb)}{kb}\right]^n, \tag{2.13}$$

where $k = |\mathbf{k}|$. If n is large, $[\sin(kb)/kb]^n$ becomes very small unless kb is small. For $kb \ll 1$ with large n, $[\sin(kb)/kb]^n$ can be approximated as

$$\left[\frac{\sin(kb)}{kb}\right]^n \approx \left[1 - \frac{k^2b^2}{6}\right]^n \approx \exp\left[-\frac{nk^2b^2}{6}\right]. \tag{2.14}$$

By putting Eq. (2.14) back into Eq. (2.13), we get

$$\begin{aligned} P(\mathbf{R}; n) &= \int \frac{\mathrm{d}\mathbf{k}}{(2\pi)^3} \exp(-i\mathbf{k}\cdot\mathbf{R}) \exp\left[-\frac{nk^2b^2}{6}\right] \\ &= \left(\frac{3}{2\pi b^2 n}\right)^{3/2} \exp\left[-\frac{3\mathbf{R}^2}{2nb^2}\right] \end{aligned} \tag{2.15}$$

where, for the last step, the standard Gaussian integral is performed for each components of the vector $\mathbf{k}$. Thus the distribution function of the end-to-end vector is Gaussian. The local structure of the chain appears only through the effective bond length b, because the local structure affects only the effective bond length but does not otherwise appear in the problem. Therefore, if we are interested in the global properties of polymers, we can introduce a different $\tau(\mathbf{R}_j)$ from Eq. (2.9),

$$\tau(\mathbf{R}_j) = \left(\frac{3}{2\pi b^2}\right)^{3/2} \exp\left(-\frac{3\mathbf{R}_j^2}{2b^2}\right), \tag{2.16}$$

with the average (root mean square) of the bond length

$$\sqrt{<\mathbf{R}_j^2>} = b, \tag{2.17}$$

which reproduces the properties of Eq. (2.13), but which is mathematically easier to handle than Eq. (2.9).

Then, the configuration of the chain composed by n Gaussian bonds is given by

$$P(\{\mathbf{R}_k\}) = \prod_{j=1}^{n} \left[\frac{3}{2\pi b^2}\right]^{3/2} \exp\left[-\frac{3\mathbf{R}_j^2}{2b^2}\right] \qquad \text{or} \tag{2.18}$$

$$P(\{\mathbf{r}_k\}) = \left[\frac{3}{2\pi b^2}\right]^{3n/2} \exp\left[-\sum_{j=1}^{n} \frac{3(\mathbf{r}_j - \mathbf{r}_{j-1})^2}{2b^2}\right]. \tag{2.19}$$

Note that Eq. (2.19) and Eq. (2.15) have different normalization constant due to different normalization conditions (the former is for each bond, the latter is for whole chain). Such a chain is called the Gaussian chain. Although the Gaussian chain does not correctly describe the local structure of the polymer, it does correctly describe the property on large length scale.

2.2 The Wiener Integral

For the two flexible polymer models discussed in section 2.1, they both obey the end-to-end distribution Eq. (2.15), and the mean-square end-to-end distance can be found as

$$< \mathbf{R}^2 >= nb^2 = Lb, \tag{2.20}$$

with

$$L = nb \tag{2.21}$$

where L is the maximum contour length of the chain at full extension, and is temperature independent. If the chain is not flexible in the length b, and the chain is long enough, we can use the equivalent gaussian links, defined by

$$l \equiv \frac{< \mathbf{R}^2 >}{L}. \tag{2.22}$$

If the equivalent chain has n gaussian links, each of average length Δs, the configuration of the Gaussian chain Eq. (2.19) can be rewritten as

$$P(\{\mathbf{r}_k\}) = \left[\frac{3}{2\pi l \Delta s}\right]^{3n/2} \exp\left[-\sum_{j=1}^{n} \frac{3(\mathbf{r}_j - \mathbf{r}_{j-1})^2}{2l\Delta s}\right]. \tag{2.23}$$

If we treat the chain configuration $\{\mathbf{r}_k\}$ as the discrete representation of the continuous curve $\mathbf{r}(s)$, we can get

$$\mathbf{r}_j - \mathbf{r}_0 = \mathbf{r}(j\Delta s) \equiv \mathbf{r}(s_j) \tag{2.24}$$

denote the position of the jth segment with respect to the first end of the chain. Take the limit $\Delta s \to 0$, $n \to \infty$, $n\Delta s = L$ to get a representation of a continuous

equivalent freely jointed chain. In this limit, the expression in the exponential of Eq. (2.23) is

$$\begin{aligned}\lim\sum_{j=1}^{n}\left[\frac{\mathbf{r}(s_j)-\mathbf{r}(s_j-\Delta s)}{\Delta s}\right]^2\Delta s &= \lim\sum_{j=1}^{n}\left[\left.\frac{\partial\mathbf{r}(s)}{\partial s}\right|_{s=s_j}\right]^2\Delta s \\ &= \int_0^L \mathrm{d}s\left[\frac{\partial\mathbf{r}(s)}{\partial s}\right]^2 \\ &= \int_0^L \mathrm{d}s[\dot{\mathbf{r}}(s)]^2 \qquad (2.25)\end{aligned}$$

Eq. (2.25) follows from the definition of derivatives and integrals in elementary calculus. In this limit, the probability $P(\{\mathbf{r}_k\})$ becomes

$$P[\mathbf{r}(s)] \propto \exp\left[-\frac{3}{2l}\int_0^L \mathrm{d}s[\dot{\mathbf{r}}(s)]^2\right]. \qquad (2.26)$$

This is the well-known Wiener distribution for flexible polymer chains.

2.3 Freely rotating chain model and worm-like chain model

The Gaussian chain model is very successful to model many flexible polymer systems. However, because the bending energy is not considered in this model, it is not good to describe semiflexible or rigid polymer systems, for example, is not good to describe the DNA chain. The wormlike-chain model was introduced by Kratky and Porod to describe semiflexible chains in which the rigidity of the polymer chains is considered [9].

The end-to-end distance of a flexible polymer chain and that with rigidity are quite different. For a rigid rod, the end-to-end distance is $L = nb$, the total contour length, while for a flexible polymer, the root mean square end-to-end distance is, $\sqrt{<\mathbf{R^2}>} = n^{1/2}b$, found from Eq. (2.20). For flexible polymer chains, there is no correlation between bonds; for polymer chains with stiffness, they do have correlation between bonds, especially for those bonds not far apart.

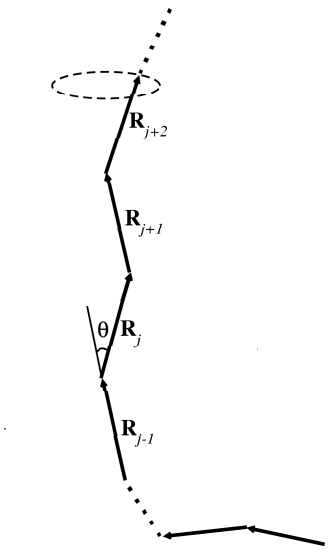

Figure 2.2: Freely rotating chain. The successive bonds form a fixed angle θ, but can freely rotate along the previous bond axis.

Consider an n bonds chain, in which the bond angles formed by successive bonds are fixed at say θ and the bond lengths are fixed at b, as shown in Fig. 2.2. The only degree of freedom left for the bond is the rotation around the axis of the previous bond. This model is called the freely rotating chain model. To calculate the mean-square end-to-end distance of the chain,

$$\begin{aligned} < \mathbf{R}^2 > &= < \sum_{j=1}^{n} \mathbf{R}_j \cdot \sum_{i=1}^{n} \mathbf{R}_i > \\ &= \sum_{j=1}^{n} \sum_{i=1}^{n} < \mathbf{R}_j \cdot \mathbf{R}_i > \\ &= \sum_{j=1}^{n} < \mathbf{R}_j^2 > + 2 \sum_{j=1}^{n} \sum_{i=j+1}^{n} < \mathbf{R}_j \cdot \mathbf{R}_i >, \end{aligned} \tag{2.27}$$

where the average is over all values of the torsion angles $\{\varphi_j\}$. The correlation between bond vectors $\mathbf{R}_j$ and $\mathbf{R}_i$ must be determined. In this model, for successive

bonds, the projection $\mathbf{R}_j$ on the direction of $\mathbf{R}_{j+1}$,

$$< \mathbf{R}_j \cdot \mathbf{R}_{j+1} >= \mathbf{R}_j \cdot \mathbf{R}_{j+1} = b^2 \cos\theta. \tag{2.28}$$

For the freely rotating chain, the component of $\mathbf{R}_j$ normal to vector $\mathbf{R}_{j+1}$ averages out to zero due to free rotations of the torsion angle φ_j. The only correlation between the bond vectors that is transmitted down the chain is the component of vector $\mathbf{R}_j$ along the bond vector $\mathbf{R}_{j+1}$. The value of this component is $b\cos\theta$. Bond vector $\mathbf{R}_{j+1}$ passes this correlation down to vector $\mathbf{R}_{j+2}$ survives due to free rotations of torsion angle φ_{j+1}. The leftover memory of the vector $\mathbf{R}_j$ at this stage is $b(\cos\theta)^2$. The correlations from bond vector $\mathbf{R}_j$ at bond vector $\mathbf{R}_i$ are reduced by the factor $(\cos\theta)^{|j-i|}$ due to independent free rotations of $|j-i|$ torsion angles between these two vectors. Therefore, the correlation between bond vectors $\mathbf{R}_j$ and $\mathbf{R}_i$ is

$$< \mathbf{R}_j \cdot \mathbf{R}_i >= b^2(\cos\theta)^{|j-i|}. \tag{2.29}$$

The end-to-end distance Eq. (2.27) becomes,

$$\begin{aligned}
< \mathbf{R}^2 > &= nb^2 + 2b^2 \sum_{j=1}^{n} \sum_{i=j+1}^{n} (\cos\theta)^{j-i} && \text{(2.30a)}\\
&= nb^2 + 2b^2 \sum_{j=1}^{n} \sum_{k=1}^{n-j} (\cos\theta)^{k} && \text{(2.30b)}\\
&= nb^2 \left[\frac{1+\cos\theta}{1-\cos\theta} - \frac{2\cos\theta}{n} \cdot \frac{1-\cos^n\theta}{(1-\cos\theta)^2} \right] && \text{(2.30c)}\\
&\approx nb^2 \left[\frac{1+\cos\theta}{1-\cos\theta} \right], && \text{(2.30d)}
\end{aligned}$$

where, in the last step, we neglect the second term for large enough n and nontrivial angle θ. For the freely rotating chain, the maximum end-to-end length (contour length) L can be found when all the bonds lie in a plane, hence

$$L = nb\cos(\theta/2). \tag{2.31}$$

It is very clear that for a given nontrivial angle $|\cos\theta| < 1$, the term $(\cos\theta)^{|j-i|}$ decays rapidly as the number of bonds between bond vectors $\mathbf{R}_j$ and $\mathbf{R}_i$ is increased,

and

$$(\cos\theta)^{|j-i|} = \exp[|j-i|\ln(\cos\theta)] = \exp\left[-\frac{|j-i|}{s_p}\right], \tag{2.32}$$

where, the last step we defined s_p as the number of bonds between bond vectors $\mathbf{R}_j$ and $\mathbf{R}_i$ when the correlation between them decays. In the length scale of local contour length $s_p b\cos(\theta/2)$ called the persistence length l_p, the correlations between bond vectors decay,

$$l_p = s_p b\cos(\theta/2) = -\frac{b\cos(\theta/2)}{\ln(\cos\theta)}. \tag{2.33}$$

Some typical persistence lengths encountered in biological systems are $l_p \approx 5mm$ for tubulin [10], $l_p \approx 20\mu m$ for actin [11, 12], and $l_p \approx 50nm$ for double-stranded DNA [13].

If we take the limit

$$b \to 0, \quad n \to \infty, \quad nb \to L, \quad \theta \to 0, \quad -\frac{b\cos(\theta/2)}{\ln(\cos\theta)} \approx \frac{b}{\theta^2/2} \to l_p \tag{2.34}$$

of the discrete the freely rotating chain, we get the worm-like chain [8]. In this case, the approximation in Eq. (2.30d) is no longer correct, because the term $\cos^n\theta$ in the limit of Eq. (2.34) is not always negligible, and

$$\cos^n\theta = \exp[n\ln(\cos\theta)] = \exp\left[-\frac{nb\cos(\theta/2)}{l_p}\right] = \exp[-\frac{L}{l_p}]. \tag{2.35}$$

Therefore, from Eq. (2.30c), the end-to-end distance becomes

$$\begin{aligned} <\mathbf{R}^2> &\approx \frac{2nb^2}{\theta^2/2} - 2b^2\frac{1-\exp[-L/l_p]}{\theta^4/4} \\ &= 2Ll_p - 2l_p^2\left\{1-\exp\left[-\frac{L}{l_p}\right]\right\} \\ &= aL - \frac{a^2}{2}\left\{1-\exp\left[-\frac{2L}{a}\right]\right\}, \end{aligned} \tag{2.36}$$

where $a = 2l_p$ is the effective Kuhn length. We should note that the definition of the Kuhn length is only for long chains, and equals to two times of the persistence length, and no definition for short chains. For convenience, we introduce the effective Kuhn length which is always equal to two times of the persistence length no

matter that the chain is long or short. There are two simple limits of this expression. The flexible limit of a worm-like chain is when the contour length is much longer than its persistence length

$$< \mathbf{R}^2 > \approx 2Ll_p = aL \quad \text{for} \quad L \gg l_p. \tag{2.37}$$

The rod-like limit of a worm-like chains is when the contour length is much shorter than its persistence length. Expanding the exponential in Eq. (2.36)

$$\exp\left[-\frac{L}{l_p}\right] \approx 1 - \frac{L}{l_p} + \frac{1}{2}\left[-\frac{L}{l_p}\right]^2 + \cdots \quad \text{for} \quad L \ll l_p, \tag{2.38}$$

and we get

$$< \mathbf{R}^2 > = L^2 \quad \text{for} \quad L \ll l_p. \tag{2.39}$$

So the wormlike chain has the similar mean-square end-to-end distance with that of the freely jointed chain only at the flexible limit. Even at this limit, there exists differences between them. The effective Kuhn length a of the freely jointed chains are assumed to be completely rigid. Worm-like chains are also stiff on length scales shorter than the effective Kuhn length, but are not completely rigid and can fluctuate and bend.

2.4 STY description

For a wormlike chain discussed in the last section, it can be characterized by the total contour length L and the persistence length l_p or the effective Kuhn length a. When the persistence length is short, the energy needed to bend a given length of the chain is less than that needed for the case of a longer persistence length. The potential energy (more information can be seen in B) per unit length stored in a bent rod is

$$E = \frac{\varepsilon}{2\Re^2}, \tag{2.40}$$

where ε is the bending force constant and $\Re$ the radius of curvature, which is defined by

$$\Re^{-1} = \left|\frac{\partial \mathbf{u}(s)}{\partial s}\right| = |\dot{\mathbf{u}}|, \tag{2.41}$$

where,

$$\mathbf{u}(s) \equiv \mathrm{d}\mathbf{r}(s)/\mathrm{d}s = \dot{\mathbf{r}}, \quad \text{and} \quad |\mathbf{u}(s)| = 1, \tag{2.42}$$

is the unit vector along the tangent direction of the curvature. This unit vector restriction is suggested by Saito-Takahashi-Yunoki (STY) [14]. The physical meaning of this restriction is clear: for an unstretchable chain, the integration of $\mathbf{u}$ along any part of the chain should equal to the end-to-end vector of it, i.e.,

$$\int_0^s \mathrm{d}t\mathbf{u}(t) = \mathbf{r}(s) - \mathbf{r}(0). \tag{2.43}$$

For a chain of contour length L, the total potential energy is

$$V = \frac{\varepsilon}{2}\int_0^L |\dot{\mathbf{u}}(s)|^2\,\mathrm{d}s = \frac{\varepsilon}{2}\int_0^L |\ddot{\mathbf{r}}|^2\,\mathrm{d}s \tag{2.44}$$

For a wormlike polymer chain, STY showed that the energy force constant ε has a simple relation with the persistence length l_p

$$l_p = \beta\varepsilon. \tag{2.45}$$

Thus, the statistical probability of a wormlike chain with persistence length l_p under the restriction Eq. (2.42) or (2.43) is given by

$$P[\mathbf{r}(s), \mathbf{u}(s)] \propto \exp\left[-\frac{l_p}{2}\int_0^L [\dot{\mathbf{u}}(s)]^2\mathrm{d}s\right] \times \prod_{s=0}^{L} \delta\left[\mathbf{r}(s) - \mathbf{r}(0) - \int_0^s \mathrm{d}t\mathbf{u}(t)\right] \tag{2.46a}$$

$$\propto \exp\left[-\frac{1}{4}\int_0^{\frac{L}{a}} [\dot{\mathbf{u}}(s)]^2\mathrm{d}s\right] \times \prod_{s=0}^{\frac{L}{a}} \delta\left[\mathbf{r}(s) - \mathbf{r}(0) - \int_0^s \mathrm{d}t\mathbf{u}(t)\right], \tag{2.46b}$$

where, in Eq. (2.46b), the chain length is rescaled in unit of the effective Kuhn length a, which does not affect the tangent vector $\mathbf{u}$.

2.5 Onsager excluded volume interaction

In the models of polymer discussed in the previous sections, we only included the interaction of a few neighboring segments or a length scale of a few persistence

lengths along the chain, and we did not include other interactions, i.e., $V = 0$. As a matter of fact, however, segments far apart along the chain do interact. One obvious interaction is that, due to the finite volume of each segment, other segments cannot come into its own region. It is called the excluded volume effect.

For a sphere with radius r in the space, the total volume other spheres with same diameter can not enter is 8 times of the volume of the sphere, indicated in Fig. 2.3a by the dotted line. Then we consider a more complex system, the excluded volume of rods with different length and cross section diameter, shown in Fig. 2.3b. Note that here we use the symbol d to denote the diameter, just to avoid the confusion with the symbol of deviation d. Since rods are anisotropic particles, the excluded volume depends on the angle formed by the considered rods. For two identical rods, which form an angle γ, in the case of the length L much larger than the cross section diameter d, Onsager exactly calculated the excluded volume [5]

$$v = 2L^2 d|\sin\gamma|, \tag{2.47}$$

which is the volume of the prism: the base is a parallelogram with each side length L, and the height is $2d$.

Based on the same rule, the excluded volume of one wormlike polymer caused by another identical wormlike polymer chain can be calculated in the following way: suppose that we can divide each chain into many tiny segments, so that all the segments are rigid rods following Eq. (2.47), then integrate along each chain, as

$$\begin{aligned} v_{worm} &= \frac{1}{2}\int_0^L \int_0^L \mathrm{d}s_1\mathrm{d}s_2 2dV_0\delta[\mathbf{r}_1(s_1)-\mathbf{r}_2(s_2)]|\sin\{\gamma[\mathbf{u}_1(s_1),\mathbf{u}_2(s_2)]\}| && \text{(2.48a)}\\ &= \frac{1}{2}\int_0^{\frac{L}{a}} \int_0^{\frac{L}{a}} \mathrm{d}s_1\mathrm{d}s_2 2a^2dV_0\delta[\mathbf{r}_1(s_1)-\mathbf{r}_2(s_2)]|\sin\{\gamma[\mathbf{u}_1(s_1),\mathbf{u}_2(s_2)]\}| && \text{(2.48b)}\\ &= \frac{1}{2}\int_0^{\frac{L}{a}} \int_0^{\frac{L}{a}} \mathrm{d}s_1\mathrm{d}s_2 v_e[\mathbf{r}_1(s_1),\mathbf{u}_1(s_1);\mathbf{r}_2(s_2),\mathbf{u}_2(s_2)], && \text{(2.48c)} \end{aligned}$$

where, V_0 is the volume of the container, which is introduced to cancel the effect of the delta function, the factor $1/2$ due to double counting, d the cross section diameter of polymer chains, delta function means the interaction only happens when they reach each other at the same position $\mathbf{r}$, angle γ now depends on the

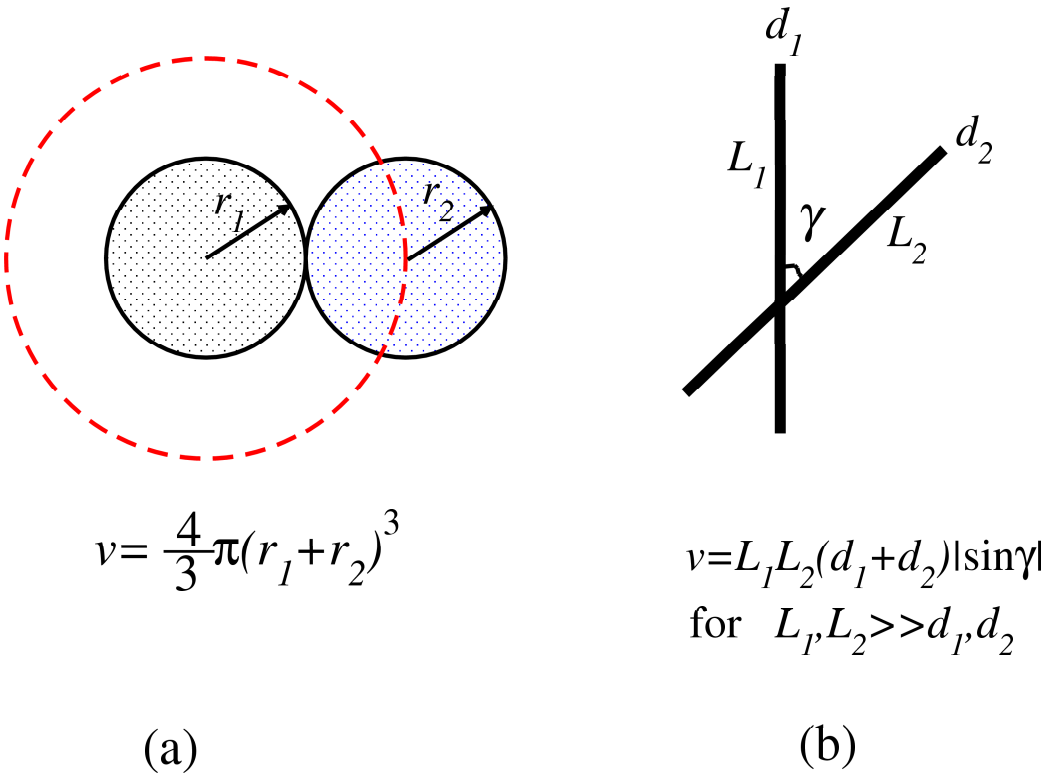

Figure 2.3: Excluded volume for two simple cases. (a) spheres with radius r_1 and r_2, respectively; (b) the two rigid rods with length and diameter of cross section $\{L_1,\ d_1\}$ and $\{L_2,\ d_2\}$, respectively, with the assumption that lengths are much larger than the radii. γ is the angle formed by them.

segment vectors $\mathbf{u}$, Eq. (2.48c) is again rescaled in the effective Kuhn length, and

$$v_e[\mathbf{r}_1, \mathbf{u}_1; \mathbf{r}_2, \mathbf{u}_2] = 2a^2 dV_0 \delta[\mathbf{r}_1 - \mathbf{r}_2]|\mathbf{u}_1 \times \mathbf{u}_2|, \tag{2.49}$$

where, because tangent vectors are unit vectors, i.e., $|\mathbf{u}| = 1$, we have used in Eq. (2.48c) $|\sin\{\gamma[\mathbf{u}_1(s_1), \mathbf{u}_2(s_2)]\}| = |\mathbf{u}_1 \times \mathbf{u}_2|$.

By including the excluded volume potential and other interactions if there exist, the configuration of a wormlike chain Eq. (2.46b) is adjusted

$$P[\mathbf{r}(s), \mathbf{u}(s)] \propto \exp\left[-\frac{1}{4}\int_0^{\frac{L}{a}} [\dot{\mathbf{u}}(s)]^2 \mathrm{d}s - \beta V\right] \times \prod_{s=0}^{\frac{L}{a}} \delta\left[\mathbf{r}(s) - \mathbf{r}(0) - \int_0^s \mathrm{d}t\mathbf{u}(t)\right], \tag{2.50}$$

where

$$\beta V = \frac{1}{2V_0}\int_0^{\frac{L}{a}}\int_0^{\frac{L}{a}} \mathrm{d}s_1 \mathrm{d}s_2 v_e[\mathbf{r}_1(s_1), \mathbf{u}_1(s_1); \mathbf{r}_2(s_2), \mathbf{u}_2(s_2)] + \beta V_{\text{other}}, \tag{2.51}$$

where βV_{other} contains all other possible potentials.

2.6 Mean field theory

Finally, the partition function for a system with N wormlike polymers contained in a volume V_0 without external field can be written as

$$Z = \frac{1}{N!}\int \prod_{i=1}^{N} D[\mathbf{r}_i(s)] D[\mathbf{u}_i(s)] P[\mathbf{r}_i(s), \mathbf{u}_i(s)] \tag{2.52}$$

where $\int D[\mathbf{r}(s)] D[\mathbf{u}(s)]$ indicates a functional integral over the range of all position and angle, that is over all possible conformations of the polymer chain.

Directly calculating the system involving interactions between elements is not easy, therefore the mean field approximation needs to be introduced. The basic underlying idea of the mean field theory is that the complicated interactions between elements in a system can be replaced by the interaction of the element with

an effective (or mean) field. In order to avoid getting lost, we give the mean field result, i.e., the wormlike chain stays in the mean field $w(\mathbf{r},\mathbf{u})$,

$$\frac{\partial q(\mathbf{r},\mathbf{u},t)}{\partial t} = \left[\nabla^2_{\mathbf{u}} - a\mathbf{u}\cdot\nabla_{\mathbf{r}} - w(\mathbf{r},\mathbf{u})\right] q(\mathbf{r},\mathbf{u},t). \tag{2.53}$$

where $q(\mathbf{r},\mathbf{u},t)$ is partial chain partition function defined by Eq. (2.66). In the following we will give the detail derivation of the mean field theory.

Introducing the microscopic distribution density function

$$\hat{\rho}(\mathbf{r},\mathbf{u}) = \sum_{i=1}^{N}\int_0^{\frac{L}{a}} \mathrm{d}s\delta[\mathbf{r}-\mathbf{r}_i(s)]\delta[\mathbf{u}-\mathbf{u}_i(s)]. \tag{2.54}$$

Then the interaction potential can be written as

$$\begin{aligned}
\exp[-\beta V] &= \int D[\rho(\mathbf{r},\mathbf{u})]\delta[\rho(\mathbf{r},\mathbf{u})-\hat{\rho}(\mathbf{r},\mathbf{u})] \\
&\quad \times \exp\left[-\frac{1}{2V_0}\int \mathrm{d}\mathbf{r}_1\mathrm{d}\mathbf{u}_1\mathrm{d}\mathbf{r}_2\mathrm{d}\mathbf{u}_2\rho(\mathbf{r}_1,\mathbf{u}_1)v_e[\mathbf{r}_1,\mathbf{u}_1;\mathbf{r}_2,\mathbf{u}_2]\rho(\mathbf{r}_2,\mathbf{u}_2)\right] \\
&= \int D[\rho(\mathbf{r},\mathbf{u})]\delta[\rho(\mathbf{r},\mathbf{u})-\hat{\rho}(\mathbf{r},\mathbf{u})] \\
&\quad \times \exp\left[-a^2 d\int \mathrm{d}\mathbf{r}\mathrm{d}\mathbf{u}_1\mathrm{d}\mathbf{u}_2\rho(\mathbf{r},\mathbf{u}_1)|\mathbf{u}_1\times\mathbf{u}_2|\rho(\mathbf{r},\mathbf{u}_2)\right],
\end{aligned} \tag{2.55}$$

where the Eq. (2.49) is substituted in the last step. By using the integral representation of the delta function

$$\begin{aligned}
\delta[\rho(\mathbf{r},\mathbf{u})-\hat{\rho}(\mathbf{r},\mathbf{u})] &\equiv \int D[w(\mathbf{r},\mathbf{u})]\exp\left\{\int \mathrm{d}\mathbf{r}\mathrm{d}\mathbf{u}w(\mathbf{r},\mathbf{u})[\rho(\mathbf{r},\mathbf{u})-\hat{\rho}(\mathbf{r},\mathbf{u})]\right\} \\
&= \int D[w(\mathbf{r},\mathbf{u})]\exp\left\{\int \mathrm{d}\mathbf{r}\mathrm{d}\mathbf{u}w(\mathbf{r},\mathbf{u})\rho(\mathbf{r},\mathbf{u})\right. \\
&\qquad \left. -\sum_{i=1}^{N}\int_0^{\frac{L}{a}}\mathrm{d}s w(\mathbf{r}_i(s),\mathbf{u}_i(s))\right\}
\end{aligned} \tag{2.56}$$

where, $w(\mathbf{r},\mathbf{u})$ is a imaginary variable, the normalization constant is absorbed by D, and in the last step, Eq. (2.54) is used. Now we are ready to rewrite the partition function of Eq. (2.52),

$$\begin{aligned}
Z &= \frac{1}{N!}\int D[\rho(\mathbf{r},\mathbf{u})]D[w(\mathbf{r},\mathbf{u})]Q^N \exp\left[\int \mathrm{d}\mathbf{r}\mathrm{d}\mathbf{u}w(\mathbf{r},\mathbf{u})\rho(\mathbf{r},\mathbf{u})\right] \\
&\quad \times \exp\left[-a^2 d\int \mathrm{d}\mathbf{r}\mathrm{d}\mathbf{u}_1\mathrm{d}\mathbf{u}_2\rho(\mathbf{r},\mathbf{u}_1)|\mathbf{u}_1\times\mathbf{u}_2|\rho(\mathbf{r},\mathbf{u}_2)\right]
\end{aligned} \tag{2.57}$$

where,

$$Q = \int D[\mathbf{r}(s)]D[\mathbf{u}(s)]P[\mathbf{r}(s),\mathbf{u}(s)]\exp\left[-\int_0^{\frac{L}{a}} \mathrm{d}s w[\mathbf{r}(s),\mathbf{u}(s)]\right] \tag{2.58}$$

is the partition function of one wormlike polymer chain in the external field w (imaginary). The main step of the self-consistent field approach consists in performing a saddle-point approximation of the integral Eq. (2.57) with respect to $w(\mathbf{r},\mathbf{u})$ and $\rho(\mathbf{r},\mathbf{u})$. Note that the imaginary number used here is just for mathematical convenience. After the saddle point approximation, the external field w is real [8, 15, 16, 17, 18].

Comparing Eq. (2.57) with the definition of the partition function

$$Z \propto \int D[\rho]D[w]\exp\{-\beta F[\rho,w]\}, \tag{2.59}$$

we get the Helmholtz free energy

$$\begin{aligned}\beta F &= \ln\left(\frac{N!}{Q^N}\right) - \int \mathrm{d}\mathbf{r}\mathrm{d}\mathbf{u} w(\mathbf{r},\mathbf{u})\rho(\mathbf{r},\mathbf{u}) \\ &\quad + a^2 d\int \mathrm{d}\mathbf{r}\mathrm{d}\mathbf{u}_1\mathrm{d}\mathbf{u}_2\rho(\mathbf{r},\mathbf{u}_1)|\mathbf{u}_1\times\mathbf{u}_2|\rho(\mathbf{r},\mathbf{u}_2).\end{aligned} \tag{2.60}$$

The grand thermodynamical potential function Ω of the system can be obtained from the relation [19],

$$\Omega = F - G, \tag{2.61}$$

where,

$$G = \mu\int \mathrm{d}\mathbf{r}\mathrm{d}\mathbf{u}\rho(\mathbf{r},\mathbf{u}) = \mu\frac{NL}{a} \tag{2.62}$$

is the Gibbs free energy, μ the segmental free energy, and totally we have N chains, each of them having L/a effective Kuhn segments. Finally the grand potential is written as

$$\begin{aligned}\beta\Omega &= \ln\left(\frac{N!}{Q^N}\right) - \int \mathrm{d}\mathbf{r}\mathrm{d}\mathbf{u} w(\mathbf{r},\mathbf{u})\rho(\mathbf{r},\mathbf{u}) \\ &\quad + a^2 d\int \mathrm{d}\mathbf{r}\mathrm{d}\mathbf{u}_1\mathrm{d}\mathbf{u}_2\rho(\mathbf{r},\mathbf{u}_1)|\mathbf{u}_1\times\mathbf{u}_2|\rho(\mathbf{r},\mathbf{u}_2) - \beta\mu\int \mathrm{d}\mathbf{r}\mathrm{d}\mathbf{u}\rho(\mathbf{r},\mathbf{u}).\end{aligned} \tag{2.63}$$

Performing the saddle point approximation with respect to the mean field $w(\mathbf{r},\mathbf{u})$ and $\rho(\mathbf{r},\mathbf{u})$, respectively, we get mean field functions

$$w(\mathbf{r},\mathbf{u}) = 2a^2 d \int \mathrm{d}\mathbf{u}_1 |\mathbf{u}\times\mathbf{u}_1| \rho(\mathbf{r},\mathbf{u}_1) - \beta\mu, \tag{2.64}$$

and

$$\rho(\mathbf{r},\mathbf{u}) = -\frac{N}{Q}\frac{\delta Q}{\delta w(\mathbf{r},\mathbf{u})}. \tag{2.65}$$

In order to solve these equations, we need to express $Q(w)$ in terms of the partial chain distribution function. Considering a partial polymer chain with length t, the end segment locating at point of $\mathbf{r}$, and pointing in the direction of $\mathbf{u}$, the distribution function is defined by

$$\begin{aligned}
q(\mathbf{r},\mathbf{u},t) &= \int_{\mathbf{r}(0)}^{\mathbf{r}(t)=\mathbf{r}} D[\mathbf{r}(s)] \int_{\mathbf{u}(0)}^{\mathbf{u}(t)=\mathbf{u}} D[\mathbf{u}(s)] \exp\left[-\frac{1}{4}\int_0^t [\dot{\mathbf{u}}(s)]^2 \mathrm{d}s\right] \\
&\quad \times \exp\left[-\int_0^t \mathrm{d}s w[\mathbf{r}(s),\mathbf{u}(s)]\right] \prod_{s=0}^{t} \delta\left[\mathbf{r}(s) - \mathbf{r}(0) - \int_0^s \mathrm{d}s'\mathbf{u}(s')\right] \qquad (2.66a) \\
&= \int_{\mathbf{u}(0)}^{\mathbf{u}(t)=\mathbf{u}} D[\mathbf{u}(s)] \exp\left[-\frac{1}{4}\int_0^t [\dot{\mathbf{u}}(s)]^2 \mathrm{d}s\right] \\
&\quad \times \exp\left[-\int_0^t \mathrm{d}s w\left\{\mathbf{r}(s) = \mathbf{r}(0) + \int_0^s \mathrm{d}s'\mathbf{u}(s'), \mathbf{u}(s)\right\}\right] \\
&\quad \times \delta\left[\mathbf{r}(t) - \mathbf{r}(0) - \int_0^t \mathrm{d}s\mathbf{u}(s)\right]\Big|_{\mathbf{r}(t)=\mathbf{r}} \qquad (2.66b) \\
&= \int \frac{\mathrm{d}\mathbf{k}}{(2\pi)^3} \exp\left\{-i\mathbf{k}\cdot[\mathbf{r}(t)-\mathbf{r}(0)]|_{\mathbf{r}(t)=\mathbf{r}}\right\} \chi(\mathbf{k},\mathbf{u},t), \qquad (2.66c)
\end{aligned}$$

where, in Eq. (2.66b), the functional integral over $\mathbf{r}(s)$ is carried out because of the delta functions; because the point t is restricted, the delta function at point t survives; $\mathbf{r}(s)$ now is the function of $\mathbf{u}$ and will not be affected by the Fourier transform, and

$$\begin{aligned}
\chi(\mathbf{k},\mathbf{u},t) &= \int_{\mathbf{u}(0)}^{\mathbf{u}(t)=\mathbf{u}} D[\mathbf{u}(s)] \\
&\quad \times \exp\left\{-\int_0^t \mathrm{d}s \left([\dot{\mathbf{u}}(s)]^2 + w[\mathbf{r}(s),\mathbf{u}(s)] - i\mathbf{k}\cdot\mathbf{u}(s)\right)\right\}, \qquad (2.67)
\end{aligned}$$

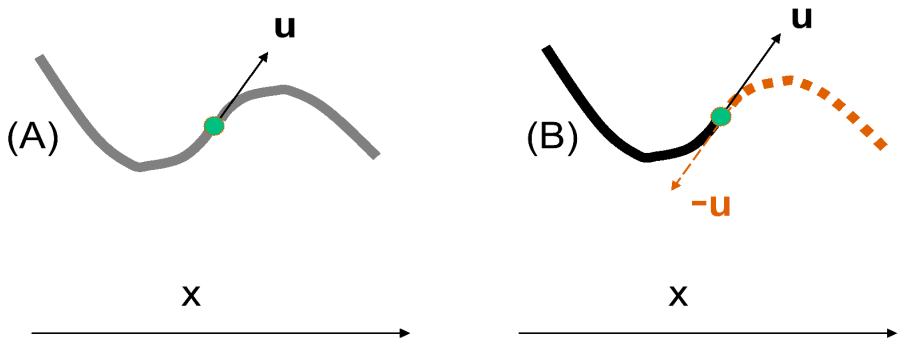

Figure 2.4: Physical meaning of the connection condition in Eqs. 2.71 and 2.72. The density distribution function for an internal segment (circle) to locate at x with a tangent vector pointing in $\mathbf{u}$ [see (A)] is the product of the distribution function for a terminal segment to locate at x with a tangent vector pointing in $\mathbf{u}$ [see solid line in (B)] and that for a terminal segment to locate at x with tangent vector pointing in $-\mathbf{u}$ [see dashed line in (B)].

which can be shown to obey the diffusion equation [15],

$$\frac{\partial \chi(\mathbf{k},\mathbf{u},t)}{\partial t} = [\nabla^2_{\mathbf{u}} + ia\mathbf{k}\cdot\mathbf{u} - w(\mathbf{r},\mathbf{u})]\chi(\mathbf{k},\mathbf{u},t). \tag{2.68}$$

Going back to the $\mathbf{r}$ space, diffusion equation for the q function is

$$\frac{\partial q(\mathbf{r},\mathbf{u},t)}{\partial t} = \left[\nabla^2_{\mathbf{u}} - a\mathbf{u}\cdot\nabla_{\mathbf{r}} - w(\mathbf{r},\mathbf{u})\right] q(\mathbf{r},\mathbf{u},t). \tag{2.69}$$

If we also reduce the spatial coordinates in the effective Kuhn length a, this equation can be rewritten as

$$\frac{\partial q(\mathbf{r},\mathbf{u},t)}{\partial t} = \left[\nabla^2_{\mathbf{u}} - \mathbf{u}\cdot\nabla_{\mathbf{r}} - w(\mathbf{r},\mathbf{u})\right] q(\mathbf{r},\mathbf{u},t) \tag{2.70}$$

Now we can rewrite the partition function Q

$$Q = \int \mathrm{d}\mathbf{r}\mathrm{d}\mathbf{u} q(\mathbf{r},\mathbf{u},t) q(\mathbf{r},-\mathbf{u},L/a-t) \tag{2.71}$$

where, the physical meaning of the product of the two q functions is that, two polymer portions with the terminal ends located at $\mathbf{r}$ are required to form a non-terminal segment at $\mathbf{r}$, and one terminal point in the direction $\mathbf{u}$, while the other

should point in the opposite direction $-\mathbf{u}$ (shown in Fig. (2.4)). Then, the density function

$$\rho(\mathbf{r},\mathbf{u}) = \frac{N}{Q}\int_0^{L/a} \mathrm{d}t q(\mathbf{r},\mathbf{u},t)q(\mathbf{r},-\mathbf{u},L/a-t). \tag{2.72}$$

From Eq. (2.66a), we can find the initial condition for the diffusion Eq. (2.69) is

$$q(\mathbf{r},\mathbf{u},0) = 1. \tag{2.73}$$

Equations (2.64) to (2.73) form a complete set of self-consistent equations for any rigidity of wormlike polymer, which can be solved numerically. First we give an initial guess of the mean field $w(\mathbf{r},\mathbf{u})$, then use the above equations, we can get one field $w'(\mathbf{r},\mathbf{u})$, compare the difference and correct initial guess. Finally we can get the self-consistent result. The rigidity is related to the ratio of the total length L and the effective Kuhn length a.

Chapter 3

Isotropic nematic interface of the wormlike polymers

The isotropic nematic interface has been the focus of theoretical [20, 21, 22, 23, 24, 25, 26, 27] and experimental study [28, 29, 30, 31] for many decades, for fundamental importance and industrial applications. One important thing is to estimate the interface tension at the boundary between the isotropic phase and the nematic phase of polymer chains. Going back to early studies, due to the difficulty of solving the interfacial problem, Holyst and Poniewierski [20] assumed a step function for the total density of the interface and found rod-like polymers have lowest interface tension at a tilt angle of 60 degree between the interface and the nematic director. While Doi and Kuzuu [22], Moore and McMullen [21] applied a wider interface and found that rod-like polymers favor a tilt angle of 90°. Chen (and his coworkers) solved the problem numerically without those assumption of the interface of both rod-like polymers [23] and flexible polymers [24], and found that for both cases, polymers prefer to be parallel to the interface. However, Shundyak and Roij [27] pointed that the accuracy of Chen's work in [23] needs to be improved and 15% lower tension was found, while Koch and Harlen [26] argued that the tension is about 50% higher and the equilibrium profiles are non-monotonic. On the experiment side, another Chen and coworkers studied the interface tensions between isotropic and anisotropic phases of solutions of the polymers poly(n-hexyl isocyanate) [28, 29],

schizophyllan [30] and cellulose crystallites [31]. They found the measured values are in the range predicted by the theoretical work. However, due to the difficulty of numerical simulations for semiflexible polymer chains, most numerical simulations were focused on the two limits of the model, one is the flexible limit, where the contour length L is much larger than the effective Kuhn length a of polymers, the other is the rigid rods limit, where $L \ll a$.

To study the properties of finite flexibility of polymers is the main interest of this chapter. In the following, we will study the two limits first to compare with the results reported by forerunners and clarify the uncertainties, then the interface of semiflexible polymers.

3.1 Isotropic nematic interface

In order to solve the problem of the isotropic-nematic interface numerically, we need to expand the completed set of the self-consistent equations Eq. (2.64) to Eq. (2.73) by the spherical-harmonic series,

$$w(\mathbf{r},\mathbf{u}) = \sum_{l,m} w_{l,m}(\mathbf{r}) Y_{l,m}(\mathbf{u}), \quad \text{where} \quad \sum_{l,m} \equiv \sum_{l=0}^{\infty} \sum_{m=-l}^{l}, \tag{3.1}$$

$$\rho(\mathbf{r},\mathbf{u}) = \frac{1}{a^2 d} \sum_{l,m} \rho_{l,m}(\mathbf{r}) Y_{l,m}(\mathbf{u}), \tag{3.2}$$

and

$$q(\mathbf{r},\mathbf{u},t) = \frac{1}{\sqrt{a^2 d}} \sum_{l,m} q_{l,m}(\mathbf{r},t) Y_{l,m}(\mathbf{u}), \tag{3.3}$$

where, Y is the spherical-harmonic series, having the form

$$Y_{l,m}(\mathbf{u}) = Y_{l,m}(\theta,\varphi) = \sqrt{\frac{2l+1}{4\pi}\frac{(l-m)!}{(l+m)!}} P_{l,m}(\cos\theta) e^{im\varphi}, \tag{3.4}$$

where $P_{l,m}(\cos\theta)$ is the associated Legendre polynomial, and the coefficient leads to the normalization condition

$$\int \mathrm{d}\mathbf{u} Y^*_{l,m}(\mathbf{u}) Y_{l_1,m_1}(\mathbf{u}) = \delta_{l,l_1}\delta_{m,m_1}. \tag{3.5}$$

Since functions w, ρ and q are all real functions, the expansion coefficients must have the following properties,

$$w_{l,m}(\mathbf{r}) = w^*_{l,-m}(\mathbf{r})(-1)^m, \tag{3.6}$$

$$\rho_{l,m}(\mathbf{r}) = \rho^*_{l,-m}(\mathbf{r})(-1)^m, \tag{3.7}$$

and

$$q_{l,m}(\mathbf{r},t) = q^*_{l,-m}(\mathbf{r},t)(-1)^m. \tag{3.8}$$

By using the addition theorem of spherical harmonics, we expand the excluded volume interaction kernel $|\mathbf{u}_1 \times \mathbf{u}_2|$ in spherical-harmonic series [32],

$$|\mathbf{u}_1 \times \mathbf{u}_2| = \sum_{l,m} \frac{4\pi}{2l+1} d_l Y_{l,m}(\mathbf{u_1}) Y^*_{l,m}(\mathbf{u}_2) \tag{3.9}$$

where

$$d_0 = \frac{\pi}{4} \tag{3.10a}$$

$$d_l = 0 \qquad l \text{ odd} \tag{3.10b}$$

$$d_l = -\frac{\pi(2l+1)l!(l-2)!}{2^{2l+1}(\frac{l}{2}-1)!(\frac{l}{2})!(\frac{l}{2})!(\frac{l}{2}+1)!} \qquad l \text{ even.} \tag{3.10c}$$

The partition function Q now is

$$Q = \int \mathrm{d}\mathbf{r} \sum_{l,m} q_{l,m}(\mathbf{r},t) q_{l,m}(\mathbf{r}, L/a - t). \tag{3.11}$$

Rewriting the mean field equations Eq. (2.64) and Eq. (2.72) by the spherical-harmonics series, and multiply both sides of the equations by $Y^*_{l,m}(\mathbf{u})$ and integral over $\mathbf{u}$, then we get

$$w_{l,m}(\mathbf{r}) = \frac{8\pi}{2l+1} d_l \rho_{l,m}(\mathbf{r}) - \sqrt{(4\pi)}\beta\mu, \tag{3.12}$$

and

$$\rho_{l,m}(\mathbf{r}) = \frac{N}{Q} \int_0^{L/a} \mathrm{d}t \sum_{l_1,m_1} \sum_{l_2,m_2} q_{l_1,m_1}(\mathbf{r},t) q_{l_2,m_2}(\mathbf{r}, L/a - t) I_{l_1,m_1,l_2,m_2,l_3,-m_3} (-1)^{m_3}, \tag{3.13}$$

where the constant

$$\begin{aligned} I_{l_1,m_1,l_2,m_2,l_3,m_3} &= \int \mathrm{d}\mathbf{u} Y_{l_1,m_1}(\mathbf{u}) Y_{l_2,m_2}(\mathbf{u}) Y_{l_3,m_3}(\mathbf{u}) \\ &= \int \mathrm{d}\mathbf{u} Y_{l_1,m_1}(\mathbf{u}) Y_{l_2,m_2}(\mathbf{u}) Y^*_{l_3,-m_3}(\mathbf{u}) (-1)^{m_3} \\ &= (-1)^{m_3} \left[\frac{(2l_1+1)(2l_2+1)}{4\pi(2l_3+1)} \right]^{1/2} \times C(l_1,l_2,l_3;0,0,0) \\ &\quad \times C(l_1,l_2,l_3;m_1,m_2,-m_3), \end{aligned} \tag{3.14}$$

where, $C(l_1,l_2,l_3;m_1,m_2,m_3)$ is the Clebsch-Gordan coefficient. Note that by this definition, the constant I is invariant in exchanging its coefficient pairs (l_i,m_i).

For the diffusion-like equation (2.69), special attention should be paid to the term $\mathbf{u}\cdot\nabla_{\mathbf{r}}$. There exist two sets of coordinates in the system: one is the spatial coordinate $(\mathbf{r})\equiv(x,y,z)$, the other is the polar coordinate $\mathbf{u}\equiv(u_x,u_y,u_z)$. In the general case, these two sets coordinates do not have a particular relation. Note that $\mathbf{u}$ is also a unit vector, so $\mathbf{u}=\sin\theta\cos\varphi\hat{u}_x+\sin\theta\sin\varphi\hat{u}_y+\cos\theta\hat{u}_z$, where $\hat{u}_x,\hat{u}_y,\hat{u}_z$ are unit vector along three axes in the polar coordinate, θ and φ the polar angles. The diffusion like equation (2.70) is

$$\begin{aligned} &\frac{\partial}{\partial t} q_{l,m}(\mathbf{r},t) = -l(l+1) q_{l,m}(\mathbf{r},t) \\ &-(-1)^m \sqrt{\frac{4\pi}{3}} \sum_{l_1,m_1} \begin{pmatrix} \frac{1}{\sqrt{2}}[I_{1,-1,l_1,m_1,l,-m} - I_{1,1,l_1,m_1,l,-m}]\hat{u}_x \\ \frac{i}{\sqrt{2}}[I_{1,-1,l_1,m_1,l,-m} + I_{1,1,l_1,m_1,l,-m}]\hat{u}_y \\ I_{1,0,l_1,m_1,l,-m}\hat{u}_z \end{pmatrix} \cdot \begin{pmatrix} \frac{\partial}{\partial x}\hat{x} \\ \frac{\partial}{\partial y}\hat{y} \\ \frac{\partial}{\partial z}\hat{z} \end{pmatrix} q_{l_1,m_1}(\mathbf{r},t) \\ &\qquad - \sum_{l_1,m_1} \sum_{l_2,m_2} w_{l_1,m_1}(\mathbf{r}) q_{l_2,m_2}(\mathbf{r},t) I_{l_2,m_2,l_1,m_1,l,-m,} (-1)^m \end{aligned} \tag{3.15}$$

with the initial conditions

$$q_{0,0}(\mathbf{r},0) = \sqrt{4\pi}. \tag{3.16}$$

The simple case of Isotropic-Nematic interface problems is that densities vary only in one spatial dimension, say the x axis. Then we can specify the relation between the two sets of the coordinates. Since the y,z axes are translational invariant, they form a plane paralleling to the interface if there exists, so we can choose the $x-z$ plane, in which the nematic director lies, i.e., u_z lies in the $x-z$ plane, as

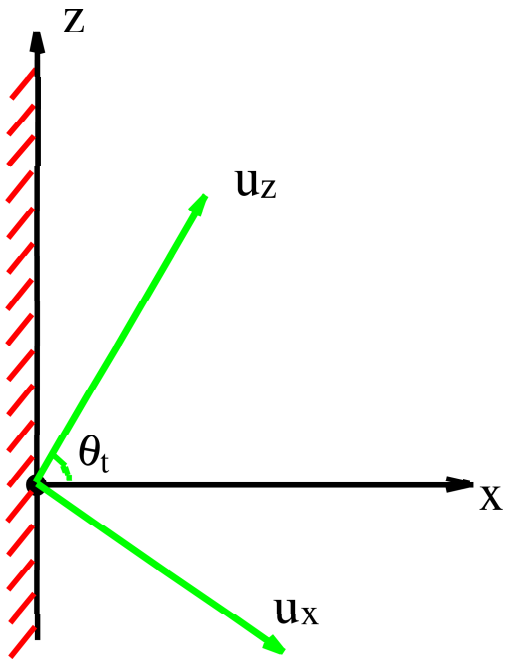

Figure 3.1: Definition of the coordinate system. The x axis is along the normal of the interface. The spherical polar coordinates for describing $\mathbf{u}$ are defined in the u-coordinate frame, while the bulk nematic director is along the u_z axis, y axis parallels to u_y axis.

shown in Fig. 3.1. The angle θ_t formed by x axis and u_z axis is called the tilt angle. For this one dimensional case, all the variables in terms of $\mathbf{r}$ in the self-consistent equations are now in terms of x, i.e.,

$$\begin{aligned} w(\mathbf{r},\mathbf{u}) &\rightarrow w(x,\mathbf{u}), & w_{l,m}(\mathbf{r}) &\rightarrow w_{l,m}(x), \\ \rho(\mathbf{r},\mathbf{u}) &\rightarrow \rho(x,\mathbf{u}), & \rho_{l,m}(\mathbf{r}) &\rightarrow \rho_{l,m}(x), \\ q(\mathbf{r},\mathbf{u},t) &\rightarrow q(x,\mathbf{u},t), & q_{l,m}(\mathbf{r},t) &\rightarrow q_{l,m}(x,t), \\ \int \mathrm{d}\mathbf{r} &\rightarrow A\int \mathrm{d}x, \end{aligned} \tag{3.17}$$

where A is the area of the interface. After adopting the one dimensional coordinate system, the dotted term in Eq. (3.15) can be simplified and the equation finally

can be rewritten as

$$\begin{aligned}\frac{\partial}{\partial t}q_{l,m}(x,t) &= -l(l+1)q_{l,m}(x,t) - (-1)^m\sqrt{\frac{4\pi}{3}}\sum_{l_1,m_1}\frac{\partial q_{l_1,m_1}(x,t)}{\partial x} \\ &\quad\times\left\{\sin\theta_t\frac{I_{1,-1,l_1,m_1,l,-m} - I_{1,1,l_1,m_1,l,-m}}{\sqrt{2}} + \cos\theta_t I_{1,0,l_1,m_1,l,-m}\right\} \\ &\quad - \sum_{l_1,m_1}\sum_{l_2,m_2} w_{l_1,m_1}(x)q_{l_2,m_2}(x,t)I_{l_2,m_2,l_1,m_1,l,-m,}(-1)^m. \qquad (3.18)\end{aligned}$$

Adopting the coordinate system shown in Fig. 3.1, for any fixed tilt angle θ_t, $q(x,\mathbf{u},t)$ has the following symmetry properties:

$$q(x,\mathbf{u},t) = q^*(x,\mathbf{u},t) = q(x,\mathbf{u}_y,t), \qquad (3.19)$$

where $\mathbf{u}_y = (\theta,-\varphi)$ is the mirror image of $\mathbf{u} = (\theta,\varphi)$ when the $\mathbf{u}_y = 0$ plane is considered to be the reflection mirror. Hence the coefficient $q_{l,m}(x,t)$ has these properties:

$$q_{l,m}(x,t) = q^*_{l,m}(x,t) = (-1)^m q_{l,-m}(x,t). \qquad (3.20)$$

By using these symmetry properties, we can reduce the number of independent variables in the actual calculation.

The numerical calculation is as the following: for wormlike chains, we can divide them into a large number $\aleph$ of divisions, each division having a tiny length $\Delta t = L/a/\aleph = n/\aleph \ll 1$, i.e., $\aleph$ is much larger than the effective Kuhn segments number n; the space is also divided into a certain number of slots, basically more points were assigned to the interface region where our interests are; with the initial condition of Eq. (3.16), and proper guess values of the mean field $w_{l,m}(x)$, Equation (3.18) can be evaluated for all q variables, from which we can get Q, ρ, and w, which can be used for the next iteration. In the updating the iteration, the Crank-Nicholson algorithm is implemented. The step stops after enough iterations, and all the variables converge to the final values. In the calculation, we use the assumption that the tilt angle is fixed across interface region.

The approach mentioned above is ready to study all cases from rigid rod-like polymers to flexible polymers, because the flexibility is only related to the ratio of the total contour length L to the effective Kuhn length a, and the value of the ratio

L/a is the only difference among those cases. Define a variable to characterize the flexibility of polymers is necessary

$$\alpha \equiv \frac{L}{a}. \tag{3.21}$$

For the case of $\alpha \ll 1$, the effective Kuhn length is very long compared to the contour length, the polymer looks like a rigid rod, and the upper integral limit $\alpha = L/a$ is very small. In the opposite case, $\alpha \gg 1$, the effective Kuhn length is very short compared to the contour length, the polymer looks like a coil and the upper integral limit $\alpha = L/a$ is very large.

The diffusion equation (3.18) is quite general. The density function Eq. (3.13) is strongly related to the value of the upper integral limit α. The diffusion equation "allows the particles diffuse at a certain speed". The upper limit α is the "time" for particles to diffuse. If "time" is short, the particles can not reach any other position, i.e., the effects can not be transmitted. For a rigid rod case, the "time" is very short, and variables are almost independent on $\mathbf{u}$, "stay" around the initial values, which means the term ∇^2_{u} contributes little to the results. If "time" is very long, the particles can reach any point, the effects can be transmitted. With "time" enough long, an "equilibrium state" is reached and will not change any more with more "time". It means that in the case of $\alpha \gg 1$, the term $\frac{\partial}{\partial t} q_{l,m}(x,t)$ contributes little to the results. This is the flexible limit of polymers. Much work has been contributed to these two limit cases by neglecting either ∇^2_u or $\frac{\partial}{\partial t} q_{l,m}(x,t)$ to study the system of rigid rod-like polymers or flexible polymers, respectively.

In our calculation, we included all these terms, and investigated the cases with different flexibilities. In the following, we discuss the properties of the phase coexistence for different α.

3.2 Interface of the flexible cases: $\alpha = 10$

In practice, we truncate the expansion in Eqs. (3.1-3.3) after the $l = 10$ term. For $\alpha = 10$, we divide the contour length L/a into $\aleph = 5000$, and for the spatial discretization, because we are interested in the interface region, more points should

be assigned to that region. For the system, we should have such boundaries: far apart from the interface region, we should recover the bulk phases, i.e., $x = -\infty$, where we have the isotropic phase, and $x = \infty$, where we have the nematic phase. So we redefine a spatial variable ξ by

$$\xi = \tanh\left(\frac{x\sqrt{1+(1/\alpha)^2}}{2}\right). \tag{3.22}$$

By this definition, we put most of the points into the region which is about $5 \sim 10$ times of the interfacial width, for polymers from the flexible limit to the rigid rod limit. For rigid rod limit, this equation is rewritten in term of L rather than a, as Eq. (3.45). The interval $x = (-\infty, \infty)$ now becomes $\xi = (-1, 1)$, which is equally divided into $N_\xi = 160$ piece, each having $\Delta\xi = 0.0125$. The differential term in the diffusion equation (3.18) is written as $\partial q_{l,m}/\partial x = [(1-\xi^2)\sqrt{1+(1/\alpha)^2}/2]\partial q_{l,m}/\partial\xi$. The derivative of $q_{l,m}(x,t)$ with respect to ξ is approximated by using a finite difference scheme.

One of the difficulties is that we need the fixed-point iteration scheme to update the variables $w_{l,m}(x)$ in Eq. (3.12), i.e.,

$$w_{l,m}^{i+1}(x) = w_{l,m}^{i}(x)(1-c) + c\left\{\frac{8\pi}{2l+1} d_l \rho_{l,m}(x) - \sqrt{(4\pi)}\beta\mu\right\}^i, \tag{3.23}$$

where, the superscript i, and $i+1$ are the ith and $(i+1)$th iteration, respectively, c the fixed-point step. In order to make the iteration converge, c is quite small practically. In the case of $\alpha = 10$, $c = 0.001$ is used, which make the updating of w quite inefficient and the running time of the program as long as weeks for a simple test.

We adopt the definition of the orientational order which is characterized by the statistical average of the tensor $\frac{1}{2}(3\mathbf{uu} - \mathbf{I})$ [24],

$$\begin{aligned}\mathcal{S}(x) &= \frac{\int \mathrm{d}\mathbf{u}\frac{1}{2}(3\mathbf{uu}-\mathbf{I})\rho(x,\mathbf{u})}{\int \mathrm{d}\mathbf{u}\rho(x,\mathbf{u})} \\ &= \frac{1}{2\sqrt{5}\rho_{0,0}(x)}\begin{pmatrix} \sqrt{6}\rho_{2,2}(x) - \rho_{2,0}(x) & 0 & \sqrt{6}\rho_{2,1}(x) \\ 0 & -\sqrt{6}\rho_{2,2}(x) - \rho_{2,0}(x) & 0 \\ \sqrt{6}\rho_{2,1}(x) & 0 & 2\rho_{2,0}(x) \end{pmatrix}\end{aligned} \tag{3.24}$$

After diagonalizing the matrix, we get the principle order parameter $S(x)$,

$$S(x) = \frac{1}{4\sqrt{5}\rho_{0,0}(x)}\Big\{\rho_{2,0}(x)+\sqrt{6}\rho_{2,2}(x) + \Big[9\rho_{2,0}^2(x)+6\rho_{2,2}^2(x)+24\rho_{2,1}^2(x)-6\sqrt{6}\rho_{2,0}(x)\rho_{2,2}(x)\Big]^{\frac{1}{2}}\Big\}. \quad (3.25)$$

Integrating $\rho(x,\mathbf{u})$ over the spherical polar variables, we find the spatial variation for the number density

$$C(x) = a^2 d\int \mathrm{d}\mathbf{u}\rho(x,\mathbf{u}) = (4\pi)^{1/2}\rho_{0,0}(x). \quad (3.26)$$

Figure 3.2 shows us the density profile for different tilt angles $\theta_t = 0$, $\frac{\pi}{12}$, $\frac{\pi}{6}$, $\frac{\pi}{4}$, $\frac{\pi}{3}$, $\frac{5\pi}{12}$ and $\frac{\pi}{2}$, respectively.

One important task is to find the interface tension of the system. First we look at the bulk phase to get the pressure of the system. For the bulk phase, functions are independent of the spatial coordinate,

$$q(x,\mathbf{u},t) = q(\mathbf{u},t), \quad (3.27)$$
$$w(x,\mathbf{u}) = w(\mathbf{u}), \quad (3.28)$$
$$\int \mathrm{d}\mathbf{r} = V_0, \quad (3.29)$$

and

$$Q = V_0\int \mathrm{d}\mathbf{u}q(\mathbf{u},t)q(-\mathbf{u},L/a-t) = V_0Q', \quad (3.30)$$
$$\rho(\mathbf{u}) = \frac{N}{Q}\int_0^{L/a}\mathrm{d}tq(\mathbf{u},t)q(-\mathbf{u},L/a-t) = \frac{N}{V_0Q'}\rho'(\mathbf{u}), \quad (3.31)$$

where, Q' and ρ' are independent of the volume. Hence, the grand potential of the system (Eq. (2.63)) is

$$\beta\Omega = \ln\left(\frac{N!}{(V_0Q')^N}\right) - \frac{N}{Q'}\int \mathrm{d}\mathbf{u}w(\mathbf{u})\rho'(\mathbf{u}) + \frac{a^2dN^2}{V_0Q'^2}\int \mathrm{d}\mathbf{u}_1\mathrm{d}\mathbf{u}_2\rho'(\mathbf{u}_1)|\mathbf{u}_1\times\mathbf{u}_2|\rho'(\mathbf{u}_2) - \frac{\beta\mu N}{Q'}\int \mathrm{d}\mathbf{u}\rho'(\mathbf{u}). \quad (3.32)$$

The pressure can be found by

$$\begin{aligned}\beta p &= -\left(\frac{\beta\partial\Omega}{\partial V_0}\right)_{N,T} \\ &= \frac{N}{V_0}+\frac{a^2dN^2}{V_0^2Q'^2}\int \mathrm{d}\mathbf{u}_1\mathrm{d}\mathbf{u}_2\rho'(\mathbf{u}_1)|\mathbf{u}_1\times\mathbf{u}_2|\rho'(\mathbf{u}_2) \\ &= \frac{a}{L}\int \mathrm{d}\mathbf{u}\rho(\mathbf{u})+a^2d\int \mathrm{d}\mathbf{u}_1\mathrm{d}\mathbf{u}_2\rho(\mathbf{u}_1)|\mathbf{u}_1\times\mathbf{u}_2|\rho(\mathbf{u}_2), \qquad (3.33)\end{aligned}$$

where, for convenience, the grand potential is used in the definition of the pressure because the Gibbs free energy has no contribution. In the last step, Eqs. (3.30) and (3.31) were used. The main point here is just to avoid the extensive variables N, V_0, and to use the intensive variables ρ.

For the bulk phase, the grand thermodynamical potential at equilibrium $\beta\Omega_e^I = -\beta pV_0 = -V_0[\frac{a}{L}\int \mathrm{d}\mathbf{u}\rho(\mathbf{u})+a^2d\int \mathrm{d}\mathbf{u}_1\mathrm{d}\mathbf{u}_2\rho(\mathbf{u}_1)|\mathbf{u}_1\times\mathbf{u}_2|\rho(\mathbf{u}_2)]$. In the presence of an interface, the contribution from different area to the grand thermodynamical potential is different, while the pressure should keep constant crossing the interface and equals to that of the bulk phase. Then we get $\beta\Omega_e = -A\int \mathrm{d}x[\frac{a}{L}\int \mathrm{d}\mathbf{u}\rho(x,\mathbf{u})+a^2d\int \mathrm{d}\mathbf{u}_1\mathrm{d}\mathbf{u}_2\rho(x,\mathbf{u}_1)|\mathbf{u}_1\times\mathbf{u}_2|\rho(x,\mathbf{u}_2)] = -\beta pV_0+\beta\sigma A$, where $\beta\sigma$ is the interface tension, and A the area of the interface. So the interface tension of the system,

$$\beta\sigma = \frac{1}{A}\left[\beta\Omega_e - \beta\Omega_e^I\right] = \int_{-\infty}^{+\infty}\mathrm{d}x\beta\Theta(x), \qquad (3.34)$$

where,

$$\beta\Theta(x) = \frac{4\pi}{ad}\left[\frac{\rho_{0,0}^I-\rho_{0,0}(x)}{\alpha\sqrt{4\pi}}+d_0(\rho_{0,0}^I)^2-\sum_{l,m}\frac{d_l}{2l+1}\rho_{l,m}^2(x)\right], \qquad (3.35)$$

is called the tension contribution, where $\alpha = L/a$ is the flexibility of polymers. Note that the first term in Eq. (3.35) is inverse proportional to α, so in the flexible limit, α is very large, such that this term vanishes [24]. However, in the opposite limit, $\alpha = 0$, this term does not make the interface tension infinite because in that case, the width of the interface is quite small in term of the effective Kuhn length, which tends to be infinity. More discussion will be made in next section for the rigid rod limit.

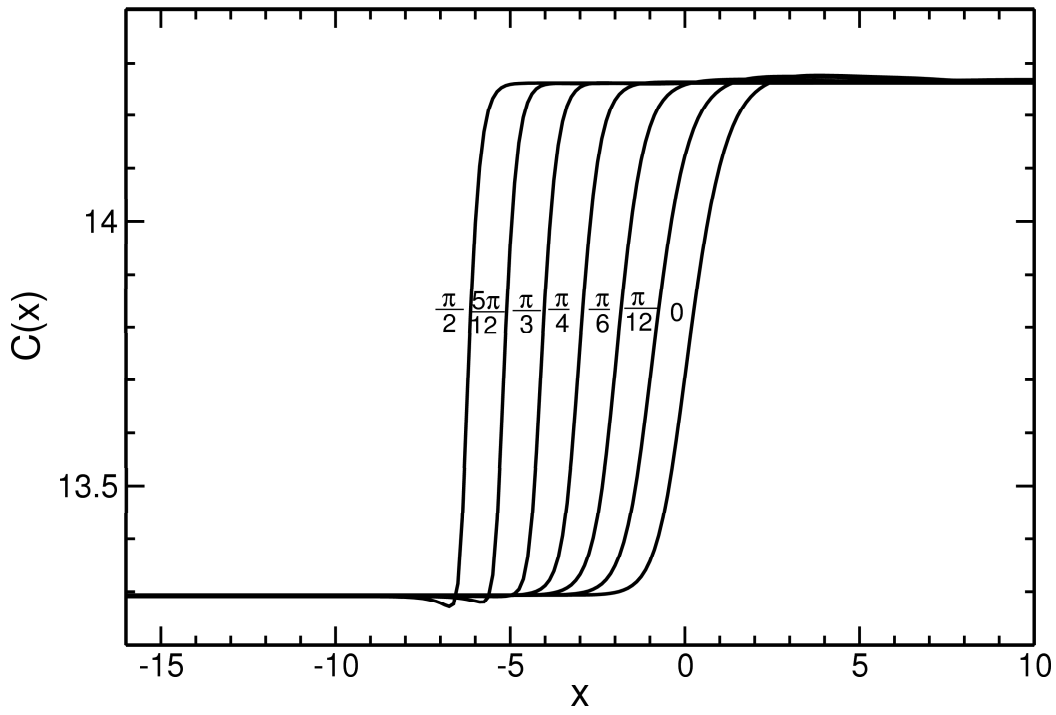

Figure 3.2: Density profile $C(x)$ at the IN interface for $\alpha = 10$. The centers of the profiles are shifted by a in order to display them clearly for different title angles, which are indicated in the figure.

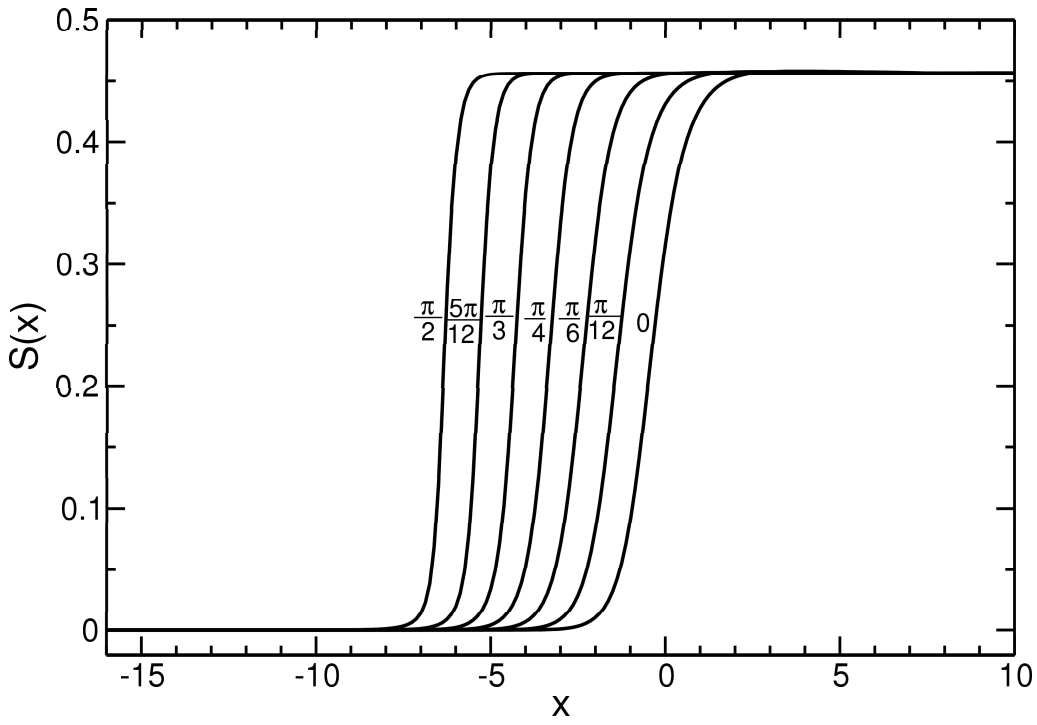

Figure 3.3: Order profile $S(x)$ at the IN interface for $\alpha = 10$. The centers also shifted by a. The tilt angles are indicated in the figure.

The profiles of the density $C(x)$, the order parameter $S(x)$, the tension contribution $\Theta(x)$ are calculated for different values of the tilt angles and are plotted as functions of x in Fig. 3.2, 3.3 and 3.4. Note that the coordinate x is reduced by a and is dimensionless here. In the calculation, the tilt angles are assumed to be fixed across the interface. In order to display clearly all profiles of different tilt angles in one plot, the center of each of the density profile and the order parameter profile is consecutively shifted by a from the previous one for each given tilt angle θ_t .

From Fig. 3.2, we see the interface width of the density profile is roughly $4a$. The interface width is getting narrower with the increase of θ_t, and the narrowest one is at $\theta_t = \pi/2$, about $2a$. The density at the two side of the interface are $C_i = 13.28$ and $C_n = 14.27$, which agree with those obtained from the bulk phase density [33] for the case of $\alpha = 10$. But these numbers are different from those obtained from the flexible limit [24], which are $C_i = 13.046$ and $C_n = 14.029$. The reason is that the case for $\alpha = 10$ is not the flexible limit. In principle, we can calculate the case for any α, no matter how large its value is to approach the flexible limit. But, in practice, we need to use the fixed point iteration (Eq. (3.23)), and the step c is getting smaller with α getting bigger, which makes the efficiency of updating $w_{l,m}(x)$ to decay rapidly. The empirical formula for the relation between them is $c \sim 0.01/(\alpha + 0.1)$. However, from figures (order parameter in figure 3, number density difference in figure 4, etc.) in reference [33] compared with Khokhlov and Semenov's work [7], we can see that after $\alpha > 10$, the lines almost flat, which means $\alpha = 10$ is big enough to study the interface properties of the flexible polymers.

Figure 3.3 shows the order parameter profile. The value of the nematic phase is $S_n = 0.456$, which, similar with the density profile, agrees with that of the bulk phase and is different from that in the flexible limit, which is $S_n = 0.4618$. The width of the order parameter for $\theta_t = 0$ is about $4a$, while that for $\theta_t = \pi/2$ is about $2a$, which is very similar with the width of density profile.

Figure 3.4 shows the tension contribution profiles, and the interface tension σ is plotted in Fig. 3.5 for different tilt angles. We see that different area has different contributions to the interface tension. On both sides far away from the interface, there is no contribution to the tension. The contribution ranges (profile widths) have similar features with those of the order parameter profiles, around

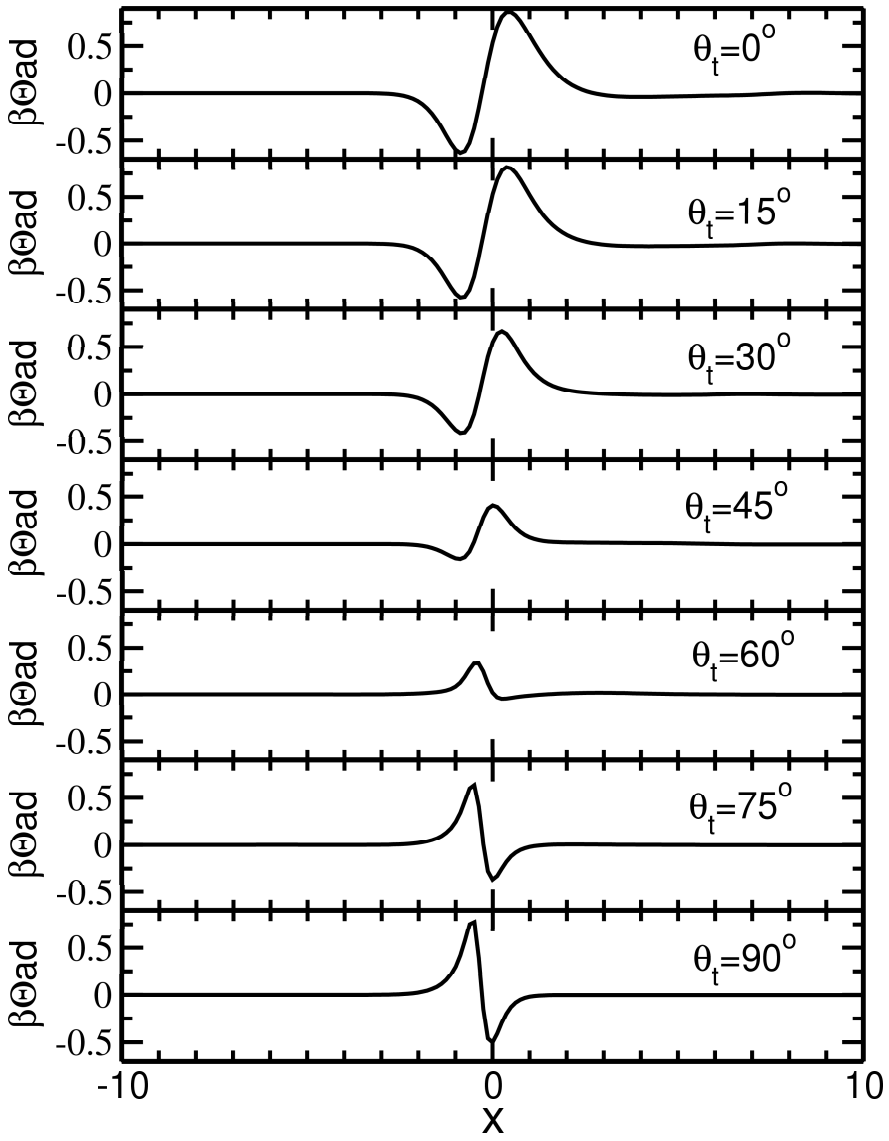

Figure 3.4: Tension contribution profile $\Theta(x)$ at the IN interface for $\alpha = 10$. From the top to the bottom, the tilt angles are 0, 15, 30, 45, 60, 75 and 90, respectively.

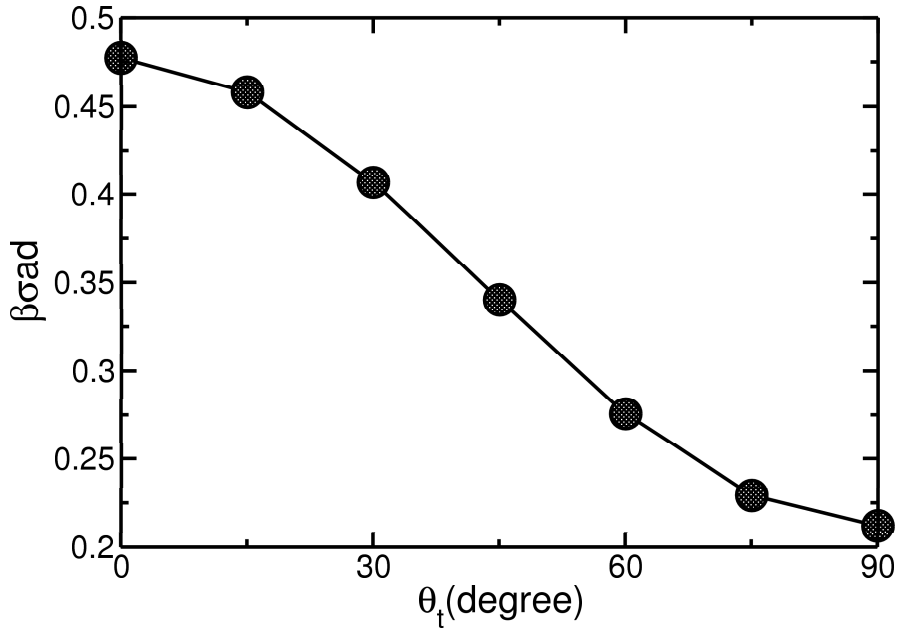

Figure 3.5: The interface tension σ as a function of the tilt angles θ_t for $\alpha = 10$.

$4a$ for $\theta_t = 0$ and decreases to $2a$ for $\theta_t = \pi/2$. The interesting thing is that, in the contribution range, for different tilt angles, the profiles have different shapes. For small tilt angles, $\theta_t \leq \pi/4$, the profile decreases first from the isotropic side (left side), then increases sharply and decreases again (up-down-up) until reaching the nematic side, i.e., on the isotropic side, the net contribution to the tension is negative, and the major contribution is from the nematic side. For large tilt angles, $\theta_t \geq \pi/3$, however, situation is totally different. The profile increases first from the isotropic phase, then decreases sharply and increases again (down-up-down) until reaching the nematic side. The major contribution comes from the isotropic side and negative contribution exists on the nematic side. Similar phenomenon is found by the study of McDonald and Allen [25], who did the MC simulation about the isotropic-nematic interface of rigid rods, using Onsager's density functional theory. We will present the results of rigid rod-like polymer in the next section, and the profiles have similar up-down-up or down-up-down properties with those presented in Fig (3.4). However, the strange thing is that our profiles are on the opposite side of theirs. Our profile for $\theta_t = 0$ is similar with theirs for "planar" (tilt angle is $\pi/2$), while ours for $\theta_t = \pi/2$ is similar with theirs for "normal" (tilt angle is 0), although we all get the lowest energy when the tilt is $\pi/2$.

As for the interface tension σ obeys similar features obtained by Cui *et al* [24]. The minimum interface tension is about 0.215 ± 0.010 with the tilt angle $\pi/2$. The polymers prefer to be parallel to the interface.

3.3 Interface of the rigid cases: $\alpha = 0$

Secondly, we study the isotropic-nematic interface of the opposite limit, the rigid rod polymers, i.e., $\alpha = 0$. One question may arise since $\alpha = L/a$ is the upper limit of the integral, which makes the density function trivial in Eq. (3.13). This is because all lengths are reduced by the effective Kuhn length a, which now is an infinity number. The isotropic-nematic interface for rigid rod-like polymers are in the length scale of the contour length L, much less than the effective Kuhn length a. Since our interests are in the interface region, which is in the length scale of the contour length, we'd better have rewritten those equations in terms of L rather

than a for this special case.

In the following study, we will find that the width of the interface is always in the length scale of the mean-square of end-to-end distance over the contour length, i.e., $< R^2 > /L$, which is equal to a for flexible limit, and equal to L for rigid rod limit. However, $< R^2 > /L$ by Eq. (2.36) is too complicated to be used to reduce the spatial variables for any possible α. More discussions on it will be made about it later.

Reducing all the variables by the contour length L instead of the effective Kuhn length a in the previous sections, and expanding them by the spherical harmonics, we get the equations in one dimension,

$$w(x, \mathbf{u}) = \sum_{l,m} w_{l,m}(x) Y_{l,m}(\mathbf{u}), \tag{3.36}$$

$$\rho(x, \mathbf{u}) = \frac{1}{L^2 d} \sum_{l,m} \rho_{l,m}(x) Y_{l,m}(\mathbf{u}), \tag{3.37}$$

and

$$q(x, \mathbf{u}, t) = \frac{1}{\sqrt{L^2 d}} \sum_{l,m} q_{l,m}(x, t) Y_{l,m}(\mathbf{u}). \tag{3.38}$$

The partition function Q now is

$$Q = \int \mathrm{d}x \sum_{l,m} q_{l,m}(x, t) q_{l,m}(x, 1-t), \tag{3.39}$$

where the reduced chain is labeled from 0 to 1. And

$$w_{l,m}(x) = \frac{8\pi}{2l+1} d_l \rho_{l,m}(x) + \sqrt{(4\pi)} \beta\mu, \tag{3.40}$$

$$\rho_{l,m}(x) = \frac{N}{Q} \int_0^1 \mathrm{d}t \sum_{l_1,m_1} \sum_{l_2,m_2} q_{l_1,m_1}(x, t) q_{l_2,m_2}(x, 1-t) I_{l_1,m_1,l_2,m_2,l_3,-m_3} (-1)^{m_3}. \tag{3.41}$$

In the differential equation of Eq. (3.18), after we adopt the reduced variable, the first term in the right hand side receives a factor of L/a, which kills the term,

therefore the equation is rewritten as

$$\begin{aligned}\frac{\partial}{\partial t}q_{l,m}(x,t) &= -(-1)^m\sqrt{\frac{4\pi}{3}}\sum_{l_1,m_1}\frac{\partial q_{l_1,m_1}(x,t)}{\partial x} \\ &\quad\times\left\{\sin\theta_t\frac{I_{1,-1,l_1,m_1,l,-m}-I_{1,1,l_1,m_1,l,-m}}{\sqrt{2}}+\cos\theta_t I_{1,0,l_1,m_1,l,-m}\right\} \\ &\quad-\sum_{l_1,m_1}\sum_{l_2,m_2}w_{l_1,m_1}(x)q_{l_2,m_2}(x,t)I_{l_2,m_2,l_1,m_1,l,-m,}(-1)^m. \qquad (3.42)\end{aligned}$$

The interface tension equation for rigid rod-like polymers is

$$\beta\sigma=\int_{-\infty}^{+\infty}\mathrm{d}x\beta\Theta(x), \qquad (3.43)$$

where

$$\beta\Theta(x)=\frac{4\pi}{Ld}\left[\frac{\rho^I_{0,0}-\rho_{0,0}(x)}{\sqrt{4\pi}}+d_0(\rho^I_{0,0})^2-\sum_{l,m}\frac{d_l}{2l+1}\rho^2_{l,m}(x)\right]. \qquad (3.44)$$

Note that the first term in the right side is not a small contribution to the interface tension.

In the calculation, for $\alpha=0$, we divide the contour length into $\aleph=500$, and the spatial discretization is defined by Eq. (3.22) but in terms of L rather than in term of a which is for other cases, i.e., in the rigid case, the spatial variable x is reduced by L,

$$\xi=\tanh(\frac{x\frac{L}{a}\sqrt{1+(1/\alpha)^2}}{2})=\tanh(\frac{x}{2}). \qquad (3.45)$$

ξ is again divided into $N_\xi=160$ piece, each having $\Delta\xi=0.0125$. The fixed point iteration is also needed here, and the fixed point step $c=0.1$ is used.

Figures 3.6 and 3.7 show the density profile $C(x)$ and order parameter profile $S(x)$, respectively. The centers of the profiles shifted as before to see them clearly. The density of isotropic at the left side is $C_i=4.19$, while that of nematic phase is $C_n=5.32$, the order parameter of nematic phase is $S_n=0.789$, which agree with the previous data [33]. The width of profiles are very similar with that for $\alpha=10$, the interfacial width of both the density profile and order profile are about $4\sim5L$.

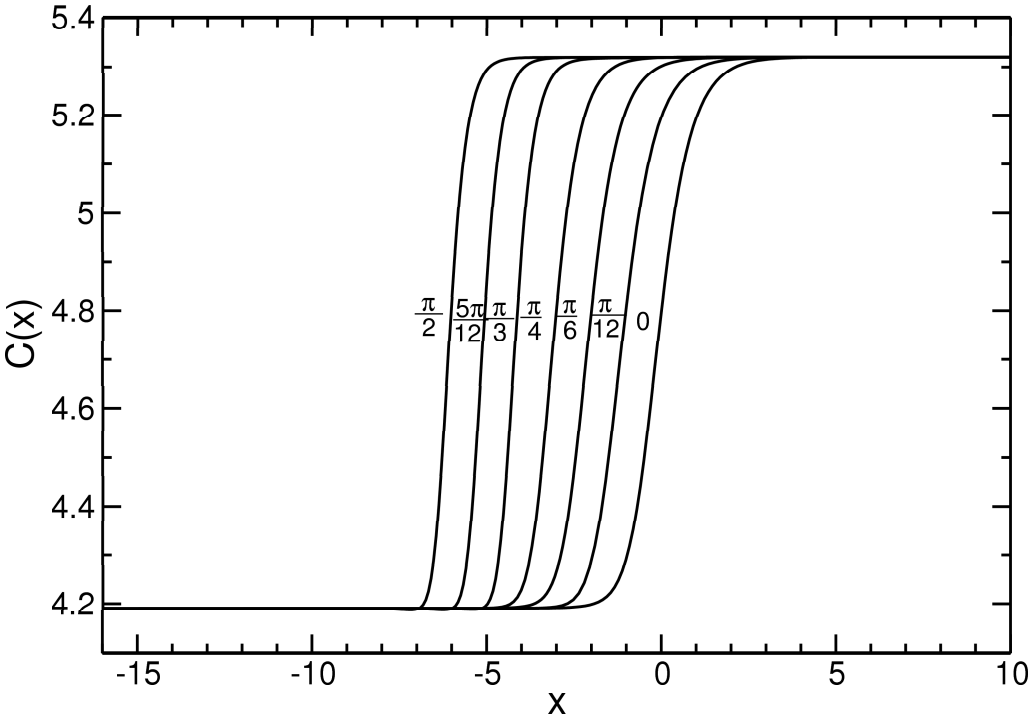

Figure 3.6: Density profile $C(x)$ at the IN interface for $\alpha = 0$. The centers of the profiles are shifted by the contour length L for different title angles, which are indicated in the figure.

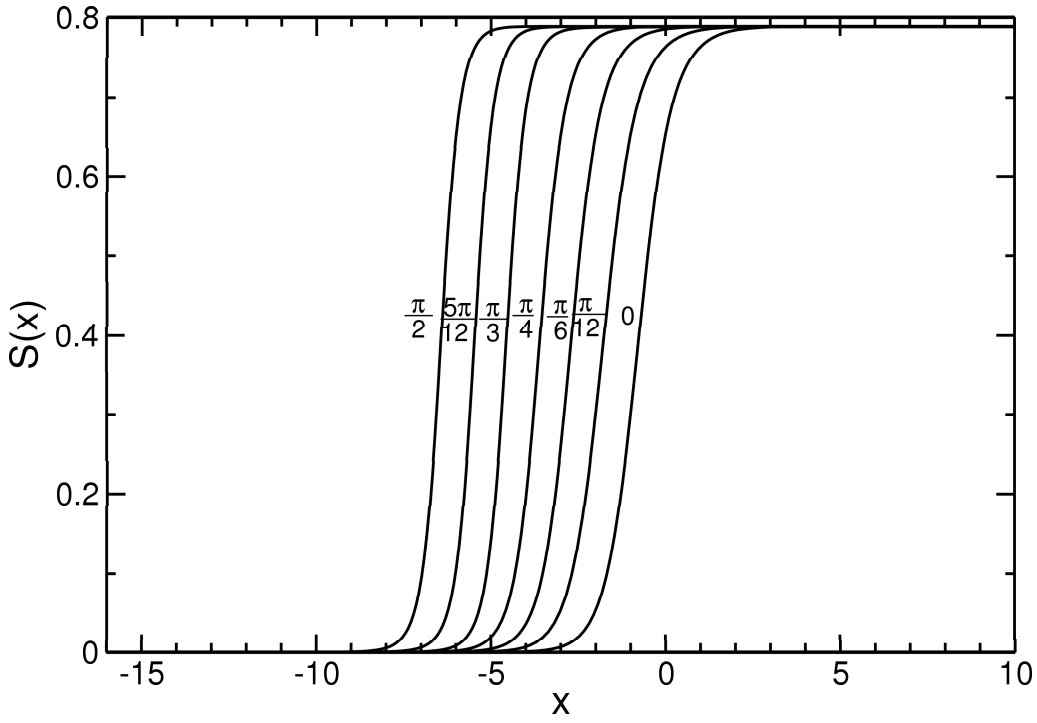

Figure 3.7: Order profile $S(x)$ at the IN interface for $\alpha = 0$. The centers also shifted by L. The tilt angles are indicated in the figure.

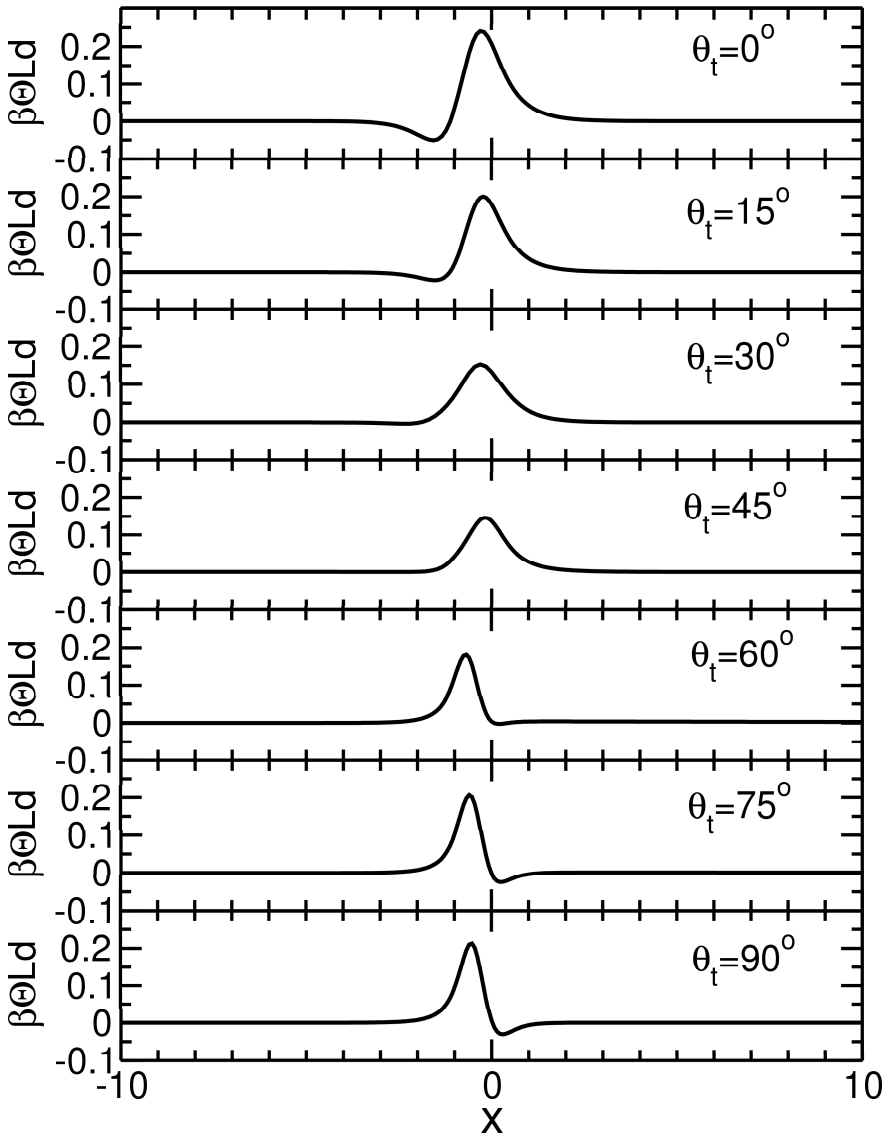

Figure 3.8: Tension contribution profile $\Theta(x)$ at the IN interface for $\alpha = 0$. From the top to the bottom, the tilt angles are 0, 15, 30, 45, 60, 75 and 90, respectively.

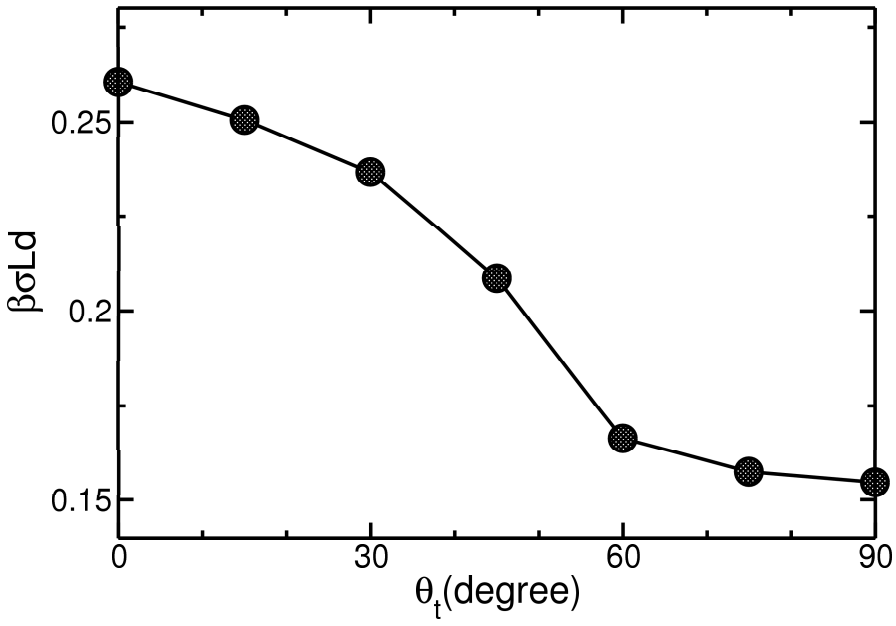

Figure 3.9: The interface tension σ as a function of the tilt angle θ_t for $\alpha = 0$.

Figures 3.8 and 3.9 show the tension contribution profiles $\Theta(x)$ and interface tension σ, respectively. The similar features have been found on the plots. The tension contribution profiles exhibit the same down-up-down for small tilt angles and up-down-up for large tilt angles. But the drop on the profile is not as deep as that we found for $\alpha = 10$ compared with the increasing part. And the change from down-up-down to up-down-up happens at smaller tilt angle than that for $\alpha = 10$. At $\theta_t = \pi/6$, we almost can not see the concave (the decrease part) on the profile, with positive contribution cross the interface.

The lowest interface tension is at $\theta_t = \pi/2$, i.e., when polymers are parallel to the flat interface. The value is 0.155 ± 0.010, which is slightly lower than that found in [23], but very close to the value 0.156 ± 0.001 found by Shundyak and van Roij [27], who used a refined spatial grid by putting more points in the range of the interface to recalculate the interfacial problem reported in [23]. They found that 40 grid points used by Chen to the spatial range $[-5L, 5L]$, the grid points per rod length $M = 40/10L = 4/L$, is not enough. $M = 20/L$, i.e., 200 grid points for that range is enough to make the interface tension converge. However, after we redefined the spatial coordinate by Eq. (3.45), $M = 30/L$ is in the interfacial range (about $4L$), despite only 160 points were used for all the space, from negative infinity to positive infinity.

3.4 Interface of the semiflexible cases: $\alpha = 1$

In this section, $\alpha = 1$ is studied. In this case, the effective Kuhn length a is equal to the total contour length L. Both formula are good for this section, but we'd like to adopt those on the section for flexible cases, i.e., to rescale the space by a, regarding the rigid limit as a special one. The contour length is divided into $\aleph = 2000$, and the spatial discretization is as Eq. (3.22). The fixed point step $c = 0.01$ is used.

The density profile $C(x)$, order parameter profile $S(x)$, tension contribution profile $\Theta(x)$ and interface tension σ are plotted in Fig. 3.10, 3.11, 3.12 and 3.13, respectively. $C_i = 15.85$, $C_n = 16.90$ and $S_n = 0.445$ all agree with the bulk data. The interesting thing is the width of the profiles are quite narrow compared with

those found for both limits, where we found the width are about $4a$ for $\alpha = 10$ and $4L$ for $\alpha = 0$ with $\theta_t = 0$, although they obey the property that width decreases with the increase of the tilt angles and that of $\theta_t = 0$ is about half of that of $\theta_t = \pi/2$. The widest width on the density and order parameter for $\alpha = 1$ is about $2a$ or $2L$.

To find out why the width is somehow "narrower", we turn to the end-to-end distance of polymer chains. For $\alpha = 1$, from Eq. (2.36), we can find the mean-square end-to-end distance over the contour length of polymers is $l_c \equiv < R^2 > /L = L\{1 - [1 - \exp(-2)]/2\} \approx 0.568L$, which means l_c for $\alpha = 1$ is about half of that of rigid rod limit, L, or half of that of flexible limit, a. So for $\alpha = 1$, the width of profile at $\theta_t = 0$ is also about 4 times of l_c, the equivalent segment length of polymer chain, and 2 times of l_c at $\theta = \pi/2$. One can make an guess of the relationship between the interface width and the equivalent segment length of the polymer chain: the widest width of isotropic-nematic interface at $\theta_t = 0$, is about 4 times of the ratio of the mean-square end-to-end distance to the contour length (i.e., $4l_c$), with the increase of tilt angle, the width decreases and the narrowest one is about $2l_c$ at $\theta_t = \pi/2$, from flexible polymers to rod-like polymers. Note that l_c is different from the persistent length l_p.

Figure 3.12 shows us a similar scenario with those found for the two limits. The inverse of the pressure happens around $\theta_t = \pi/4$. We already mentioned that for $\alpha = 10$, it happened over $\pi/4$, while for $\alpha = 0$, it happened below $\pi/4$.

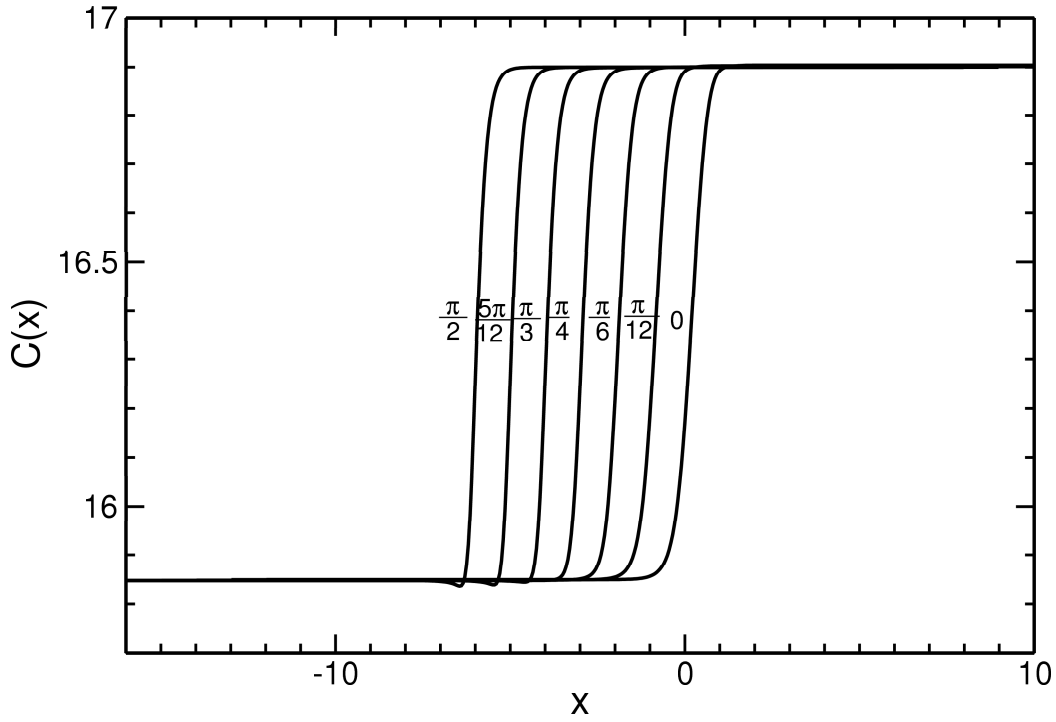

Figure 3.10: Density profile $C(x)$ at the IN interface for $\alpha = 1$. The centers of the profiles are shifted by the contour length a for different title angles, which are indicated in the figure.

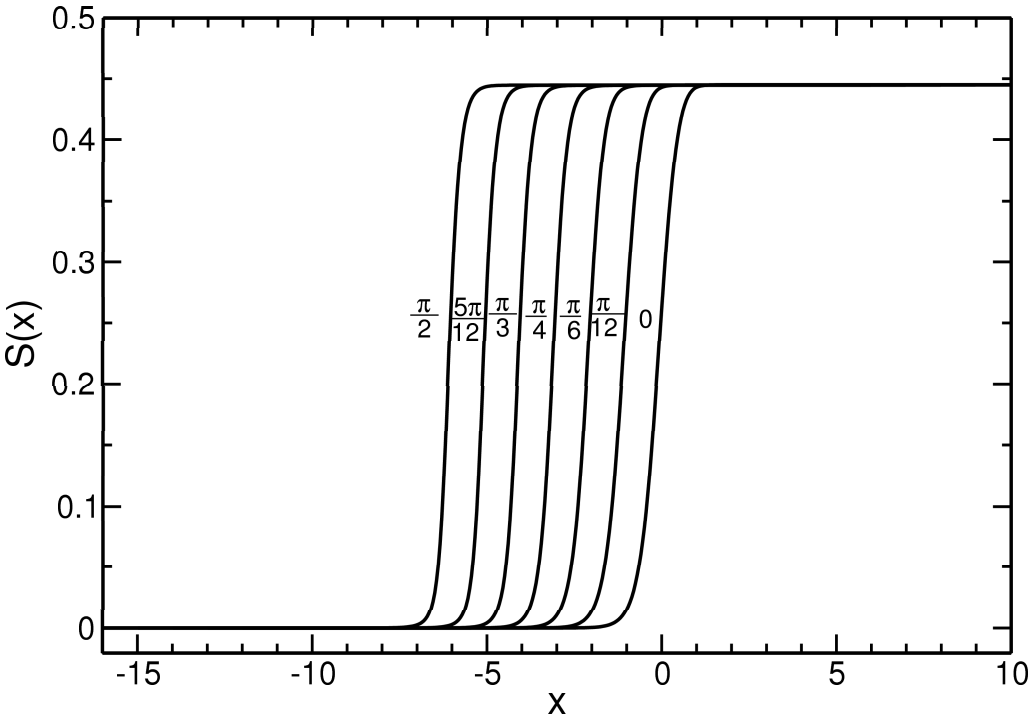

Figure 3.11: Order profile $S(x)$ at the IN interface for $\alpha = 1$. The centers also shifted by a. The tilt angles are indicated in the figure.

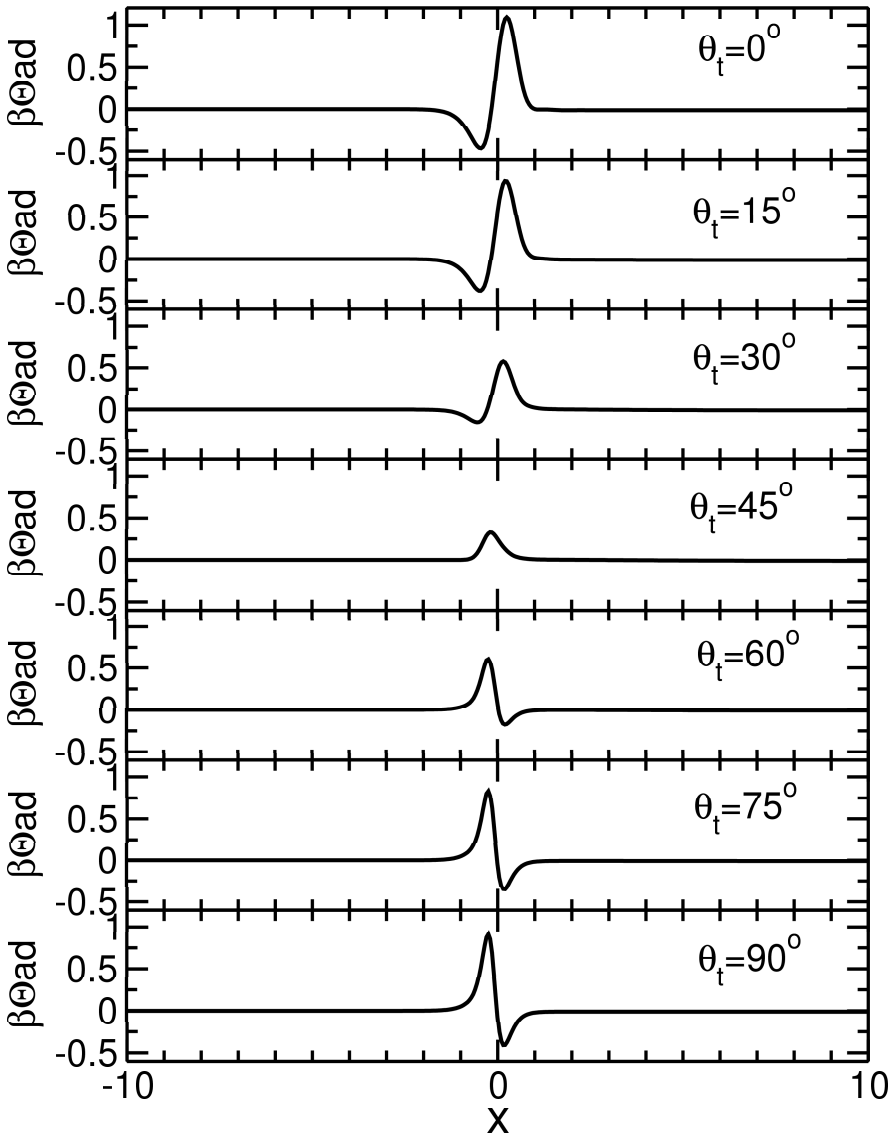

Figure 3.12: Tension contribution profile $\Theta(x)$ at the IN interface for $\alpha = 1$. From the top to the bottom, the tilt angles are 0, 15, 30, 45, 60, 75 and 90, respectively.

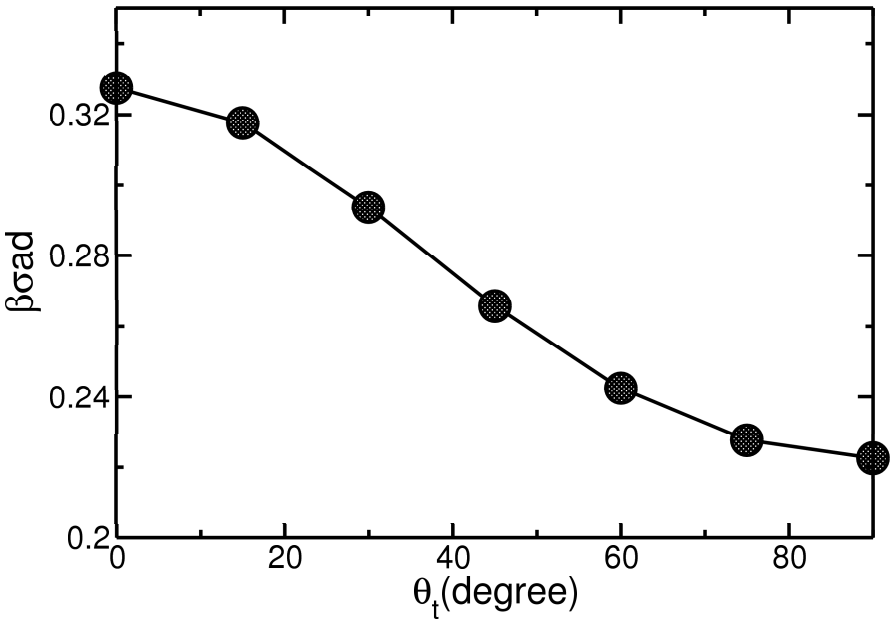

Figure 3.13: The interface tension σ as a function of the tilt angle θ_t for $\alpha = 1$.

Chapter 4

A wormlike polymer confined between hard walls

A polymer confined in certain geometry is of fundamental importance in polymer physics because it underlies some important biological processes and technological applications. This area has attracted many interests, for example, polymer confined in a spherical surface [34], polymer confined in a tube [35, 36, 37, 38], polymer confined between slit [39, 40]. The confinement of flexible polymer causes an entropy change, while the confinement of semiflexible polymer causes both energy and entropy changes.

Although a lot of work have been done in this area, there are still many open questions. So far no work has been done for a wormlike polymer confined between two hard walls, which are separated to a distance comparable to the effective Kuhn length. In this chapter, we will discuss the confinement of two types of polymer models, one is the flexible Gaussian model, and the other is wormlike chain model.

4.1 Flexible polymer confined in hard walls

To start with, we give a review of the well-formulated treatment of the structure of a flexible polymer chain in an external potential field. The flexible polymer chains

are normally modeled by the Gaussian chain model, which has been introduced in the second chapter. The configuration of a flexible polymer is usually described by a reduced continuous space curve $\mathbf{r}(t)$, where t is the contour coordinate varying from 0 to L/a, L the total contour length, a the effective Kuhn length. The statistical weight of a flexible polymer in an external field $V(\mathbf{r})$, acting on unit segment of the polymer, is described by

$$P[\mathbf{r}(t)] \propto \exp\left[-\int_0^{\frac{L}{a}} \mathrm{d}t\Big\{\frac{3}{2a^2}\Big|\frac{\mathrm{d}\mathbf{r}(t)}{\mathrm{d}t}\Big|^2 + \beta V[\mathbf{r}(t)]\Big\}\right], \tag{4.1}$$

where $\beta = 1/k_B T$, k_B the Boltzmann constant and T the temperature. The model in Eq. (4.1) is accurate for description of the physical features of a polymer where the characteristic length scale under examination is much greater than the effective Kuhn length a. Indeed, the formalism has been widely used in developing essential statistical-physics approaches to polymers [41, 35, 8].

We can follow the similar approach of Eq. (2.66a) to define the probability function, $q^g(\mathbf{r}, t)$, of finding the terminal end of a polymer segment of length t at location $\mathbf{r}$, where the superscript g denotes the Gaussian chain. Using the statistical weight in Eq. (4.1), one can show that $q^g(\mathbf{r}, t)$ satisfies [15],

$$\frac{\partial q^g(\mathbf{r}, t)}{\partial t} = [\frac{a^2}{6}\nabla^2 - \beta V(\mathbf{r})]q^g(\mathbf{r}, t). \tag{4.2}$$

To completely specify the physical problem represented in the above partial differential equation, an "initial" condition,

$$q^g(\mathbf{r}, 0) = 1, \tag{4.3}$$

needs to be supplemented. The segmental density, after the consideration of the entire polymer of length L, can be written as,

$$\rho(\mathbf{r}) = \frac{\int_0^{L/a} \mathrm{d}t q^g(\mathbf{r}, t) q^g(\mathbf{r}; L/a - t)}{\int \mathrm{d}\mathbf{r} q^g(\mathbf{r}, L/a)} \tag{4.4}$$

For an infinite square well with the surfaces perpendicular to the x axis [see Fig. 4.1A], we can write the potential $V(\mathbf{r})$ in one dimension,

$$V_{\mathrm{w}}(x) = 0 \qquad \text{for} \qquad 0 < x < W, \tag{4.5}$$

and

$$V_{\mathrm{w}}(x) = \infty \qquad \text{for} \qquad x > W \quad \text{or} \quad x < 0 \tag{4.6}$$

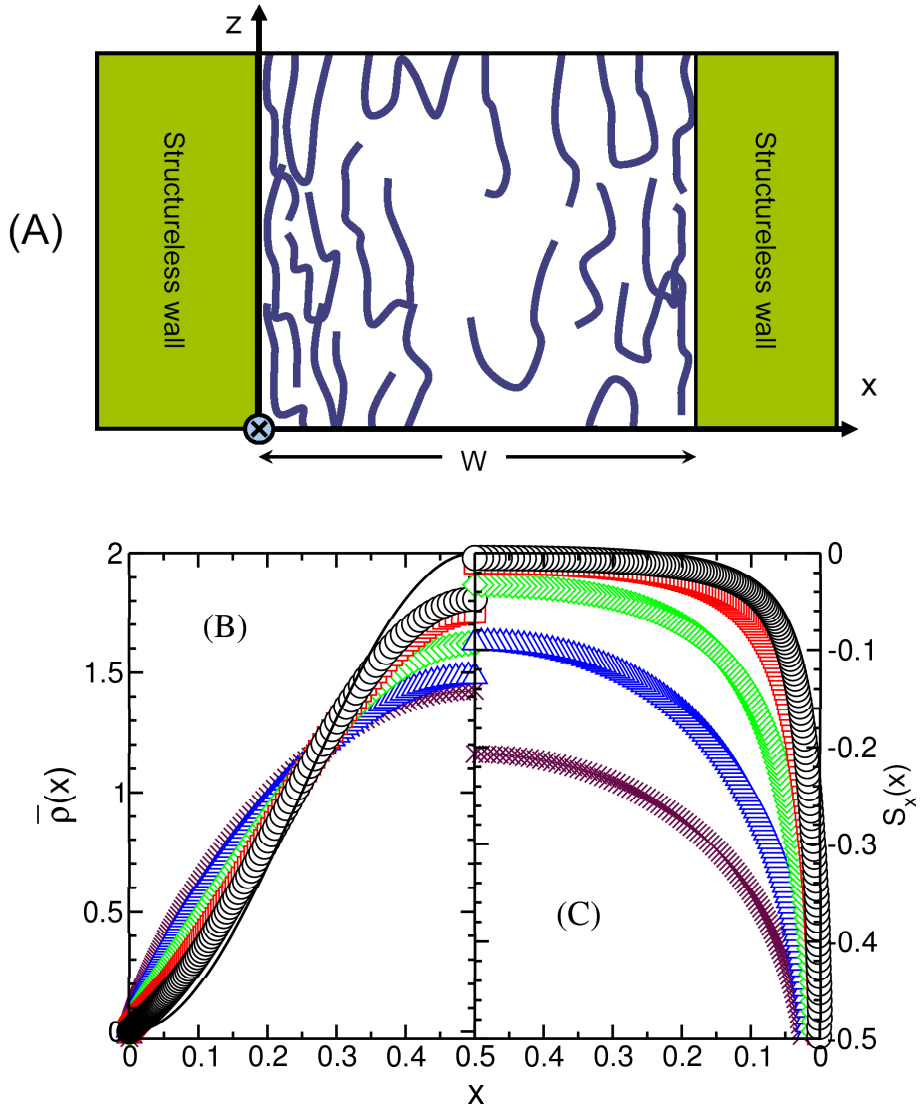

Figure 4.1: (A) Schematic diagram of wormlike chains between two parallel walls, (B) left half of the normalized segment density profile, and (C) right half of the orientational order parameter profile. The two hard walls, located at $x = 0$ and $x = W$ respectively, are assumed without any features and sterically contain wormlike chains. The solid curve in plot (B) represents the limit of $W \gg a$ and can be obtained exactly. Circles, squares, diamonds, triangles, and crosses represent the profiles obtained numerically for $W/a = 6, 4, 2, 1$ and 0.5, respectively.

For a small wall separation (the distance separated by the two walls, W), i.e., when W is much smaller than the radius of gyration of the polymer $\sqrt{La}$, the solution to the partial differential equation is dominated by the ground-state eigenfunction associated with the operator on the right-hand side of Eq. (4.2) [41]. The ground-state eigenvalue can be identified with the reduced segmental chemical potential $\beta\mu$ in this case [42]. Hence, all we need to do is to solve the eigenvalue problem of

$$-\beta\mu q_0^g(x) = \left[\frac{a^2}{6}\frac{\mathrm{d}^2}{\mathrm{d}x^2} - \beta V_{\mathrm{w}}(x)\right] q_0^g(x). \tag{4.7}$$

With the potential Eq. (4.5-4.6), Eq. (4.7) has a simple ground-state solution

$$q_0^g(x) = A\sin(\pi x/W), \tag{4.8}$$

and eigenvalue

$$\beta\mu = (\pi^2/6)(a/W)^2, \tag{4.9}$$

where A is a normalization constant. Within this ground-state dominating limit, we have $q^g(x,t) \approx q_0^g(x)\exp(-\beta\mu t)$ asymptotically; the segmental density in Eq. (4.4) can then be related to $q_0^g(x)$ by

$$\rho(x) \propto (q_0^g(x))^2, \tag{4.10}$$

which yields a normalized segmental density function for polymer confined in a wall separation W,

$$\bar{\rho}(x) = 2\sin^2(\pi x/W). \tag{4.11}$$

Half of $\bar{\rho}(x)$, between $x = 0$ and $x = W/2$, is plotted as a solid curve in Fig. 4.1B. Similar results were reported by Hsu and Grassberger [39] using the Monte Carlo simulations.

With the caution that the solution is valid in the limit $W \ll \sqrt{La}$ (the wall separation is much smaller than the radius of gyration of the polymer), a few simple conclusions can be drawn from this solution. First, the normalized density (Eq. (4.11)) is a universal function of x/W, independent of the magnitude of the effective Kuhn length a. The confinement influences the polymer segments directly near the wall boundaries; the effects of the confinement, however, propagate through

the entire polymer. To maximize the entropy, this would normally result in rearrangement of the entire polymer conformation in a length scale comparable to the radius of gyration, of the order $\sqrt{La}$. In the current system, because the dominating length scale is W, not $\sqrt{La}$, the polymer undergoes conformation change across the entire separation W. Secondly, the free energy of the polymer, F, can be written as the number of segments, L/a, multiplied by the segmental chemical potential, μ. This leads to

$$F \equiv \mu L/a \propto k_B T(\sqrt{La}/W)^2 \propto k_B T(R_0/W)^2, \tag{4.12}$$

where R_0 is the radius of gyration; the harder the polymer is squeezed between the gap (smaller W), the higher the conformation entropy is penalized. Though Eq. (4.12) is the direct result of the statistical weight in Eq. (4.1), the scaling relation between F, R_0 and W is fully consistent with the result from a simple scaling argument based on, for example, the "blob" picture [35].

4.2 STY weight for a wormlike chain in external field

Both Eqs. (4.11) and (4.12) are known results and can be found in, for example, Ref. [41]. However, for a wormlike polymer, the persistence length $l_p \equiv a/2$ can become large in comparison with a typical characteristic length scale in the system. In some systems, we are interested in cases where l_p is comparable to W. For example, a double-stranded DNA molecule has a persistence length of a few hundred $\mathring{A}$ depending on the ionic strength of the solvent, and some of the biological systems consist of DNA molecules confined in the geometry with length scales comparable to its persistence length [43, 44]. Most importantly, the orientation of an individual segment, which is particularly relevant to handling the Onsager excluded-volume interaction [5], needs to be explicitly considered.

For a flexible polymer, the statistical weight in Eq. (4.1) is a good approximation of practical systems only when the physical features in a length scale shorter than a can be ignored. In this chapter, we adopt the approach taken by STY [14] for

treating wormlike polymer chains (introduced in the second chapter), where most universal physical features at a scale less than l_p are maintained. The configuration of a polymer is still described by a continuous space curve $\mathbf{r}(t)$, but the statistical weight depends on the local curvature variation and an external potential,

$$P \propto \exp\left[-\int_0^{\frac{L}{a}} \mathrm{d}t\{\frac{1}{4}|\frac{\mathrm{d}\mathbf{u}(t)}{\mathrm{d}t}|^2 + \beta V[\mathbf{r}(t), \mathbf{u}(t)]\}\right], \tag{4.13}$$

where $\mathbf{u}(t)$ is the unit vector $\mathbf{u}(t) \equiv \mathrm{d}\mathbf{r}(t)/\mathrm{d}t$ and $V(\mathbf{r}, \mathbf{u})$ is the external potential acting on a unit segment, a function of both $\mathbf{r}$ and $\mathbf{u}$. One can show, for a "free polymer" where $V(\mathbf{r}, \mathbf{u}) = 0$, that the conformational properties described by this statistical weight recover those described by the statistical weight in Eq. (4.1), in the limit of $L \gg l_p$, and those described by a simple rigid rod model, in the limit of $L \ll l_p$ [8, 42]. In this section, for a long wormlike chain ($L \gg l_p$) confined between two walls with separation W, we demonstrate that the STY weight in Eq. (4.13) recovers the results based on (Eq. 4.7) in the limit of $R_0 \gg W \gg l_p$ (the same condition for validity of the model in Eq. (4.1), and yields different physical features in the parameter regime $R_0 \gg \sqrt{l_p W}$.

Because orientation of a polymer segment is explicitly considered in Eq. (4.13), we are able to examine a physical quantity that is a function of both $\mathbf{r}$ and $\mathbf{u}$. To this end, we are interested in the conditional probability, $q(\mathbf{r}, \mathbf{u}, t)$, that a polymer portion of length t has an end located at $\mathbf{r}$ *and* whose tangent vector point in the direction $\mathbf{u}$. The computation of $q(\mathbf{r}, \mathbf{u}, t)$ is equivalent to solving the differential equation (2.69), with the "initial" condition of Eq. (2.73). The segmental distribution function, for an internal segment of the polymer to located at $\mathbf{r}$ and with a tangent vector pointing at $\mathbf{u}$, can be written as,

$$\rho(\mathbf{r}, \mathbf{u}) = \frac{\int_0^{L/a} \mathrm{d}t q(\mathbf{r}, \mathbf{u}, t) q(\mathbf{r}, -\mathbf{u}, L/a - t)}{\int \mathrm{d}\mathbf{r}\mathrm{d}\mathbf{u} q(\mathbf{r}, \mathbf{u}, L/a)}. \tag{4.14}$$

We have already discussed in the third chapter that Eq. (4.14) is a general equation. Different ratio of L/a gives us different properties of polymers. For $L/a \ll 1$, we have the rigid rod-like polymers, on the other side, for $L/a \gg 1$, we have the flexible polymers. In the rest of this chapter, we are only concerned about

long wormlike chains where the radius of gyration of the chain, R_0, is much greater than both l_p and W. Within this parameter regime, the ground-state solution for the operator in the square brackets of Eq. (2.69) is the dominating function contributing to the free energy and segmental density distribution. Adopting the coordinate system in Fig. 4.1A, we need to obtain the ground-state solution of the eigen problem for the partial differential equation

$$-\beta\mu\psi(x,\mathbf{u}) = [\nabla_u^2 - au_x\frac{\mathrm{d}}{\mathrm{d}x} - \beta V(x,\mathbf{u})]\psi(x,\mathbf{u}), \tag{4.15}$$

where u_x is the projection of the $\mathbf{u}$ vector onto the x axis. Asymptotically for large t, we have

$$\psi(x,\mathbf{u};t) \approx \psi(x,\mathbf{u})\exp(-\beta\mu t). \tag{4.16}$$

Considering the relationship between the ρ and ψ in Eq. (4.14), we can readily write

$$\rho(x,\mathbf{u}) \propto \psi(x,\mathbf{u})\psi(x,-\mathbf{u}). \tag{4.17}$$

Note that the physical meaning of the product on the right hand sides of both Eqs. (4.14) and (4.17) have the same meaning as that in Fig. 2.4. The negative sign in front of the second $\mathbf{u}$ vector can only be omitted for systems containing a reversal symmetry in $\mathbf{u}$, such as in the case of studying the bulk properties of a nematic phase [7, 33, 45]. This fact was not always appreciated in some studies [46].

This formalism has been used for studying interfacial properties between two immiscible wormlike polymers [47] and between the isotropic and nematic states of wormlike liquid-crystal polymers [24, 48].

4.3 Recovery of the results in Section 4.1 for $W \gg a$

One of the most important features of the above formalism for $\psi(x,\mathbf{u})$ is that it recovers the formalism for $q^g(x)$, discussed in Section 4.1 for a "wide" confinement gap, $W \gg a$. In this limit, to see how Eq. (4.15) reduces to Eq. (4.7) for a

square well potential (Eqs. 4.5 and 4.6), we start by noting that the only relevant orientational variable is $u_x \equiv \mathbf{u} \cdot \hat{\mathbf{x}}$, where $\hat{\mathbf{x}}$ is a unit vector along the x axis [47].

Expanding $\psi(x, u_x)$ in terms of Legendre functions $P_l(u_x)$, we write

$$\psi(x, u_x) = \sum_{l=0}^{\infty} \psi_l(x) P_l(u_x), \tag{4.18}$$

where, at this stage, $\psi_l(x)$'s $(l = 0, 1, 2, ...)$ are undetermined functions of x. The substitution of this expression into Eq. (4.15) allows us to identify the coupled differential equations that $\psi_l(x)$'s must satisfy,

$$-\beta\mu\psi_l(x) \;=\; -l(l+1)\psi_l(x) - a\frac{l}{2l-1}\frac{\mathrm{d}}{\mathrm{d}x}\psi_{l-1}(x) - a\frac{l+1}{2l+3}\frac{\mathrm{d}}{\mathrm{d}x}\psi_{l+1}(x). \tag{4.19}$$

More specifically, the first two coupled equations, valid for $0 \le x \le W$, read

$$-\beta\mu\psi_0(x) = -\frac{a}{3}\frac{\mathrm{d}}{\mathrm{d}x}\psi_1(x), \tag{4.20}$$

and

$$-\beta\mu\psi_1(x) = -2\psi_1(x) - a\frac{\mathrm{d}}{\mathrm{d}x}\psi_0(x) - \frac{2a}{5}\frac{\mathrm{d}}{\mathrm{d}x}\psi_2(x). \tag{4.21}$$

An examination of Eq. (4.20) reveals that $\beta\mu$ is of order $(a/W)^2$ for small a/W. And the last term in Eq. (4.21) is of order $(a/W)^3$. Keeping terms of order $(a/W)^2$ or lower in Eq. (4.21), we neglect the left-hand side because it is of order $(a/W)^3$. Then Eq. (4.21) can be rewritten as

$$2\psi_1(x) = -a\frac{\mathrm{d}}{\mathrm{d}x}\psi_0(x). \tag{4.22}$$

Together with Eq. (4.20), we can easily see, when $W/a \gg 1$, $\psi_0(x)$ satisfies Eq. (4.2) , and $\psi_1(x)$ is of order (a/W). Hence, Eq. (4.2) is a special, asymptotic case of Eq. (2.69). It is known that most physical properties of a wormlike chain [obeying Eq. (4.13)] recover those of a flexible chain [obeying Eq. (4.1)] in the limit of $L \gg a$; we see here no exception for systems where $W \gg a$.

4.4 The case of $W \approx a$

We now return to the general case of $W \sim a$ that requires numerical consideration of Eq. (2.69) [24]. Cautions have to be made to impose the boundary conditions at the walls. For the geometry of hard walls described in Fig. 4.1, it is clear that the external potential $V_{\rm w}(x, \mathbf{u}) = \infty$ for $x < 0$ or $x > W$, which is a condition that would be normally invoked in a typical potential-well problem. The situation at $x = 0^+$, however, is more complex; a polymer terminal segment that points to the negative x-direction is not directly influenced by the hard-wall steric interaction, hence has a non-zero density distribution; on the other hand, a polymer terminal segment that points to the positive x-direction is subject to the hard-wall steric interaction [49]. This implies that $V_{\rm w}(0^+, \mathbf{u}) = \infty$ for $\mathbf{u} \cdot \hat{\mathbf{x}} > 0$ and $V_{\rm w}(0^+, \mathbf{u}) = 0$ for $\mathbf{u} \cdot \hat{\mathbf{x}} < 0$; according to the same rational, $V_{\rm w}(W - 0^+, \mathbf{u}) = \infty$ for $\mathbf{u} \cdot \hat{\mathbf{x}} < 0$ and $V_{\rm w}(W - 0^+, \mathbf{u}) = 0$ for $\mathbf{u} \cdot \hat{\mathbf{x}} > 0$.

To solve the eigenproblem in Eq. (4.15), we need to implement Legendre expansions for the angular dependence in both $\psi(x, \mathbf{u})$ (Eq. (4.18)) and $V_{\rm w}(x, \mathbf{u})$[32],

$$V_{\rm w}(x, \mathbf{u}) = \sum_{l=0}^{\infty} V_{{\rm w}l}(x) P_l(u_x). \tag{4.23}$$

Applying the boundary mentioned above, we get

$$\begin{aligned}
V_{{\rm w}l}(0^+) &= V_\infty \frac{2l+1}{2} \int_0^{\frac{\pi}{2}} {\rm d}\theta \sin\theta P_l(\cos\theta) && \text{(4.24a)}\\
V_{{\rm w}l}(W - 0^+) &= V_\infty \frac{2l+1}{2} \int_{\frac{\pi}{2}}^{\pi} {\rm d}\theta \sin\theta P_l(\cos\theta) && \text{(4.24b)}\\
V_{{\rm w}l}(x) &= 0 \qquad \text{for} \quad 0 < x < W, && \text{(4.24c)}\\
V_{{\rm w}l}(\text{otherwise}) &= V_\infty, && \text{(4.24d)}
\end{aligned}$$

where $\cos\theta = u_x$, and V_∞ a quite big number used to describe the infinite potential walls, and practically 5000 was used.

Using these equations, we numerically solved for any value of W/a. Figure 4.2 shows the numerical solution for the eigenvalue $\beta\mu$ as a function of W/a. Note that $\beta\mu(W/a)^2$ approaches the asymptote $\pi^2/6$ at $W/a \gg 1$, agreeing with the analytic solution to Eq. (4.2).

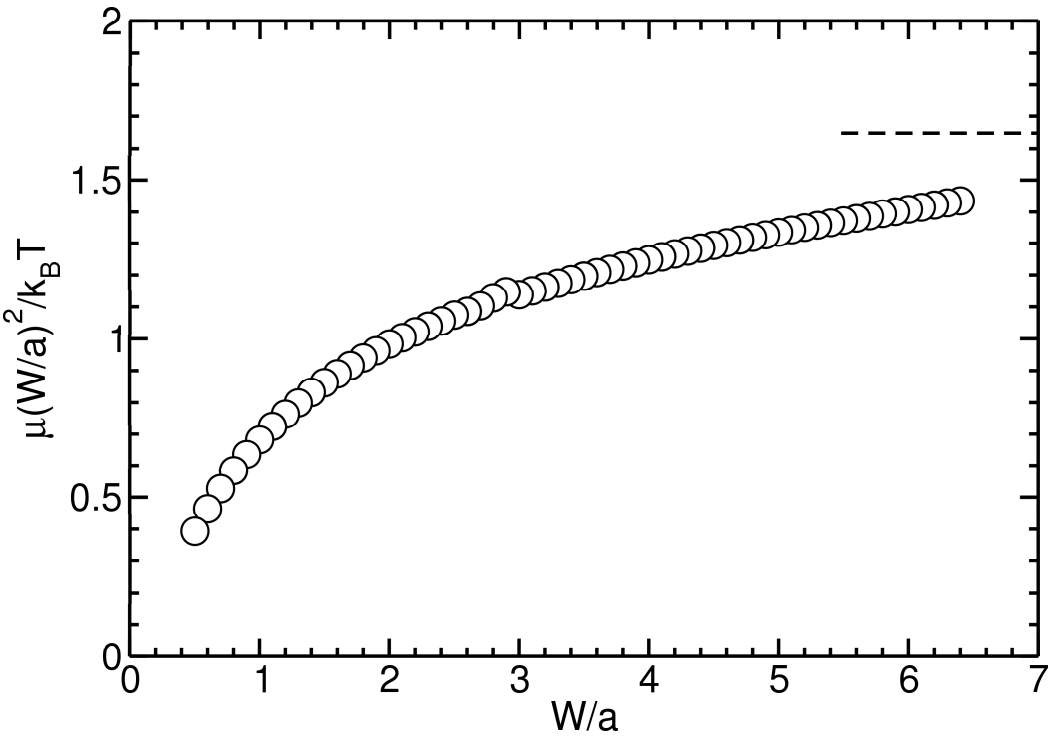

Figure 4.2: Numerical solution for the reduced chemical potential $\mu(W/a)^2/k_BT$ as a function of the reduced wall separation W/a for a wormlike chain. The dashed line represents the asymptotic limit $\pi^2/6$, based on a model for flexible chain.

The normalized segment density and order parameter profiles, $\bar{\rho}(x) = \int \mathrm{d}\mathbf{u}\rho(x,\mathbf{u})$ and $S_x(x) \equiv < P_2(\cos\theta_x) >$, are plotted in Fig. 4.1B and 4.1C for several values of W/a, where $< ... >$ is performed in reference to the conditional density probability function in Eq. (4.4) with a fixed x. The illustration shows that as W/a is decreased from a rather large value (circles where $W/a = 6$) to a small value (crosses where $W/a = 0.5$), $\bar{\rho}(x)$ deviates from the prediction based on Eq. (2) (solid curve); instead of occupying the central region between the walls to maximize the entropy, the polymer segments are forced towards the near-wall regions by the smaller separations. In the mean time, polymer segments near the walls develop significant orientational ordering, lying parallel to the walls — a value $-1/2$ for S_x would imply that the segments are perfectly parallel to the surface of the wall.

4.5 The confined wormlike polymer interacting with the Onsager approximation

So far we have discussed the structure of wormlike chains without mutual segment-segment interactions. To include excluded-volume interactions, a wormlike chain can be treated as a cylindrical filament (which can still be described by a space curve specifying the filament axis) characterized by a cross-sectional diameter d. In a typical bead-spring model for polymers where the excluded-volume interaction is usually characterized by the size of a bead, the interaction energy is independent of the orientation of the polymer bonds. However, the excluded-volume interaction of cylindrical filaments has a clear orientation dependence. In the limit $l_s \gg d$, the excluded volume between two perpendicular rigid segments of length l_s is approximately $2dl_s^2$, which is much greater than that between two parallel segments, $2\pi d^2 l_s$. Onsager derived a free energy expression based on the second-virial coefficient approximation for the excluded-volume interaction between two rods of an arbitrary relative orientation [5]. The Onsager approximation is considered accurate for long polymers [7], where $L \gg a \gg d$, a condition that can be easily satisfied by most polymer systems, in particular, DNA molecules. To describe the current system, the interaction between a polymer segment and others is approximated by

a mean-field background potential energy $U(x, \mathbf{u})$ acting on this segment. Within the Onsager approximation, this is given by [7, 24] [a],

$$\beta U(x, \mathbf{u}) = 2a^2 d \int \mathrm{d}\mathbf{u}' \rho(x, \mathbf{u}') |\mathbf{u} \times \mathbf{u}'|. \tag{4.25}$$

The potential $V(x, \mathbf{u})$ in Eq. (4.15) is now

$$V(x, \mathbf{u}) = U(x, \mathbf{u}) + V_{\mathrm{w}}(x, \mathbf{u}). \tag{4.26}$$

Equations (4.15-4.26) completely specify a set of self-consistent equations, which we can solve numerically.

We adopted a similar definition of the coordinate system defined in the third chapter. The only difference is now we have two separated walls in the space as shown in Fig. 4.3. We already mentioned the spatial variable (in Fig. 4.1(A)), the x axis is along the normal of the infinite structureless walls; the system is translational invariant in the y and z directions. The polar variables to describe $\mathbf{u}$ are defined in the tilted coordinate frame labeled by the Cartesian variables u_x, u_y, and u_z. The direction of the u_z coordinate coincides with the bulk nematic director, so that the angle between the direction of the u_z axis and the normal to the surface x is the tilt angle θ_t. The u_y direction is chosen in the same direction as the y axis. Similar with Eq. (3.15), for a fixed tilt angle θ_t, expanding in the $\mathbf{u}$ space, the variable

$$u_x = \cos\theta_t \sin\theta \cos\varphi + \sin\theta_t \cos\theta, \tag{4.27}$$

where, θ and φ are polar angles.

The nematic director is no longer along the x axis when the tilt angle is nontrivial. In the vicinity of the walls, the rotation symmetry of $\psi(x, \mathbf{u})$ is broken, which

[a] We should note that the Onsager term in Eq. A4 in reference [24] is incorrect. A '2' factor is missing on the right hand side of the formula, therefore the relative term should multiply by this factor in the following equations: Eq. 1, Eq. 7, Eq. 8, Eq. 19, Eq. 20, and Eq. 37. Note that there is another misprint in Eq. 37; the sign factor $(-1)^m$ should not be there. The correct formula is as Eq. (4.40) in present paper. The last term in Eq. 25 needs one more sign factor $(-1)^{m_1}$. Fortunately, the two equations used for calculation Eq. 12 and Eq. 25 do have a '2' factor and the code for both Eq. 25 and Eq. 37 are in the correct form, which generated correct results present in that paper.

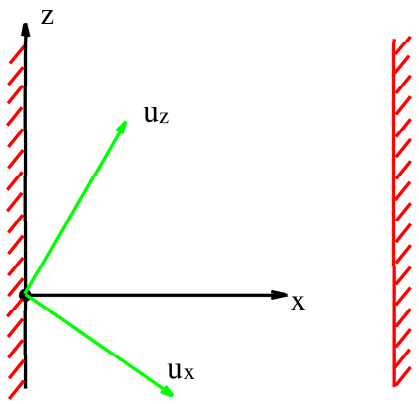

Figure 4.3: The similar definition of the coordinate system as that shown in Fig. 3.1. The x axis is along the normal of the wall. The spherical polar coordinates for describing $\mathbf{u}$ are defined in the u-coordinate frame, while the bulk nematic director is along the u_z axis.

make the Legendre functions no longer suitable for the expansion of the eigenfunction. Hence, to solve this set of self-consistent equations, we again expand all the functions by the spherical harmonics

$$\psi(x,u) = \frac{1}{\sqrt{a^2 d}} \sum_{l,m} \psi_{l,m}(x) Y_{l,m}(u), \tag{4.28}$$

where $\psi_{l,m}(x)$ is dimensionless.

For the boundary condition, again because the rotational symmetry of the system around the nematic director is no longer valid for the nontrivial tilt angle, the limits of the integral in Eq. (4.24a) and Eq. (4.24b) have been changed, which make it difficult to integrate directly. However, by using the addition theorem, we can rotate the coordinate system, and express $V_{\rm w}(x,\mathbf{u})$ by the spherical harmonics in terms of the coefficients $V_{{\rm w}l}(x)$ in Eq. (4.24),

$$V_{\rm w}(x,\mathbf{u}) = \sum_{l,m} V_{{\rm w}l,m}(x) Y_{l,m}(\mathbf{u}), \tag{4.29}$$

where

$$V_{{\rm w}l,m}(x) = V_{{\rm w}l}(x) \frac{4\pi}{2l+1} Y^*_{l,m}(\theta_t, 0), \tag{4.30}$$

where θ_t is the tilt angle.

Multiply both sides of Eq. (4.15) by $Y^*_{l,m}(\mathbf{u})$, integrate over $\mathbf{u}$, and rescale the variable x in units of the effective Kuhn length a. This procedure yields

$$\begin{aligned}
&[l(l+1)-\beta\mu]\psi_{l,m}(x)+(-1)^m\sqrt{\frac{4\pi}{3}}\sum_{l_1,m_1}\frac{\mathrm{d}\psi_{l_1,m_1}(x)}{\mathrm{d}x}\\
&\times\left[\sin(\theta_t)\frac{I_{1,-1,l_1,m_1,l,-m}-I_{1,1,l_1,m_1,l,-m}}{\sqrt{2}}+\cos(\theta_t)I_{1,0,l_1,m_1,l,-m}\right]\\
&+\sum_{\mathrm{l,m}}\frac{8\pi}{2l_1+1}(-1)^{l_4+m+m_1}d_{l_1}\psi_{l_2,m_2}(x)\psi_{l_3,m_3}(x)\psi_{l_4,m_4}(x)I_{l,-m,l_1,m_1,l_2,m_2}\\
&\times I_{l_1,-m_1,l_3,m_3,l_4,m_4}=0,
\end{aligned}\tag{4.31}$$

where the bold faced indices $\mathrm{l,m}$ in the third term indicate that the sum is over all relevant values of $l_1, l_2, l_3, l_4, m_1, m_2, m_3$, and m_4. The constant I comes from the integral of three spherical harmonics, defined by Eq. (3.14).

The density distribution function

$$\rho(x,\mathbf{u})=\frac{1}{a^2d}\sum_{l,m}\rho_{l,m}(x)Y_{l,m}(u),\tag{4.32}$$

in which the coefficient $\rho_{l,m}(x)$ is ready to be deduced from $\psi_{l,m}(x)$

$$\rho_{l,m}(x)=\sum_{l_1,m_1}\sum_{l_2,m_2}I_{l,-m,l_1,m_1,l_2,m_2}(-1)^{l_1+m}\psi_{l_1,m_1}(x)\psi_{l_2,m_2}(x).\tag{4.33}$$

In the vicinity of the walls, the functions $\psi_{l,m}(x)$ change sharply when the spatial variable x approaches them, so more representative points should be assigned to the region close to the walls. Hence, we chose a new way to define the spatial variable. In the calculation, for the left half space $[0, W/2a]$, we use a spatial variable defined by

$$\xi=\left[\frac{2ax}{W}\right]^{1/3}\tag{4.34}$$

where the interval of ξ is $[0,1]$ for the left half. The points of the right half space is just the mirror image of the left side when the $x = W/2a$ plane is chosen to be the reflection mirror,

$$2-\xi=\left[2-\frac{2ax}{W}\right]^{1/3}.\tag{4.35}$$

Hence the interval of ξ for the whole system is $[0, 2]$, which can be discretized into N_ξ equally spaced slabs. Practically, $N_\xi = 160$ was used. For the differential term $\mathrm{d}\psi_{l,m}(x)/\mathrm{d}x$ in Eq. (4.31), we have two choices to express in difference: one is to use $\mathrm{d}\psi_{l,m}(x)/\mathrm{d}x \approx (\mathrm{d}\xi/\mathrm{d}x)\Delta\psi_{l,m}(x(\xi))/\Delta\xi$; the other, used in the calculation, is to express directly

$$\frac{\mathrm{d}\psi_{l,m}(x)}{\mathrm{d}x} \approx \frac{\psi_{l,m}(x(\xi+\Delta\xi)) - \psi_{l,m}(x(\xi-\Delta\xi))}{x(\xi+\Delta\xi) - x(\xi-\Delta\xi)}. \tag{4.36}$$

For the first and the last point, respectively, the forward and backward difference was used instead of the central difference.

For the coordinate system chosen in Fig. 4.3, with an arbitrary θ_t, we already have the symmetry properties of Eq. (3.19-3.20). Besides this, the excluded-volume interaction prefers to have a tilt angle of $\pi/2$ [24, 50], which give us another symmetry properties

$$\psi(x, \mathbf{u}) = \psi^*(x, \mathbf{u}) = \psi(x, \mathbf{u}_x), \tag{4.37}$$

where $\mathbf{u}_x = (\pi - \theta, \varphi)$ is the mirror image of $\mathbf{u} = (\theta, \varphi)$ when the $\mathbf{u}_x = 0$ plane is considered to be the reflection mirror. Therefore the coefficient $\psi_{l,m}(x) = 0$ for all the odd $l + m$ terms. In practice, by using these symmetry properties, we reduced the number of independent variables, and truncate the expansion in Eq. (4.28) after the $l = 10$ term.

For the order parameter of the system, here we would like to take another definition: in the third chapter, we defined the principle order parameter in Eq. (3.25), which is according to the $\mathbf{u}$ coordinate system; here we'd like to choose that according to the spatial coordinate to see clearly the biaxial effect. With the tilt angle $\theta_t = \pi/2$, the order parameters can be expand explicitly in terms of $\rho_{l,m}$ as the following,

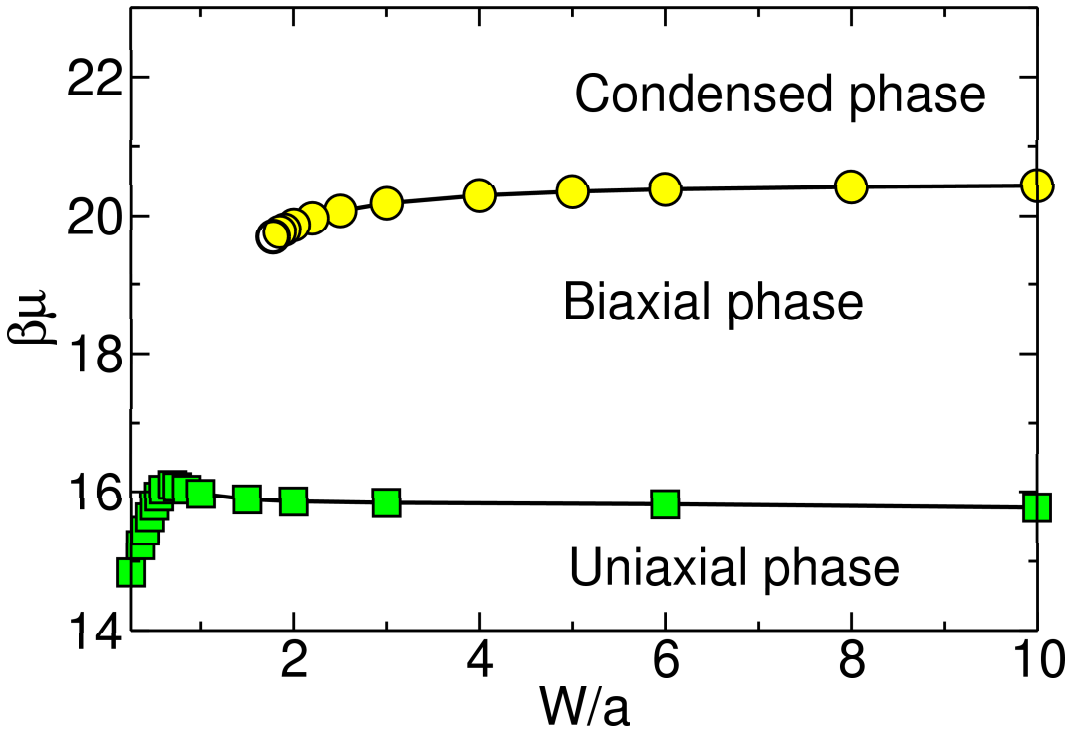

Figure 4.4: Phase diagram for wormlike chains confined between walls. The horizontal axis is the wall separation, while the vertical axis is the chemical potential per effective Kuhn segment. Filled symbols represent the numerical solution to Eqs. (4-7) based on which solid curves (first-order phase boundaries) are projected. The open symbol represents the critical point.

$$
\begin{aligned}
S_x(x) \equiv < P_2(\mathbf{u}\cdot\hat{x}) > &= \frac{\int \mathrm{d}\mathbf{u}\rho(x,\mathbf{u})\left[\frac{3}{2}\sin^2\theta\cos^2\varphi - \frac{1}{2}\right]}{\int \mathrm{d}\mathbf{u}\rho(x,\mathbf{u})} \\
&= \frac{\sqrt{6}\rho_{2,2}(x) - \rho_{2,0}(x)}{2\sqrt{5}\rho_{0,0}(x)}; \qquad (4.38a) \\
S_y(x) \equiv < P_2(\mathbf{u}\cdot\hat{y}) > &= \frac{\int \mathrm{d}\mathbf{u}\rho(x,\mathbf{u})\left[\frac{3}{2}\sin^2\theta\sin^2\varphi - \frac{1}{2}\right]}{\int \mathrm{d}\mathbf{u}\rho(x,\mathbf{u})} \\
&= \frac{-\sqrt{6}\rho_{2,2}(x) - \rho_{2,0}(x)}{2\sqrt{5}\rho_{0,0}(x)}; \qquad (4.38b) \\
S_z(x) \equiv < P_2(\mathbf{u}\cdot\hat{z}) > &= \frac{\int \mathrm{d}\mathbf{u}\rho(x,\mathbf{u})\left[\frac{3}{2}\cos^2\theta - \frac{1}{2}\right]}{\int \mathrm{d}\mathbf{u}\rho(x,\mathbf{u})} \\
&= \frac{\rho_{2,0}(x)}{\sqrt{5}\rho_{0,0}(x)}. \qquad (4.38c)
\end{aligned}
$$

With all formula mentioned above, we numerically investigate the problem of a flexible polymer confined between two walls. We have found that three distinct structures are possible, depending on the magnitude of W/a and $\beta\mu$ (see Fig. 4.4); the latter can be viewed as a controlling parameter related to the average segment density between the walls. Qualitatively, long wormlike chain can be viewed as rods of length $2l_p$ freely jointed together; the three phases found here can be compared to similar phases that appear in the system of rod-like molecules between walls [27].

The error this simulation mainly comes from two sources: one is from the finite discretization of the space, the other is that we must truncate the spherical series at a certain number. In order to calculate how big the error bar is, we chose some cases, in which we calculate the spherical harmonics series after $l = 12$, and $N_\xi = 320$, and found the error for uniaxial-biaxial transition is quite small. For example, the case of $W/a = 2$, the data are: $l = 10$, $N_\xi = 160$ is 15.855 (this number is the chemical potential at the bi-uni phase transition); $l = 10$, $N_\xi = 320$ is 15.865; $l = 12$, $N_\xi = 160$are 15.885. Thus the estimate error can be regarded as ± 0.05 for this case by using $l = 10$, $N_\xi = 160$. For biaxial-condensed transition, the data shown that even lower error bar, due to the slight stronger first order phase transition. In the case of $W/a = 6$, for $l = 10$, $N_\xi = 160$ is 20.3835; for $l = 10$,

$N_\xi = 240$ is 20.3839; for $l = 12$, $N_\xi = 160$ is 20.3848. So for B-C transition, the estimated error is about ± 0.004.

4.6 Uniaxial-Biaxial transition

Consider a system where $W/a > 1.8$ (Fig. 4.4). At low $\beta\mu$ (hence low ρ) the excluded-volume interaction between segments is less important and the orientational ordering of those near-wall segments is mainly the consequence of the steric interaction with the wall. Within a distance of a from the wall, there exists a depletion layer of polymer segments, as the segment density profiles in Fig. 4.5A show. With the increasing of distance from the wall, the segments have less steric interaction with the wall, and tend to form the bulk isotropic-like phase. From Eq. (4.38), we know only two of these three order parameters are independent $[S_x(x) + S_y(x) + S_z(x) = 0]$. At $x = 0^+$, $S_x(x)$ attains the value $S_x(0^+) = -\frac{1}{2}$, while both $S_y(x)$ and $S_z(x)$ have the value $\frac{1}{4}$, which indicates that $\rho_{2,2}(x) = 0$, the density profile is rotational invariant around the x axis, and a pancake shape distribution is present. Throughout the entire region, the *uniaxial* symmetry $S_z(x) = -S_x(x)/2$ is maintained (Figs. 4.5C and 4.5E).

Increasing the reduced segment density, which is written as

$$\tilde{\rho}(x) \equiv a^2 d\rho(x) = a^2 d \int \mathrm{d}\mathbf{u}\rho(x, \mathbf{u}) = \sqrt{4\pi}\rho_{0,0}(x), \tag{4.39}$$

corresponds to increasing $\beta\mu$. As $\beta\mu$ approaches 16 (more exactly, the solid curve associated with squares in Fig. 4.4), a phase transition to a biaxial phase, that has different orientational properties, can be seen. Khokholv and Semenov were the first to suggest that a nematic liquid-crystal phase can form provided that $\tilde{\rho}$ is high enough, where the orientation-dependent Onsager interaction is the mechanism responsible for this transition [7]. We see here the manifestation of a similar principle at work in a confined system. Polymer segments far from the wall are still oriented nearly randomly and give rise to the similar density as in a uniaxial phase. The segments close the wall begin to develop a density-enhanced layer with nematic characteristics [Fig. 4.5B]; a preferred direction parallelling to the wall surface is

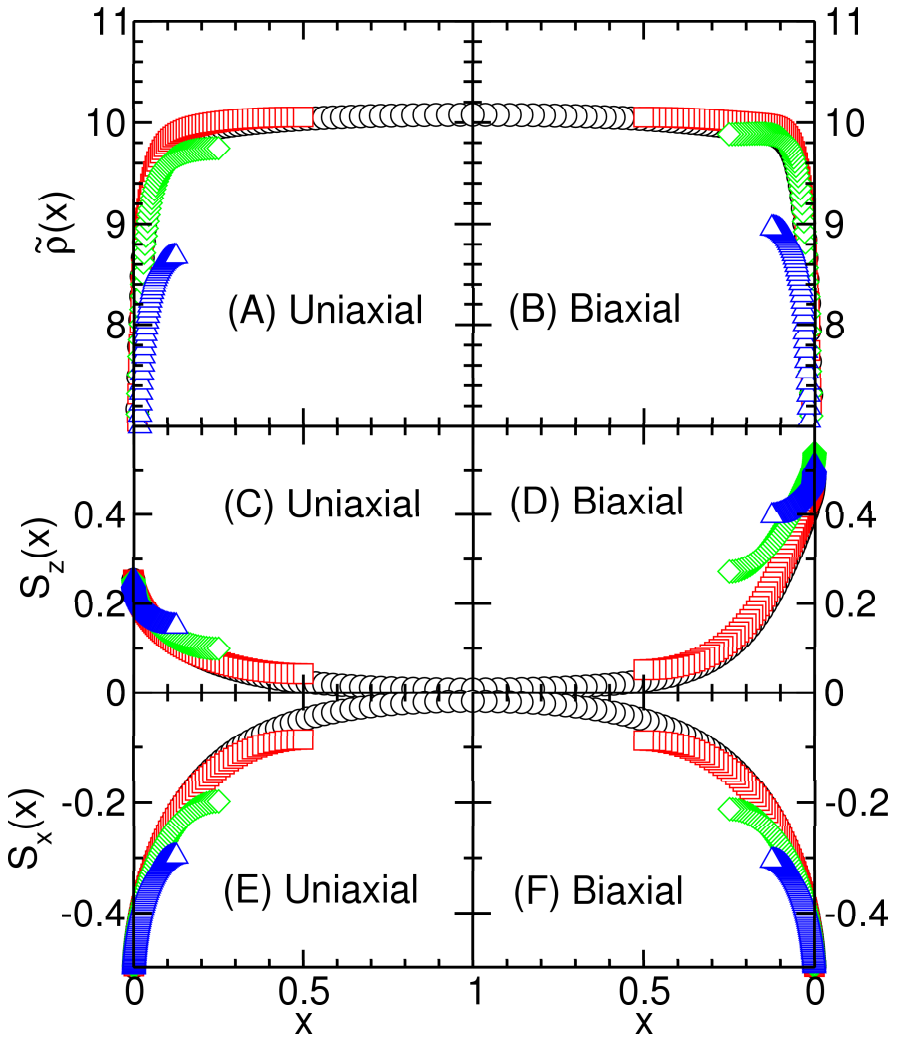

Figure 4.5: Density profiles and order parameter profiles in half space for the uniaxial (left half) and biaxial (right half) states for $W/a = 2$ (circles), 1 (squares), 0.5 (diamonds), and 0.25 (triangles) at the uniaxial-biaxial transition, corresponding to $\beta\mu = 15.86, 15.98, 15.80$ and 14.84 respectively.

selected as the local nematic direction (defined as z in Fig. 4.1). Orientational order parameters in this phase display typical biaxiality: $S_z(x) > |S_x(x)|/2$ [Fig. 4.5D and 4.5F].

Is the phase transition, caused by the presence of the walls, first order or second order? To answer this question, we calculate the surface tension $\beta\sigma$ of the two states, where the surface tension is defined by the difference between the grand thermodynamic potential of the polymer between walls and that of the bulk phase, isotropic phase, written in terms of $\rho_{l,m}$,

$$\beta\sigma = \frac{4\pi}{ad}\int_0^{W/a} \mathrm{d}x \left[d_0[\rho^I_{0,0}(x)]^2 - \sum_{l,m} \frac{d_l \rho^2_{l,m}(x)}{2l+1} \right], \tag{4.40}$$

which is the flexible limit of the tension definition by Eqs. (3.34, 3.35). Figure 4.6A's show the surface tensions of the uniaxial $\beta\sigma_{\mathrm{u}}$ (dashed lines) and the biaxial phases $\beta\sigma_{\mathrm{b}}$ (solid lines) as function of the chemical potential $\beta\mu$ for the wall separation of $W/a = 2, 1, \frac{1}{2}$ and $\frac{1}{4}$, respectively. Each case appears a typical second order phase transition. However, closely examining them, we found these two lines in each case did cross each other. The surface tension difference between the uniaxial and biaxial phases $\beta\Delta\sigma = \beta\sigma_{\mathrm{u}} - \beta\sigma_{\mathrm{b}}$ against the chemical potential are shown in Fig. 4.6B's. Figure 4.6C's are the square root of the difference $\sqrt{\beta\Delta\sigma}$, where for negative data, we find the square root of the absolute value and multiply by the negative sign. All the lines in Fig. 4.6C's have the negative parts, which indicate the surface tension lines do cross each other. So the phase transition is a weak first order transition. The crossing point is the phase transition point, i.e., the point where the surface tension of the biaxial phase is lower than that of the uniaxial phase when we increase the chemical potential $\beta\mu$ from a point where the uniaxial phase is stable. It is easy to see that for wider wall separation, the negative part on the profile of $\sqrt{\beta\Delta\sigma}$ is smaller. However, we examined the infinite wall separation (a half system, with one wall at $x = 0$ point, and $W/2a = \infty$), which is still a weak first order phase transition.

The phase diagram of uniaxial-biaxial transition is shown by the square-symbols in Fig. 4.4. This uniaxial-biaxial phase transition line is replotted in Fig. 4.7A (the chemical potential against the inverse of the wall separation), in order to see clearly

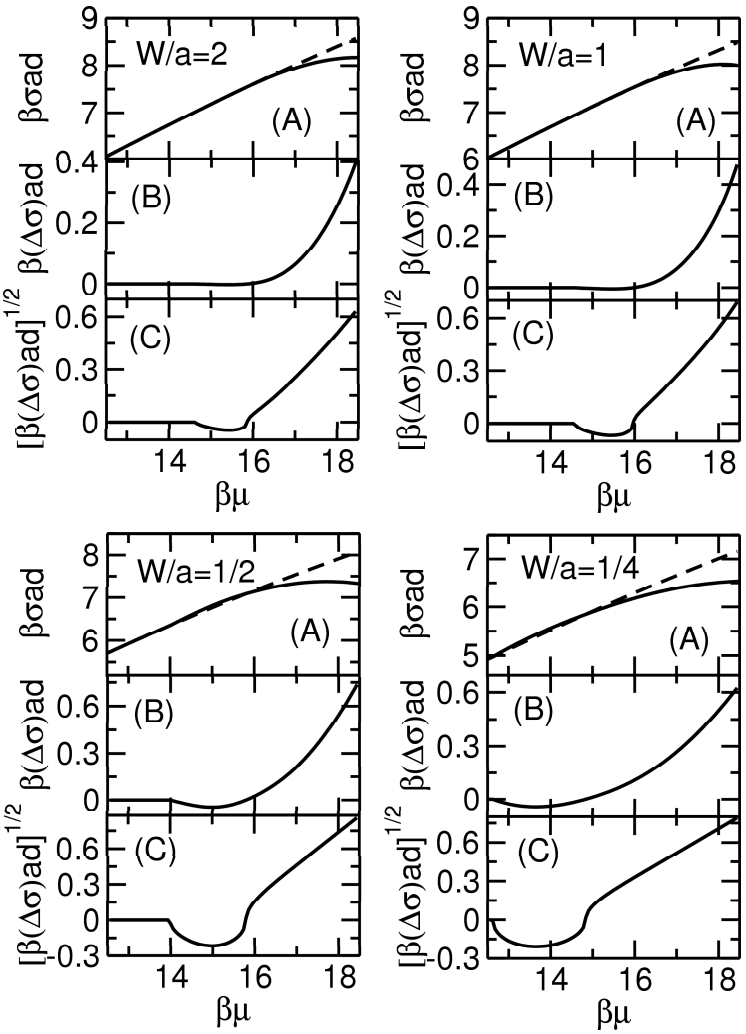

Figure 4.6: Surface tension of the uniaxial and the biaxial phases for different wall separation as functions of $\beta\mu$. (A) the solid line is the surface tension of the biaxial phase $\beta\sigma_{\rm b}$, while the dashed line of the uniaxial phase $\beta\sigma_{\rm u}$; (B) the difference of the surface tension between these two phases; (C) the square root of the difference.

what happens for large wall separation. For wider wall separation, the chemical potential tends to be a constant. It can be explained that, at the uniaxial-biaxial phase transition, the biaxial layers are developed only in the area close to the walls. Far away from the wall, the segments of the polymer do not have the steric interaction with the wall; due to the lower density (below the value in the isotropic phase of the bulk isotropic-nematic transition), the bulk isotropic-like phase exists in the middle area. The existing isotropic phase between the two biaxial layers has no contribution to the phase transition. This can also be seen on Fig. 4.5, for wider wall separation (for example $W/a = 2$), in the middle area, the density profile (Fig. 4.5B) is flat, and the order parameters (Fig. 4.5D, F) tends to zero.

Comparing the density profiles for the uniaxial and biaxial phases shown in Fig. 4.5A and 4.5B, respectively, we can see that in the two phases, the densities are different from each other, especially for narrower wall separation. Integrate the density profile throughout the whole space, we get the total amount of the polymer confined between the two walls,

$$R_i = a^2 d \int_0^{W/a} \mathrm{d}x\mathrm{d}\mathbf{u}\rho_i(x,\mathbf{u}) = \int_0^{W/a} \mathrm{d}x\tilde{\rho}_i(x), \tag{4.41}$$

where i can be u, b and c, which stand for the uniaxial state, the biaxial state and the condensed state, respectively. The difference of R between the uniaxial phase and biaxial phase at the phase transition point

$$\Delta R = R_\mathrm{b} - R_\mathrm{u} = \int_0^{W/a} \mathrm{d}x[\tilde{\rho}_\mathrm{b}(x) - \tilde{\rho}_\mathrm{u}(x)], \tag{4.42}$$

which is shown by the uptriangle-symbol line in Fig. 4.7B. The peak of the profile appears around $a/W \approx 1.8$, which is different from the peak of the phase transition (Fig. 4.7A) around $a/W \approx 1.5$. We can see that the difference of the density R appears to be a constant for large wall separation ($a/W \leq 0.4$). It again shows us that the biaxial phase is mainly a surface phenomenon where a thin layer is developed in the length scale of the effective Kuhn length a. When the wall separation is larger than $2a$, the segments of polymer away from the walls are not affected by the walls, and the isotropic state is present, which has no contribution to the phase transition.

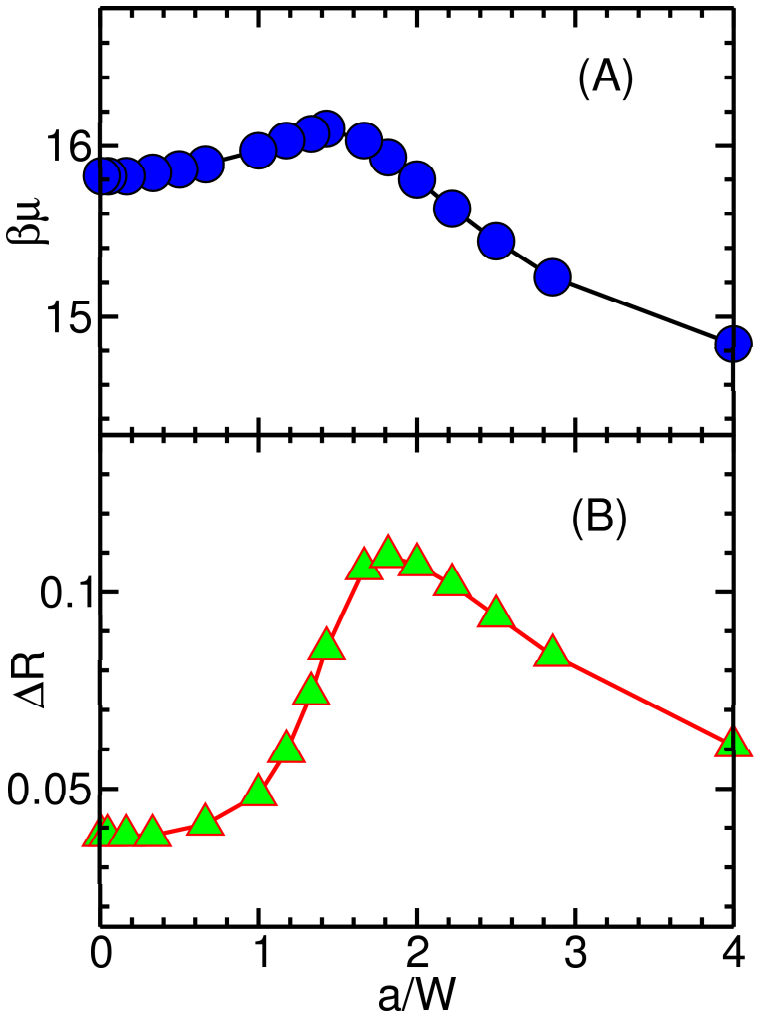

Figure 4.7: (A) the chemical $\beta\mu$ as function of the inverse of the wall separation a/W at the uniaxial-biaxial transition, (B) the density difference between the two phases ΔR against a/W.

4.7 Biaxial-Condensed transition

As the overall density is further increased, the biaxial phase remains stable as long as the density far from the wall is below the value in the isotropic phase of the bulk isotropic-nematic transition, $\tilde{\rho}_{\rm I} = 13.046$ (corresponding to $\beta\mu_{\rm IN} = 20.49$) [24, 33]. The density-enhanced layer near the wall develops stronger nematic characteristics and the local density may even exceed $\tilde{\rho}_{\rm N} = 14.029$, the value in the nematic phase of the bulk IN transition. The thickness of the surface layer expands beyond a and develops into a thick partial wetting layer. For very large W/a, this behavior of the biaxial phase continues until $\beta\mu$ reaches $\beta\mu_{\rm IN}$, where the thickness of the wetting layer diverges, which results in complete wetting by the nematic phase at a single wall [49]. For smaller W/a, however, the dense wetting layers extending from both walls tend to merge, resulting in a new *(capillary) condensed* phase, which becomes stable after $\beta\mu$ reaches the solid phase boundary associated with the circles in Fig. 4.4. After this phase transition, the density within the entire space between the walls jumps to a value comparable to $\tilde{\rho}_{\rm N}$. Orientational order parameters still display typical biaxiality: $S_z(x) > |S_x(x)|/2$, but the average order parameter S_z grows and approximately reaches the asymptotic value $S_z = 0.4618$, found for the bulk isotropic-nematic transition [24, 33]. Ultimately, as $W/a \to \infty$, the first-order biaxial-condensed transition becomes the bulk isotropic-nematic transition.

This scenario of three stable phases needs to be revised for $W/a < 1.8$. Because the space between the walls is so narrow, the system does not support the adequate development of the partial wetting biaxial state; the latter might already have a wetting width that exceeds W/a. Figure 4.9 shows us surface tension of the biaxial state and condensed state against the chemical potential near the phase transition point for different wall separations (more data is shown by the close-circle symbol in Fig. 4.4). For $W/a = 6$, the two line crosses each other with large angle; for $W/a = 2$, the angle formed by lines almost disappear. For even narrower wall separation, the crossover between the partial wetting and condensed states is continuous without any signature of a phase transition. The first order biaxial-condensed phase transition terminated at the critical point (the open symbol in Fig. 4.4). The open symbol on the phase diagram will be determined later.

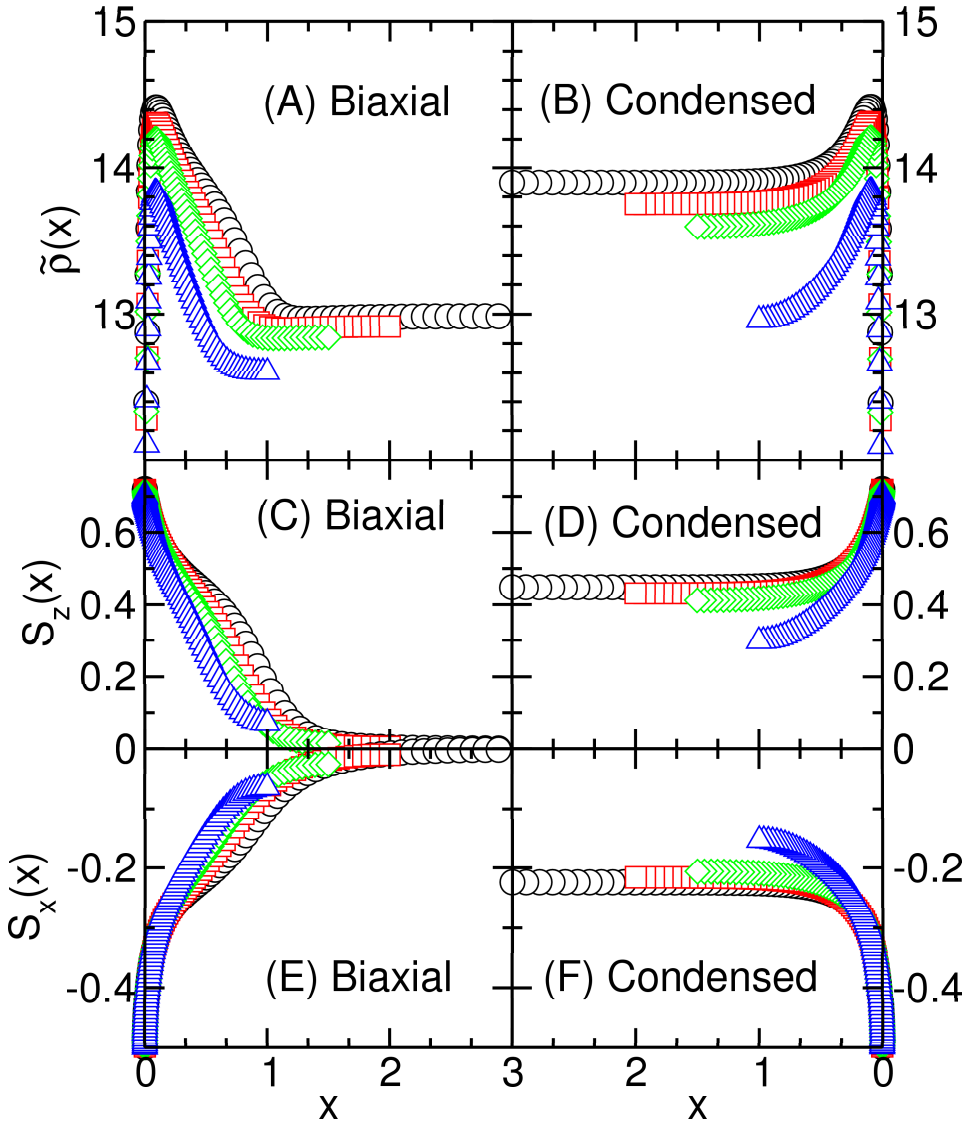

Figure 4.8: Density and order parameter profiles in half space for the condensed (right half) and biaxial (left half) states for $W/a = 6$ (circles), 4 (squares), 3 (diamonds), and 2 (triangles) at the biaxial-condensed transition, corresponding to $\beta\mu = 20.4, 20.3, 20.1$, and 19.8 respectively.

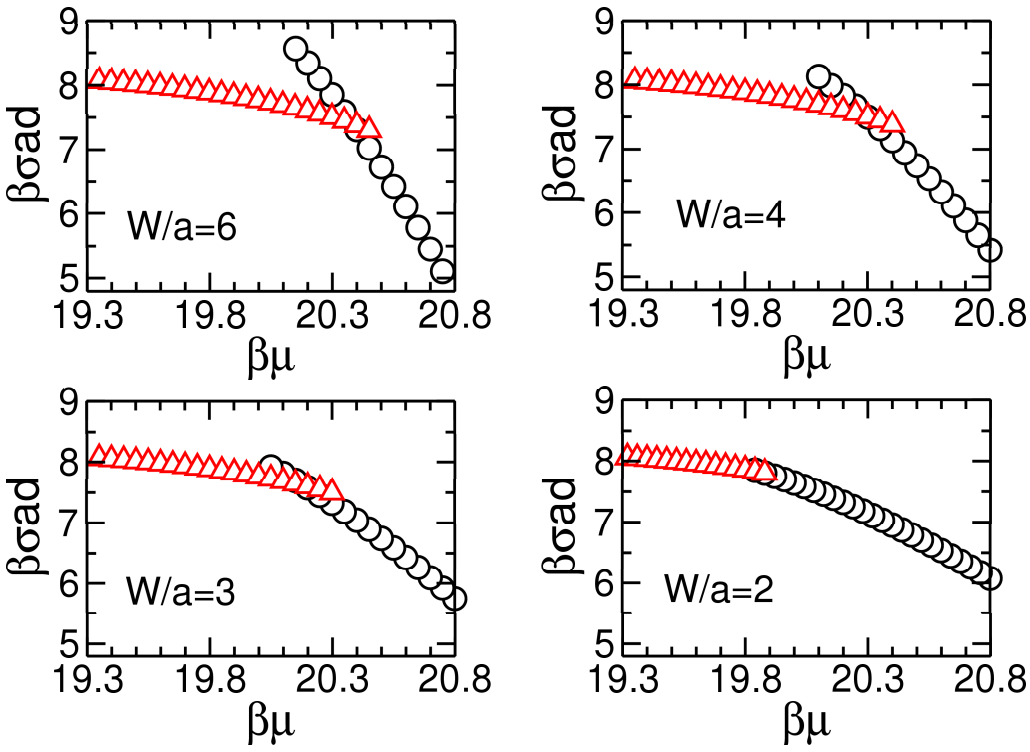

Figure 4.9: Surface tension of the biaxial phase (triangles) and the condensed phase (circles) as function of chemical potential for $W/a = 6, 4, 3$ and 2, respectively.

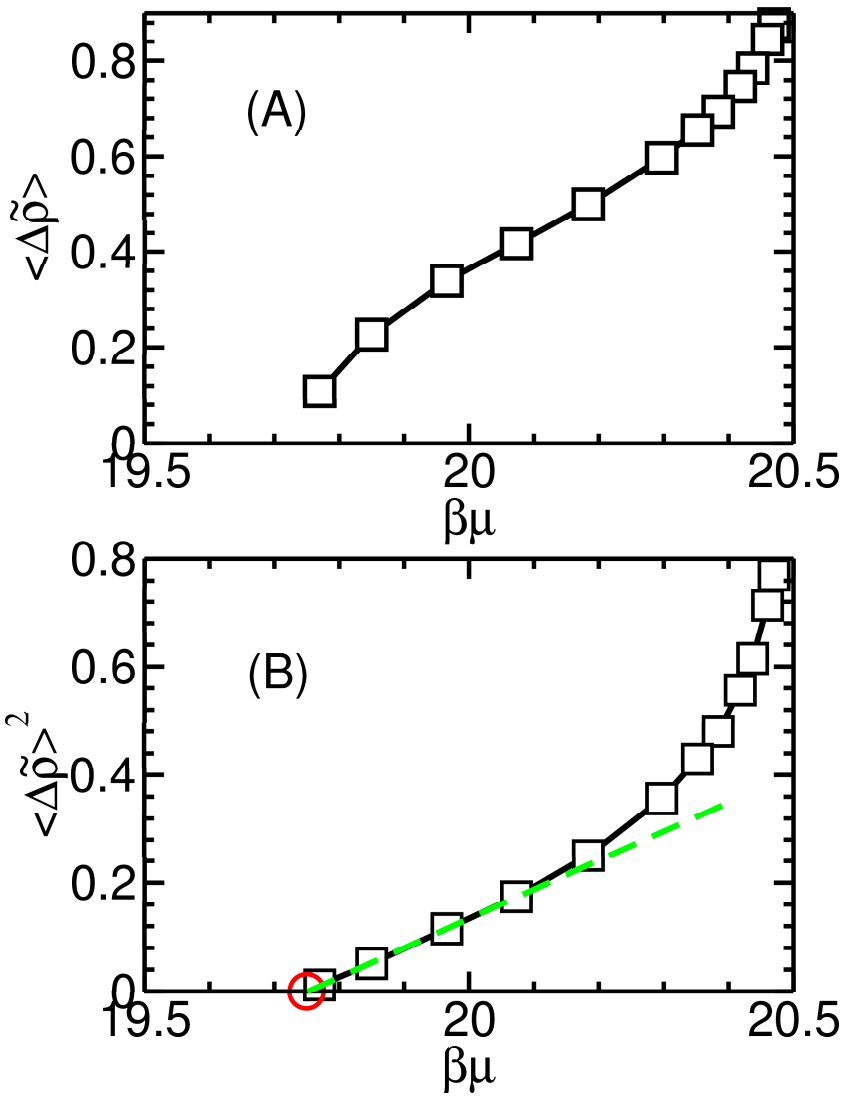

Figure 4.10: (A) the difference of average density as function of the chemical potential at the biaxial-condensed phase transition point, (B) the square of the difference of average density as function of the chemical potential. The circle is the estimated critical point ($\beta\mu = 19.75$) when the square of the difference of average density is zero.

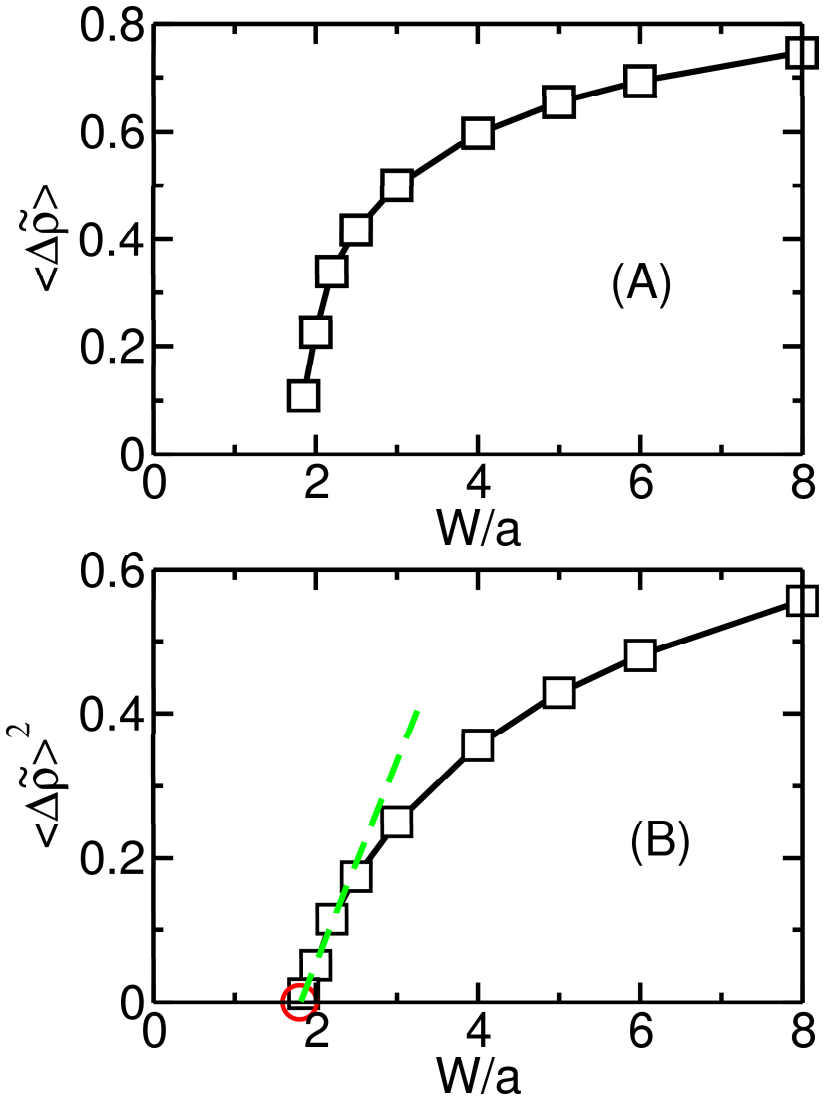

Figure 4.11: (A) the difference of the average density as function of the wall separation. (B) the square of the difference of the average density as function of the wall separation. The asymptotic line crosses x axis around $W/a = 1.8$.

From Fig. 4.9, we can see that for wider wall separation, the phase separation is at higher chemical potential. For $W/a = 6$, the phase transition happens at $\beta\mu \approx 20.4$, which is close to the bulk isotropic-nematic phase transition point. While the phase transition point for $W/a = 3$ is at $\beta\mu \approx 20.1$, and $W/a = 2$ is at $\beta\mu \approx 19.85$, which means the density-enhanced layers merged easier for narrower wall separation and phase transition at lower chemical potential.

Closing to the critical point, the two surface tension lines can not be distinguished easily (can not find the crossing point). To determine the critical point is of interest. Going back to Figs. 4.8A and 4.8B, we find that the density for biaxial phase changes much slower than that of the condensed phase when the wall separation changes, i.e., the density difference for the two phase getting smaller when the wall separation decreases. The first order phase transition terminates at a point where the density difference at the phase transition disappears.

We have discussed in the previous section that the uniaxial-biaxial phase transition is mainly a surface phenomenon, which is characterized by the difference of the total amount of polymer confined between two walls (Eq. (4.42)). However, for the biaxial-condensed phase transition, it is mainly contributed from the middle area, and the difference of the average density between the walls is more useful. The difference of the average density can be simply defined as

$$< \Delta\tilde{\rho} > \equiv < \tilde{\rho} >_{\rm c} - < \tilde{\rho} >_{\rm b} \equiv \frac{aR_{\rm c}}{W} - \frac{aR_{\rm b}}{W}, \tag{4.43}$$

where $< \tilde{\rho} >_c$ and $< \tilde{\rho} >_b$ are the average densities for the condensed phase and biaxial phase, respectively, $R_{\rm c}$ and $R_{\rm b}$ the total amount of polymer confined between the walls defined by Eq. (4.41) for the condensed and biaxial phase, respectively.

Figures 4.10A and 4.10B show the average density difference and the square of the average density difference against the chemical potential at the biaxial condensed phase transition, respectively. From Fig. 4.10B, we can see that, close to the critical point, the critical behavior $< \Delta\tilde{\rho} >^2 \sim (\beta\mu - \beta\mu_{\rm c})$ is clear, where $\beta\mu_{\rm c}$ is the critical chemical potential, and the value is $\beta\mu_{\rm c} = 19.75 \pm 0.05$. The similar critical behavior is found on the relationship between the square of the difference of the average density and the wall separation, which is shown in Fig. 4.11B, i.e.,

$< \Delta\tilde{\rho} >^2 \sim (W/a - W_c/a)$, where $W_c/a = 1.80 \pm 0.10$ is the critical wall separation. Hence, the critical point of the biaxial-condensed phase transition is at ($W_c/a = 1.80$ and $\beta\mu_c = 19.75$) shown by the open circle on the phase diagram Fig. 4.4.

Van Roij and coworkers [51] studied of the confinement of hard-rods by two hard walls, based on the Zwanzig model, in which the orientations are restricted to three orthogonal directions. The interaction is chosen as Onsager type. A very similar phase diagram is plotted with three phases, uniaxial, biaxial and condensed phases. The biaxial-condensed phase transition terminates at a critical point when the wall separation is 2.08 ± 0.01 times of the length of the rods, while the critical point in this thesis for flexible polymer is at the point when the wall separation is 1.80 ± 0.10 times of the length of the effective Kuhn length. In his paper, the coexistence curve for biaxial-condensed transition is plotted as a function of average number density.

In order to compare the plot to our results, we also plot the coexistence curves in Fig. 4.12. Figure 4.12A is '$a/W - < \tilde{\rho} >$' (the inverse of wall separation versus the average density) coexistence phase diagram. The coexistence curves are shown by diamond-symbol line for the condensed phase and by square-symbol line for the biaxial phase, respectively. The two lines merged at the critical point found in the early discussion for narrower wall separation. At wider wall separation, the two densities tend to the values of the isotropic phase and the nematic phase of the bulk isotropic-nematic phase transition, respectively, ($C_I = 13.048$ and $C_N = 14.039$ [24]), shown by the two cross symbols ($\times$). The triangle symbols are the curves with fixed chemical potential, which is very similar to the P-V diagram of the gas-liquid phase transition. It is similar to that of the rigid rod case. Besides the two curves (uniaxial-biaxial transition and biaxial-condensed transition curves shown in Fig. 4.12) meet at different wall separation, the density is also different. The critical density for their figure is between the bulk coexistence densities C_I and C_N, and ours is lower than the bulk coexistence densities. The reason is that for lower average density the narrower wall separation causes the phase transition to happen at lower chemical potential.

Figure 4.12B is '$\beta\mu - < \tilde{\rho} >$' (the chemical potential versus the average density)

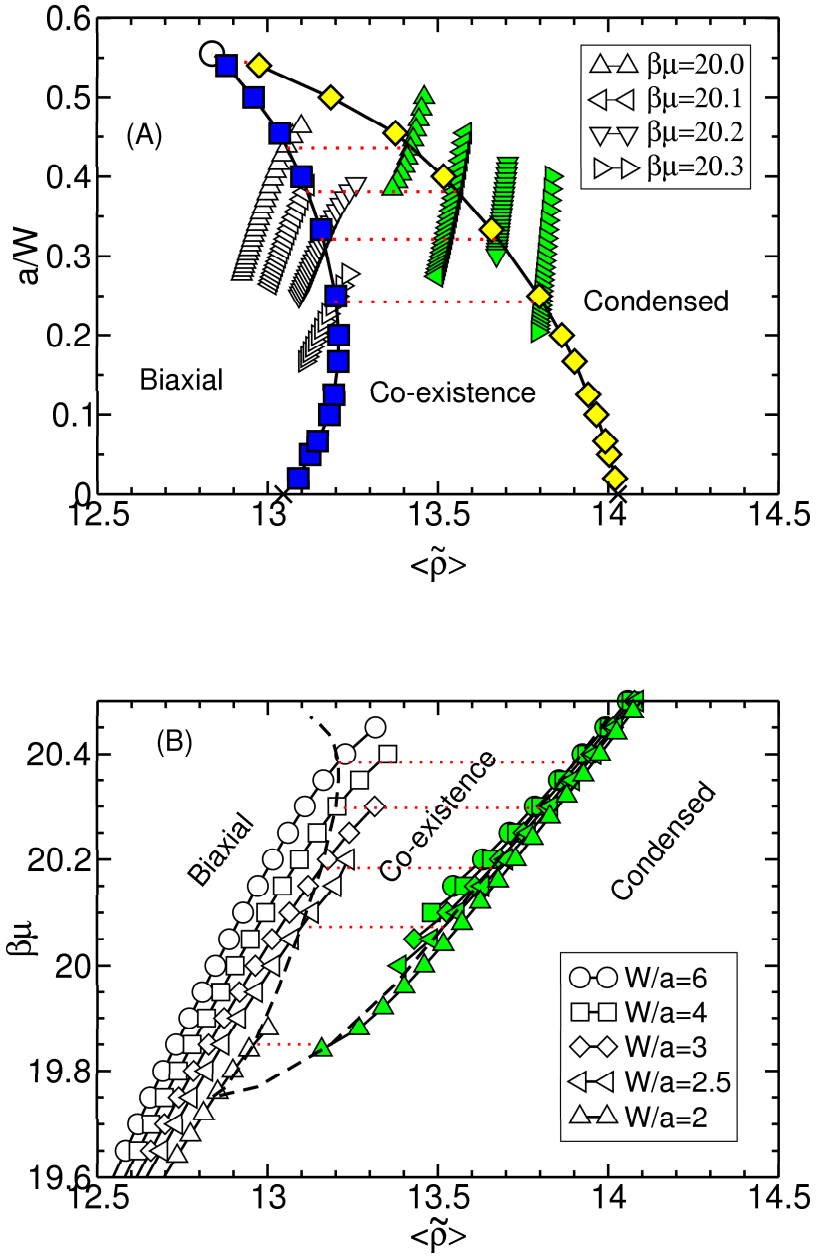

Figure 4.12: The coexistence curve for the biaxial-condensed nematic phase transition.(A) the inverse of wall separation against the average densities. (B) the chemical potential against the average densities.

coexistence phase diagram. The dashed lines are the coexistence curves and they merged at the critical point. The symbolled lines are for fixed wall separation. With the increase of the chemical potential, the density increases. When it reaches the coexistence curve, the density jumps from the value of the biaxial phase to that of the condensed phase. The jumps are shown by the dotted lines.

Chapter 5

Summary

In this thesis, we have discussed two nematic ordering problems of semiflexible (wormlike) polymers: one is the study of the isotropic-nematic interfaces of polymers for some typical cases (flexible, rod-like and intermediate), and the other is the study of a very long wormlike polymer confined between two infinite flat hard walls.

By using the functional integral approach, the mean field theory of semiflexible polymers in the three dimensions was introduced. This numerical procedure of the general form has been developed before in the work of Chen and coworkers [24]. The interaction of the segments of polymers is that of the Onsager excluded volume type.

In the study of isotropic-nematic interfaces, the numerical calculations have been performed to investigate the phase coexistence for different type of polymers. The profiles of density , order parameter, tension contribution and the interface tension have been given for polymers with the flexibility $\alpha = 10$, $\alpha = 0$ and $\alpha = 1$, which represent the three typical cases, the flexible one, the rod-like one, and the intermediate one, respectively. For these three cases, we found that the interface tension is always a monotonic function of the tile angle and has a minimum at $\theta_t = \pi/2$. The contribution to the interface tension for different tilt angle comes from different area. For $\theta_t = 0$, the major contribution comes from the nematic phase side, while for $\theta_t = \pi/2$, the major contribution comes from the isotropic

phase side. The interface width is also a monotonic function of tilt angle and has a minimum at $\theta_t = \pi/2$, and is proportion to the ratio of the mean-square end-to-end distance to the total contour length for these three cases. The simulation results are consistent with work by other people.

In the study of the confinement, we investigated the case of a long polymer confined between two flat hard walls, which are separated by a distance comparable to the effective Kuhn length of polymer chain for wormlike chain model with or without the Onsager excluded volume interaction. The domination of ground-state is assumed for the long polymer. For wider wall separation, without Onsager excluded volume interaction, the wormlike chain recovers most of the properties of a Gaussian chain. However, for the wall separation comparable with the effective Kuhn length, the Gaussian chain model is no longer good for the polymer confinement. Including the interaction, the numerical simulation show that three phases, uniaxial, biaxial and condensed phases may exist. The results are compared with the similar findings for the hard-rod fluid.

Appendix A

Virial expansion of excluded interaction

The following is to evaluate the excluded interaction of hard particles. Based on the method developed by Mayer and Mayer, assuming additive forces:

$$w = w_N[(q_1), ..., (q_N)] = \sum_{i=1}^{N} \sum_{j=1}^{i-1} w_{i,j}, \tag{A.1}$$

$$w_{i,j} = w_2[(q_i), (q_j)] \tag{A.2}$$

where (q_i) are the coordinates of the ith particle. We use Mayer function

$$f_{i,j} = f_{i,j}[(q_i), (q_j)] = \exp[-w_{i,j}/k_B T] - 1 \tag{A.3}$$

So the interaction between the particles are

$$\begin{aligned} \exp[-w] &= \exp[-\sum_{i=1}^{N} \sum_{j=1}^{i-1} w_{i,j}] \\ &= \prod_{i=1}^{N} \prod_{j=1}^{i-1} (1 + f_{i,j}) \\ &= 1 + \sum_{i=1}^{N} \sum_{j=1}^{i-1} f_{i,j} + \frac{1}{2} \sum_{i=1}^{N} \sum_{j=1}^{i-1} \left(\sum_{i'=1}^{N} \sum_{j'=1}^{i'-1} \right)' f_{i,j} f_{i',j'} + \cdots \end{aligned} \tag{A.4}$$

where prime on the summation means (i', j') should be different from (i, j). .....

Mayer and Mayer obtain an expansion for the integral in terms of the irreducible cluster integrals

$$\alpha_1 = \frac{1}{V}\int f_{1,2} d\mathbf{r}_1 d\mathbf{r}_2 \tag{A.5}$$

$$\alpha_2 = \frac{1}{2V}\int f_{1,2} f_{1,3} f_{2,3} d\mathbf{r}_1 d\mathbf{r}_2 d\mathbf{r}_3. \tag{A.6}$$

It is not very easy to calculate α easily. In the following we first do some calculation on spheres, which is the easiest one. For two hard spheres, the potential is only depending on the distance between them

$$w_{i,j} = \begin{cases} \infty, & r_{1,2} < 2R; \\ 0, & r_{1,2} \geq 2R\ . \end{cases} \tag{A.7}$$

where R is the radius of the sphere, $r_{1,2} = |\mathbf{r}_{1,2}|$, and $\mathbf{r}_{1,2} = \mathbf{r}_2 - \mathbf{r}_1$ so the Mayer function will be

$$f_{i,j} = \begin{cases} -1, & r_{1,2} < 2R; \\ 0, & r_{1,2} \geq 2R\ . \end{cases} \tag{A.8}$$

For the second order virial expansion

$$\begin{aligned} \alpha_1 &= \frac{1}{V}\int f_{1,2} d\mathbf{r}_1 d\mathbf{r}_2 \\ &= \frac{1}{V}\int d\mathbf{r}_1 \int f_{1,2} d\mathbf{r}_{1,2} \\ &= -\frac{4\pi}{3}(2R)^3 \end{aligned} \tag{A.9}$$

For the third order virial expansion

$$\begin{aligned} \alpha_2 &= \frac{1}{2V}\int f_{1,2} f_{1,3} f_{2,3} d\mathbf{r}_1 d\mathbf{r}_2 d\mathbf{r}_3 \\ &= \frac{1}{2V}\int d\mathbf{r}_1 \int f_{1,2} d\mathbf{r}_{1,2} \int f_{1,3} f_{2,3} d\mathbf{r}_{2,3} \\ &= -\frac{1}{2V}\int d\mathbf{r}_1 \int_0^{2R} 4\pi r_{1,2}^2 dr_{1,2} \frac{2\pi}{3}(2R)^3 \left(1 - \frac{r_{1,2}}{4R}\right)^2 \left(2 + \frac{r_{1,2}}{4R}\right) \\ &= -\frac{80}{3}\pi^2 R^6 \end{aligned} \tag{A.10}$$

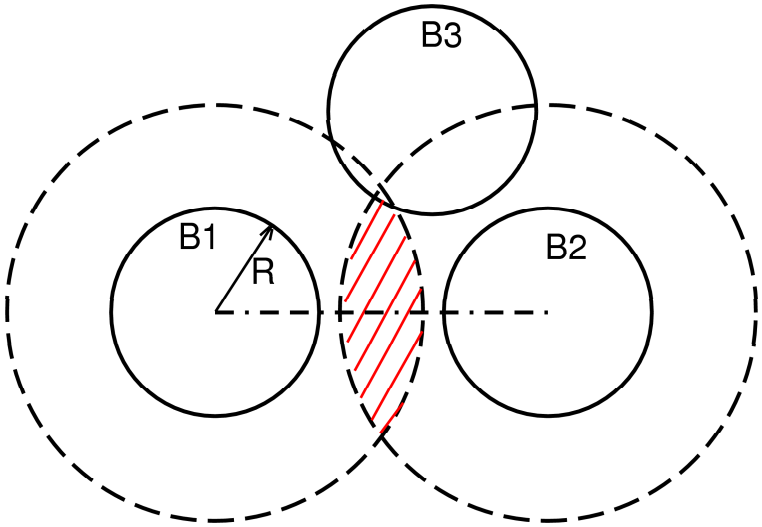

Figure A.1: Schematic diagram of the second and third virial expansion of hard spheres

Then we got the relation between the second order and the third order expansion is

$$-\alpha_2 = \left(\frac{15}{64}\right)\alpha_1^2. \tag{A.11}$$

This the result for spheres.

As for rods with length l and diameter D, the calculation is on the same way, but much more complicated. Onsager got the results for second order with $l \gg D$

$$\alpha_1 = -2l^2 D \sin\gamma_{12} \tag{A.12}$$

where γ is the angle formed by two rods. Onsager also gave the estimate of the third virial expansion as

$$\alpha_2 = -(2D)^3[l^3(\sin\gamma_{12}/\sin\phi_3) + O(l^2 D)] \tag{A.13}$$

where γ_{12} is angle formed by rod 1 and 2, and ϕ_3 is the angle formed by the plane12 and plane13. So the relation between the second order and the third order expansion is

$$-\frac{\alpha_2}{\alpha_1^2} \simeq \left(\frac{(2D)^3 l^3(\sin\gamma_{12}/\sin\phi_3)}{[2l^2 D\sin\gamma_{12}]^2}\right) \tag{A.14}$$

$$\sim \frac{D}{l} \tag{A.15}$$

Since $l \gg D$ then we can cut off after the second virial expansion. Fig A.2 shows us the third virial expansion of three rods perpendicular to each other. The third virial expansion is about the $D^3 l^3$, which is agree with the above result.

We should note that if the three rods are nearly coplanar, ϕ_3 would be so small, and with nontrivial angle γ_{12}, α_2 will be infinite, the above relation between the estimate second and third order will be revised to

$$-\frac{\alpha_2}{\alpha_1^2} = O(1). \tag{A.16}$$

This is a case of two dimension problem. At three dimension, if the density is not so high, the above revision is not necessary.

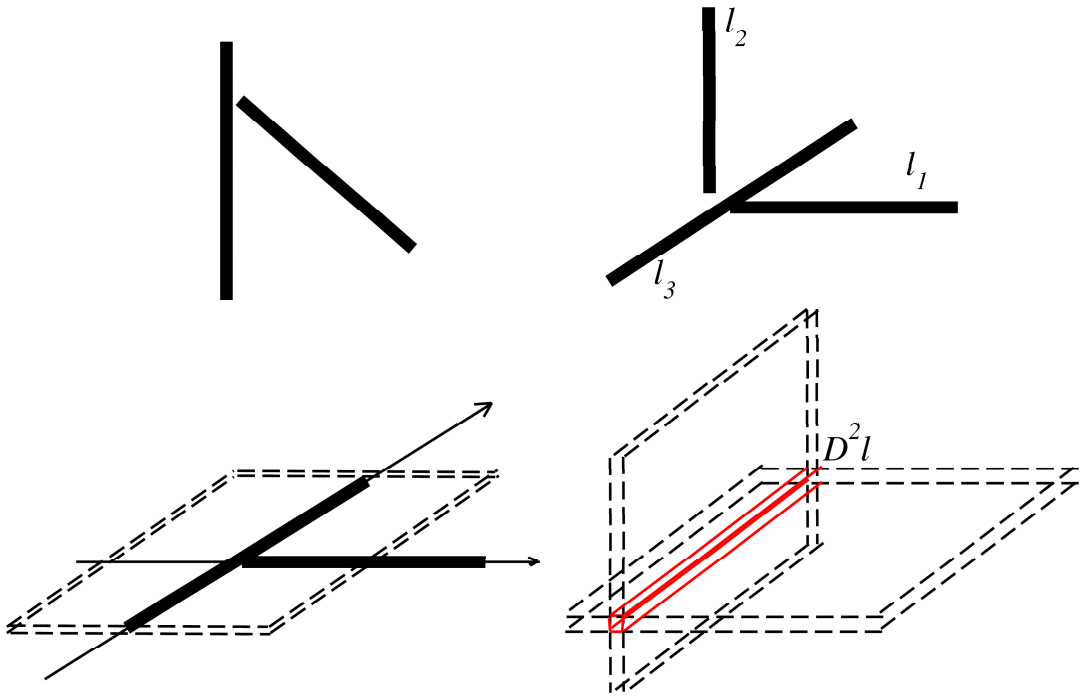

Figure A.2: Schematic diagram of the second and third virial expansion of hard rods. The left side shows the second virial expansion, which is a box of volume $l^2 D$. The right side is the third virial expansion, which is $\sim D^2 l \cdot D l^2 = D^3 l^3$.

Appendix B

Bending energy of hard rods

According to Hooke's law, the angle is proportional to the force on the rod's

$$f \sim \theta \tag{B.1}$$

then the potential stored in the unit length of the rod is

$$E \sim \frac{\theta^2}{2} \tag{B.2}$$

From Fig. B.1 we see that the relationship between θ and the radius of the curve $\Re$

$$\tan\frac{\theta}{2} = \frac{b/2}{\Re} \tag{B.3}$$

Since $\theta \ll 1$

$$\theta \simeq \frac{b}{\Re} \tag{B.4}$$

Then we get

$$E \sim \frac{1}{2\Re^2} \tag{B.5}$$

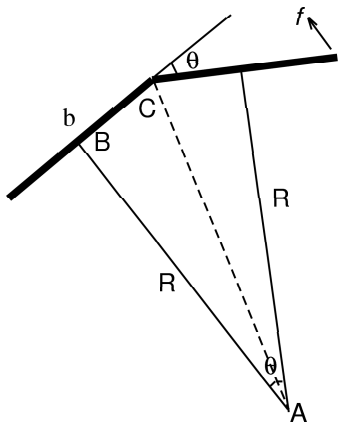

Figure B.1: Explaining the bending energy. Two conjunctive segments with length b along the wormlike chain form an angle θ, $\Re$ are the radius of the curve.

Bibliography

[1] http://moebius.physik.tu-berlin.de/lc/lcs.html.

[2] P.-G. D. Gennes and J. Prost, *The Physics of Liquid Crystals*, 2 ed. (Clarendon, Oxford, 1992).

[3] G. J. Vroege and H. N. W. Lekkerkerker, Rep. Prog. Phys. **55**, 1241 (1992).

[4] http://www.accessexcellence.org/RC/VL/GG/structure.html.

[5] L. Onsager, Ann. N. Y. Acad. Sci. **51**, 627 (1949).

[6] R. Zwanzig, J. Chem. Phys. **39**, 1714 (1963).

[7] A. R. Khokhlov and A. N. Semenov, Physica **112A**, 605 (1982).

[8] K. F. Freed, Adv. Chem. Phys. **22**, 1 (1972).

[9] O. Kratky and G. Porod, Recl. Trav. Chim. **68**, 1106 (1949).

[10] F. Gittes, B. Mickey, J. Nettleton, and J. Howard, J. Cell Biol. **120**, 923 (1993).

[11] J. Kas, H. Strey, M. Barmann, and E. Sackmann, Europhys. Lett. **21**, 865 (1993).

[12] A. Ott, M. Manasco, A. Simon, and A. Libchaber, Phys. Rev. E **48**, 1642 (1993).

[13] C. Frontale, E. Dore, A. Ferraute, and E. Gratton, Biopolymers **18**, 1353 (1979).

[14] N. Saito, K. Takahashi, and Y. Yunoki, J. Phys. Soc. Jpn **22**, 219 (1967).

[15] E. Helfand, J. Chem. Phys. **62**, 999 (1975).

[16] K. M. Hong and J. Noolandi, Macromolecules **14**, 727 (1981).

[17] F. Schmid, J. Phys.: Condens. Matter **10**, 8105 (1998).

[18] D. Duchs and D. E. Sullivan, J. Phys.: Condens. Matter **14**, 12189 (2002).

[19] E. Helfand and Y. Tagami, J. Chem. Phys. **57**, 1812 (1972).

[20] R. Holyst and A. Poniewierski, Phys. Rev. A **38**, 1527 (1988).

[21] B. G. Moore and W. E. McMullen, Phys. Rev. A **42**, 6042 (1990).

[22] M. Doi and N. Kuzuu, J. Appl. Polym. Sci.: Appl. Polym. Symp. **41**, 65 (1985).

[23] Z. Y. Chen and J. Noolandi, Phys. Rev. A **45**, 2389 (1992).

[24] S.-M. Cui, O. Akcakir, and Z. Y. Chen, Phys. Rev. E **51**, 4548 (1995).

[25] A. J. McDonald, M. P. Allen, and F. Schmid, Phys. Rev. E **63**, 010701 (2001).

[26] D. L. Koch and O. G. Harlen, Macromoleculars **32**, 219 (1999).

[27] K. Shundyak and R. van Roij, J. Phys.: Condens. Matter **13**, 4789 (2001).

[28] W. L. Chen, T. Sato, and A. Teramoto, Macromolecules **29**, 4283 (1996).

[29] W. L. Chen, T. Sato, and A. Teramoto, Macromolecules **31**, 6506 (1998).

[30] W. L. Chen, T. Sato, and A. Teramoto, Macromolecules **32**, 1549 (1999).

[31] W. L. Chen and D. G. Gray, Langmuir **18**, 633 (2002).

[32] I. S. Gradshteyn and I. M. Ryzhik, *Tables of Integrals, Series, and Products* (Academic, New York, 1980).

[33] Z. Y. Chen, Macromolecules **26**, 3419 (1993).

[34] A. J. Spakowitz and Z. G. Wang, Phys. Rev. Lett. **91**, 166102 (2003).

[35] P.-G. D. Gennes, *Scaling Concepts in Polymer Physics* (Connell University Press, Ithaca, N.Y., 1993).

[36] L. Livadaru and H. J. Kreuzer, New J. Phys. **5**, 95 (2003).

[37] T. Dotera and Y. Y. Suzuki, Phys. Rev. E **62**, 5318 (2000).

[38] T. W. Burkhardt, J. Phys. A: Math. Gen. **30**, L167 (1997).

[39] H. P. Hsu and P. Grassberger, J. Chem. Phys. **120**, 2034 (2004).

[40] Y. L. Chen *et al.*, J. Chem. Phys. **120**, 2034 (2004).

[41] M. Doi and S. F. Edwards, *The theory of polymer dynamics* (Oxford University Press, New York, 1988).

[42] A. Y. Grosberg and A. R. Khokhlov, *Statistical physics of Macromolecules* (American Institute of Physics, N.Y., 1994).

[43] D. E. Smith, S. J. Tans, S. Grimes, D. L. Anderson, and C. Bustamente, Nature **413**, 748 (2001).

[44] R. E. Strzelecka, M. W. Davidson, and R. L. Rill, Nature **331**, 457 (1988).

[45] T. Odijk, Macromolecules **19**, 2313 (1986).

[46] D. V. Kuznetsov and W. Sung, Macromolecules **31**, 2679 (1998).

[47] D. C. Morse and G. H. Fredrickson, Phys. Rev. Lett. **73**, 3235 (1994).

[48] A. Y. Grosberg and D. V. Pachmov, Liq. Cryst. **10**, 539 (1991).

[49] Z. Y. Chen and S.-M. Cui, Phys. Rev. E **52**, 3876 (1995).

[50] H. Kimura and H. Nakano, J. Phys. Soc. Jpn. **54**, 1730 (1985).

[51] R. van Roij, M. Dijkstra, and R. Evans, J. Chem. Phys. **113**, 7689 (2000).